ANALYTICAL AND EXPERIMENTAL STUDY OF HIGH VELOCITY IMPACT ON COMPOSITE PLATES

A Thesis

Submitted to the College of Engineering

Of Nahrain University in Partial Fulfillment

Of the Requirements for the Degree of

Doctor of Philosophy

in

Mechanical Engineering

by

Ali Hussain Mohammad Al Hilli

B.Sc. 1996

M.Sc.1999

Muharram **1426**

February **2006**

Certification

We certify that the this thesis entitled ”**Analytical and Experimental Study of High Velocity Impact on Composite Plates** ” was prepared by **Ali Hussain Mohammad Al-Hilli,** under our supervision at Nahrain University/ College of **Engineering**, in partial fulfillment of the requirements for the Degree of **Doctor of Philosophy** in **Mechanical Engineering**.

Signature:
Name: **Dr. Kadhim H. Ghlaim**
(Supervisor)
Date: / / 2006

Signature:
Name: **Prof. Dr. Hisham Tawfiq**
(Supervisor)
Date: / / 2006

Signature:
Name: **Prof. Dr. Hisham Tawfiq**
(Head of Department)
Date: / / 2006

Certificate

We certify, as an examining committee, that we have read this thesis entitled " **Analytical and Experimental Study of High Velocity Impact on Composite Plates**" and examined the student **Ali Hussain Mohammad Al-Hilli** and found that the thesis meets the standard for the Degree of **Doctor of Philosophy** in **Mechanical Engineering**.

Signature:
Name: **Dr. Kadhim H. Ghlaim**
(Supervisor)
Date: / 4 /2006

Signature:
Name: **Prof. Dr. Hisham Tawfiq**
(Supervisor)
Date: / 4 /2006

Signature:
Name: **Dr. Fawaz Abbas T. Najim**
(Member)
Date: / 4 /2006

Signature:
Name: **Asst. Prof. Dr. Samira K. Radi**
(Member)
Date: / 4 /2006

Signature:
Name: **Asst. Prof. Dr. Talal A. Jabbar**
(Member)
Date: / 4 /2006

Signature:
Name: **Asst. Prof. Dr. Ahmad AL -Beiroti**
(Member)
Date: / 4 /2006

Signature:
Name: **Prof. Dr. Muhsin J. Jweeg**
(Chairman)
Date: / 4 /2006

Approval of the College of Engineering

Signature:
Name: **Prof. Dr. Fawzi M. Al-Naima**
(Dean)
Date: / 4 /2006

Abstract

Fiber reinforced composite materials are used increasingly in many military and civil applications due to their excellent mechanical properties like high specific strength, specific stiffness, resistance to corrosion, increased fatigue life among others. However, one of the main concerns in the use of advanced composites is their poor translaminar properties, which become critical under situations like impact loading. Composites that are used in aerospace and land based structural components are often subjected to high velocity impact threats like broken engine parts, turbine blades, fragments from bombs, shells, mortars, …etc.

In this work, the energy absorbed due to impact of small rigid projectile on composite materials targets is studied analyticaly and experimentally. Analytically, the energy absorbed due to impact of conical nose projectiles on composite laminates is investigated. Four types of observed energies are studied. They are the strain energy due to deformation of plate (contact energy), the large deformation near the impact zone, the delamination energy and the energy losses due to friction.

The equation of motion of plates is solved for the transient contact load at high velocity with its boundary conditions. Large deformation of delaminated zone is derived assuming a deformation shape formulation to calculate the penetration depth and delamination radius. Delamination energy is calculated by solving the delamination failure criteria with equation of motion. Friction energy is calculated assuming constant friction coefficient.

The experimental work is divided into two parts. First, fabrication and testing the mechanical properties of woven laminate composite materials. Three types of fibers are used which are E-Glass, Carbon, and Kevlar fibers with different types of weave style. The matrices used are epoxy and polyester. Fabrication of matrix and composite samples is done by using successful new molding materials as the (paste for pans), and

ceramic plate with x-ray films. The sets of standard tests are done to measure the needed mechanical properties. From these tests new woven factors are evaluated which are the ratios of mechanical properties for the woven composite to that for equivalent cross-ply composite. It is found that these factors were higher for Kevlar composite for the same matrix material. It was higher for fiber-reinforced epoxy than the fiber reinforced polyester. And it is increased as the yarn section increased and the end satin increased.

Second, testing the manufactured composite plates for the ballistic impact, for this reason, an Impact rig is designed and built using special type of gun made for this purpose with clamped fixation for the square target plate. The computerized counter device is designed for measuring the incident and resting velocity, and to evaluate the approximate penetration time. This rig is used to compare theoretical results with tests, and also to study the effect of hybrid arrangement on the impact.

The results show that the contact energy has a lower value for the energy absorbed, the delamination and large deformation energy are increased as the incident velocity increased until reaching the ballistic velocity limit then they remain constant. The friction energy remaining increased without affecting the ballistic limit. The absorbing energy was increased with increasing the thickness of the plates. The resistance of the carbon composites is shown to be lower than the Kevlar composite and higher than the E-Glass composite.

To improve the impact properties of the E-Glass, a layer of Kevlar is added to the composite, a 3-location of Kevlar lamina was used to reinforce the E-Glass, which at the front, back and center of the composite. Results of this work indicate that the damage is well contained within the Kevlar lamina. However, ballistic limit is higher for the composite that has the Kevlar layer in the back of the target, while it is lower for the case when the Kevlar layer is in the front location.

List of Contents

Nomenclature

Symbols		Notations
A	=	Area (m^2)
a	=	Delamination radius (m)
a	=	Width of plate (m)
b	=	Length of plate (m)
E	=	Young modulus (MPa)
F	=	Friction force (N)
G	=	Modulus of rigidity (MPa)
h	=	Plate thickness (m)
J	=	Area moment of inertia (m^4)
LG	=	Gauge length of tensile specimen (m)
LO	=	Overall length of tensile specimen (m)
m	=	Cosine of orientation angle
n	=	Sine of orientation angle
N	=	Normal force (N)
q	=	Impact force (N)
R	=	Deformation radius (m)
t	=	Time (s)
T1	=	Time period for the incident screen of chronograph (s)
T2	=	Time period through the impact take place (s)
T3	=	Time period for the resting screen of chronograph (s)
u	=	Displacement in x-direction (m)
U	=	Energy (Joule)
V	=	Velocity (m/s)
v	=	Volume fraction

W	=	Woven Factor
w	=	Displacement in y-direction (deflection) (m)
x	=	Direction through the length of plate (m)
y	=	Direction through the width of plate (m)
z	=	Direction thought the thickness of the plate (m)
α	=	Shear correction factor (5/6)
β	=	Angle
ε	=	Longitudinal Strain
ϕ	=	Projectile cone angle
γ	=	Shear strain
κ	=	Curvature (m^{-1})
μ	=	Friction coefficient
ν	=	Poisson's ratio
θ	=	Slope
ρ	=	Density (kg/m^3)
σ	=	Longitudinal stress (MN/m^2)
τ	=	Shear stress (MN/m^2)

Matrix Notations

$[\overline{Q}_{ij}]$	=	Reduced stiffness matrix through coordinate axis
[A]	=	Axial stiffness matrix
[a]	=	Inverse of axial stiffness matrix
[B]	=	Axial –bending stiffness matrix
[D]	=	Bending torsion stiffness matrix
[Q]	=	Reduced stiffness principle axis

Subscript

∞	=	Infinite satin
break	=	Break point for strain
c	=	Contact
del	=	Delamination
E	=	Young modulus
F	=	Fiber
F	=	Friction
G	=	Modulus of rigidity
i	=	Layer I
L	=	Longitudinal
Ld	=	Large deformation
m	=	Matrix
n	=	Maximum available for matrix (delamination failure criteria)
p	=	Projectile
pi	=	Incident for projectile
Po	=	Resting for projectile
r	=	Polar coordinate an radius axis
s	=	Ultimate for matrix (delamination failure criteria)
T	=	Tensile
ult	=	Ultimate
w	=	Weave
ν	=	Poisson's ratio
θ	=	Polar coordinate an angle axis

Abbreviations

3eskp	=	**3-e**nd **s**atin **K**evlar **p**olyester **c**omposite
5escp	=	**5-e**nd **s**atin **c**arbon **p**olyester **c**omposite
5esgp	=	**5-e**nd **s**atin E-**g**lass **p**olyester **c**omposite
CCA	=	**C**omposite **C**ylinder **A**ssemblage
CCCC	=	Rectangular plate **C**lamped on all **F**our edges
FRP	=	**F**iber **R**einforced **P**lastic
NIJ	=	**N**ational **I**nstitute of **J**ustice
p1ge	=	**P**lain 2.5*2.5 E-**g**lass **e**poxy **c**omposite
p1gp	=	**P**lain 2.5*2.5 E-**g**lass **p**olyester **c**omposite
p2gp	=	**P**lain 12.5*12.5 E-**g**lass **p**olyester **c**omposite
P-55	=	Carbon high modulus
PAN	=	**P**oly**a**crylo**n**itrile
pcp	=	**P**lain **c**arbon **p**olyester **c**omposite
rangp	=	**Ran**dom E-**g**lass **p**olyester **c**omposite

List of Tables

List of Figures

Chapter One

General Introduction

1.1General:

Composite materials are widely used in the aerospace, marine, automobile industries and military armored systems etc. This class of materials exhibits many superior properties including high specific strength and stiffness, good formability, and corrosion resistance [1]. Among the most preferment is the laminated fiber composite, which some of them passes in the higher specific moduli, such as Kevlar and carbon fiber composites. The specific strength and stiffness are significantly greater than monolithic materials such as steel and aluminum, which make them attractive for numerous weight critical applications [2].

Impact events can be categorized into four-velocity ranges; low, high, ballistic, and hyper velocity. Low velocity impact may include situations such as dropped tool (<30 m/s) where as high velocity impact might include a bird colliding with an airplane (30-250 m/s). Ballistic impact events include situations such as a projectile fired from a gun at speed in excess of 250 m/s. Finally, orbital traveling in outer- space at velocities up to 20,000 m/s are considered hypervelocity impact events. The low, high and ballistic impact events are the focus of this work. There is a growing need in the military and civil applications for composite materials [3].

1.2 Composite Materials

Mankind has been aware of composite material since several hundred years before Christ applied innovations to improve the quality of life. Although it is not clear as to how man understood the fact that mud bricks made sturdier houses if lined with straw, he used them to make buildings that lasted. Ancient pharaohs made their slaves, used bricks with straw to enhance the structural integrity of their buildings, some of which testifies to the wisdom of the dead civilization even today.

Contemporary composites resulting from research and innovation from the past few decades have progressed from glass fiber for automobile bodies to particulate composites for aerospace and a range of their applications.

Fibers or particles embedded in the matrix of another material would be the best example of modern composite materials, which are mostly structural. Laminates are composites materials where different layers of materials give them the specific characteristics of composite materials having a specific function to perform. Fabrics have no matrix to fall back on, but in them a specific character. Reinforcing material generally withstand maximum load and serve the desirable properties [4].

In matrix based structure composites, the matrix serve two paramount purposes via binding the reinforcement phase in place and deforming to distribute the stress among the constituent reinforcement materials under the applied force. Figures 1-1 and 1-2 show some kinds of fibers and matrices respectively.

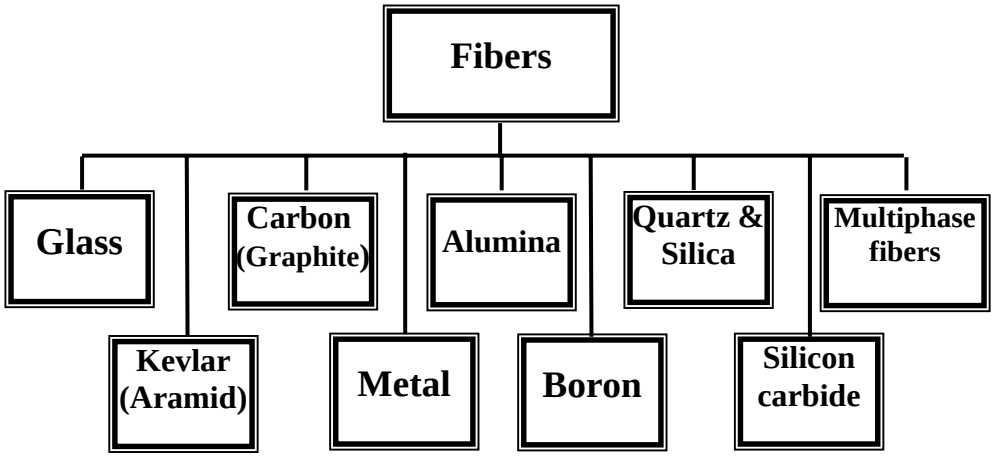

Figure 1-1 Some Kinds of Fibers [5].

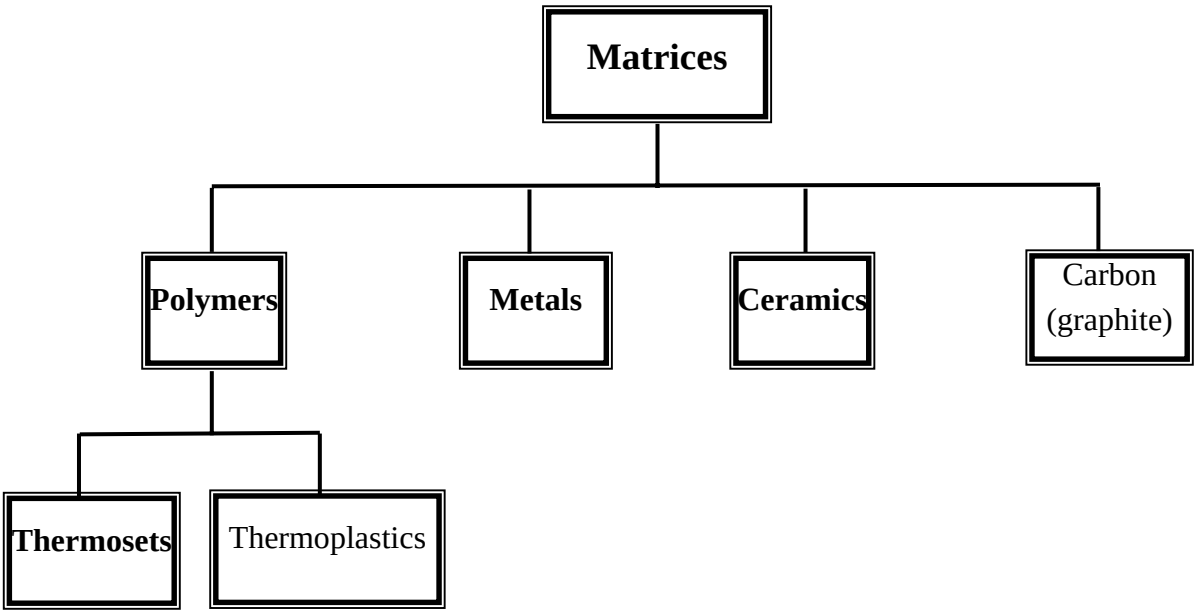

Figure 1-2 Some Kinds of Matrices [5].

The plots of the specific tensile strength (strength/density) versus specific modulus (modulus/density) for various fiber-reinforced composite are shown in Fig. 1-3.

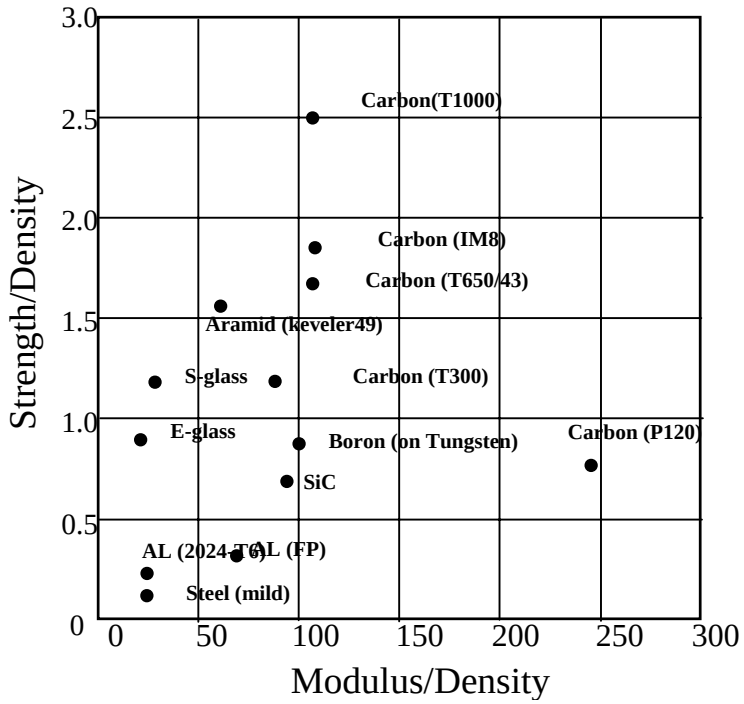

Figure 1-3 The specific tensile strength versus specific modulus for various fiber-reinforced composite (65% V_F) with epoxy matrix and for Steel and Aluminum [2].

The fiber feature and geometry is important for the behavior of the composite laminate. The geometrical classification can be shown in Fig. (1.4)

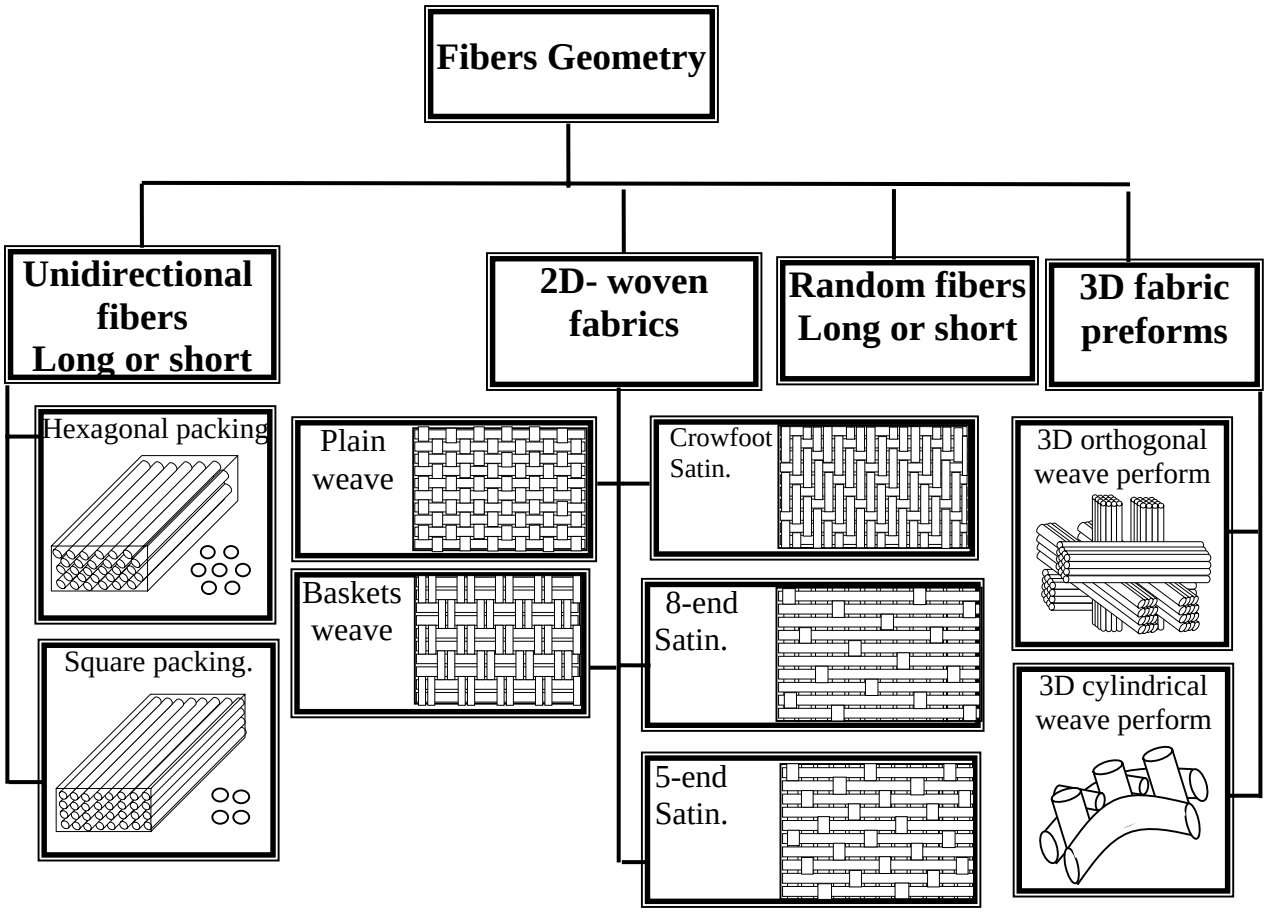

Figure. 1-4 Some kinds of fibers geometry [2,5].

1.2.1 Woven Fibrous Composites

Woven fiber reinforced plastics are becoming increasingly important as they have the following advantages over laminates made from individual layers of unidirectional materials:

- Improving formability and drape
- Bi-directional reinforcement in a single layer
- Improving impact resistance
- Balanced properties in the fabric plane

The woven composite is formed by interlacing two sets of threads, the warp and the weft, in a wide variety of weaves and balances.

Fibers can be woven into many different types of weave pattern, widths, and thicknesses. The warp yarns, or ends, lie in the lengthwise (machine) direction of fabric, whereas the filling yarns, or picks, lie crosswise, at right angles to warp yarn. Fabric construction is specified by the number of warp yarns per centimeter of fabric width and the number of filling yarn per centimeter in the lengthwise direction. Therefore fabric weight, thickness, and breaking strength are proportional to the number and types of warp and filling yarn used in the weaving.

Variety of weave patterns can be used to interlace the warp and filling yarns to form a stable fabric {see Fig. 1-4}. The weave pattern controls the handling characteristics of a fabric and, to some degree, the properties of a product that uses it as reinforcement. Some applications require that all fabric construction variables be specifically designed so that the desired performance criteria can be met.

The plain weave, which interlaces one warp yarn over and under one filling yarn, demonstrates the greatest degree of stability with respect to yarn slippage and fabric distortion; yarn count and content, however, also contribute to fabric stability.

The basket weave has two or more warp yarn that interlace over and fewer than two or more filling yarns. Although the basket weave is less stable than the plain weave, it is more pliable and will conform more to simple contours.

A crowfoot satin weave has one warp yarn interlacing over three and under one filling yarn in an irregular pattern, resulting in a pliable fabric capable of conforming to complex or compound contours[6].

The 8-end satin weave has one warp yarn interlacing over seven and less than one filing yarn in an irregular pattern, which yields a pliable fabric that will readily conform to compound contours. Since this weave pattern allows a comparatively high yarn count per centimeter and fewer fiber distortion, it translates better strength properties in all directions than a tighter weave, such as the plain weave. A variation of the 8-end satin weave is the 5-end satin weave.

Generally, the longer the float, which is the portion of a warp or filling yarn that extends unbound over two or more yarn lying 90^{o} to it, the higher the composite strength extended the length of the float, which reduces the interlacing frequency,

increasing the composite strength for all kinds of fibrous reinforcements. The transition from the plain a weave to a crowfoot weave also results in improving the composite mechanical properties [7].

1.3 Impact Problems

1.3.1 Definition

Impact resistance is the ability of a material to absorb and dissipate energies under impact or shock loading. The response to impact loads ranges from localized damage to total disintegration. Even local damage can be serious since it can lead to delamination and other effects. During impact loading fracture modes may be significantly different than static tensile failure. This is particularly true for strain rate sensitive materials [8].

1.3.2 Impact Measurement Techniques

Impact testing is normally performed with a swinging or a dropping weight. The object of these tests is to measure the amount of energy transferred or "lost" from the striking body. For bodies without flaws or notches, the transferred energy consists of energy to initiate crack and energy to propagate a crack. The two common swinging weight impact test methods are the Charpy and Izod methods shown in Fig. 1-5. In these methods a notched bar is impacted by a striker-pendulum released from a standard height. The height of the pendulum swing past the impact is a measure of the amount of energy absorbed by the impact. The shorter the after-swing the greater the energy absorbed by the specimen and hence the greater impact resistance or toughness.

The absorbed energy is expressed per unit cross section of specimen. Typical results of Charpy and Izod impact tests on unidirectional composites and common structural alloys are given in Table 1-1. Among the composites, impact resistance is strongly influenced by the ductility or strain to fracture of the fiber. This can be seen

in Table 1-1 where the S-glass composite has very high impact resistance, while high modulus carbon fiber composites have low impact resistance.

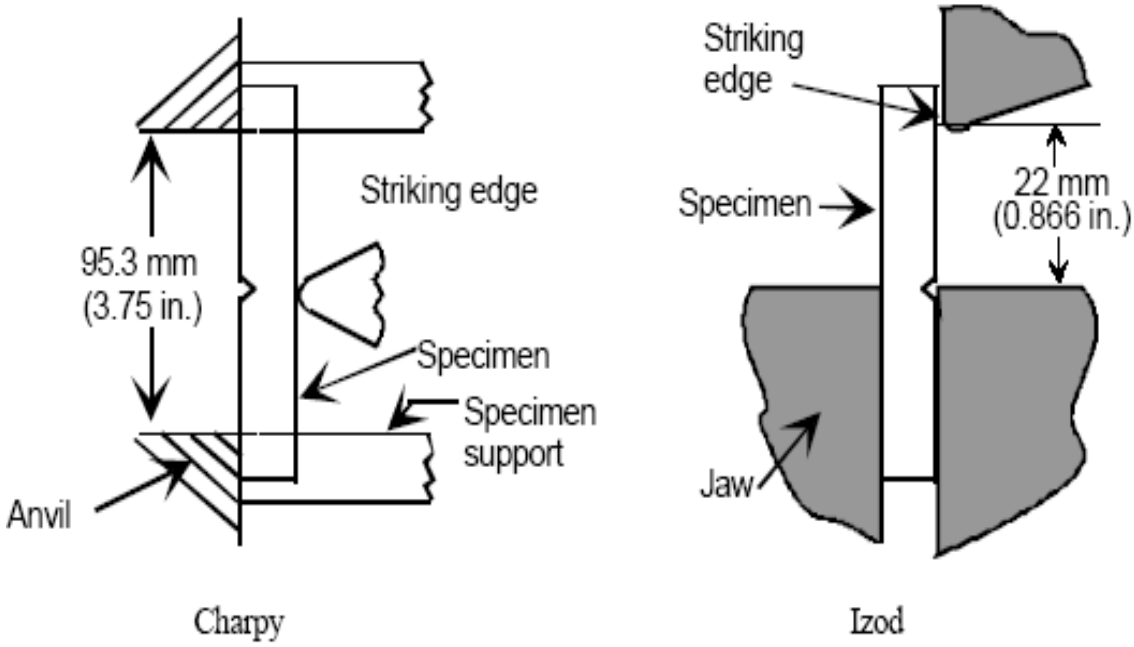

Figure 1-5 Swinging weight impact-testing methods[3]

In recent years the drop-weight method has become the preferred technique for impact testing of composites because a greater range of testing parameters is possible and the results are more readily analyzed. A typical drop-weight testing apparatus is shown in Fig. 1-6. In the drop-weight test the energy absorbed by structure prior to failure resulting from high strain rate or impact load. Drop-weight test stands are equipped with load measuring devices (usually load cells) either in the specimen supporting platforms as shown in Fig. 1-6 or in the top. Photoelectric cells are used to time the top velocity just prior impact. High-speed cameras can also be used to record the impact events and the propagation mode. A typical load-time curve recorded by these devices is illustrated in Fig. 1-7. The initial rise in the load-time curves corresponds to the fracture initiation phase. In some cases a local peak is recorded due to matrix cracking. The maximum load corresponds to fiber

fracture. The portion of the trace beyond the maximum corresponds to the propagation phase.

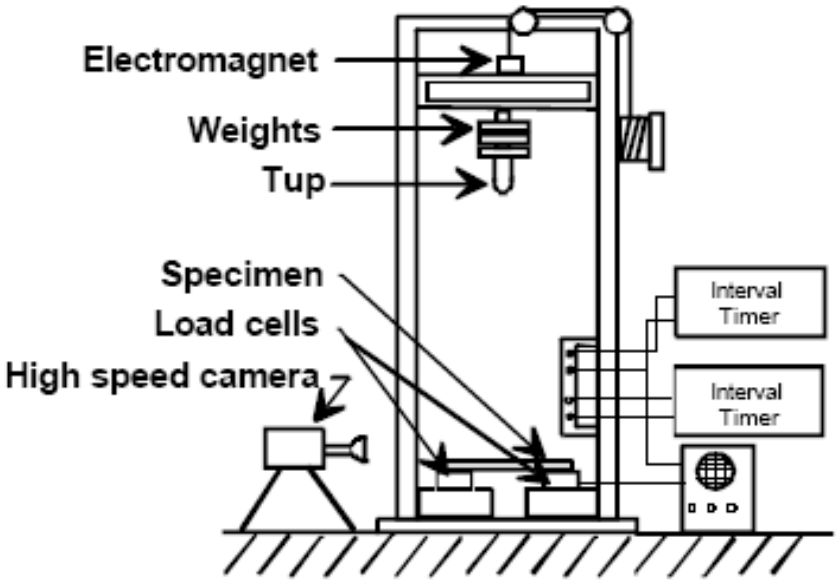

Figure 1-6 Drop-weight impact measuring apparatus [3]

Table 1.1 V-Notched Charpy and Izod impact of unidirectional composites [3]

Material	Impact energy J/m^2	
	Charpy	Izod
S-glass/epoxy V_F= 55%	5078	-
B/Epoxy	816-1313	-
Kevlar/epoxy	2189	1094
AS Carbon/epoxy	701	219
HMS Carbon/Epoxy	161	58
T300 Carbon/epoxy	919	438
4340 Steel	1459	-
6061-T6 Aluminum Alloy	1022	-
7075-T6 Aluminum Alloy	438	-

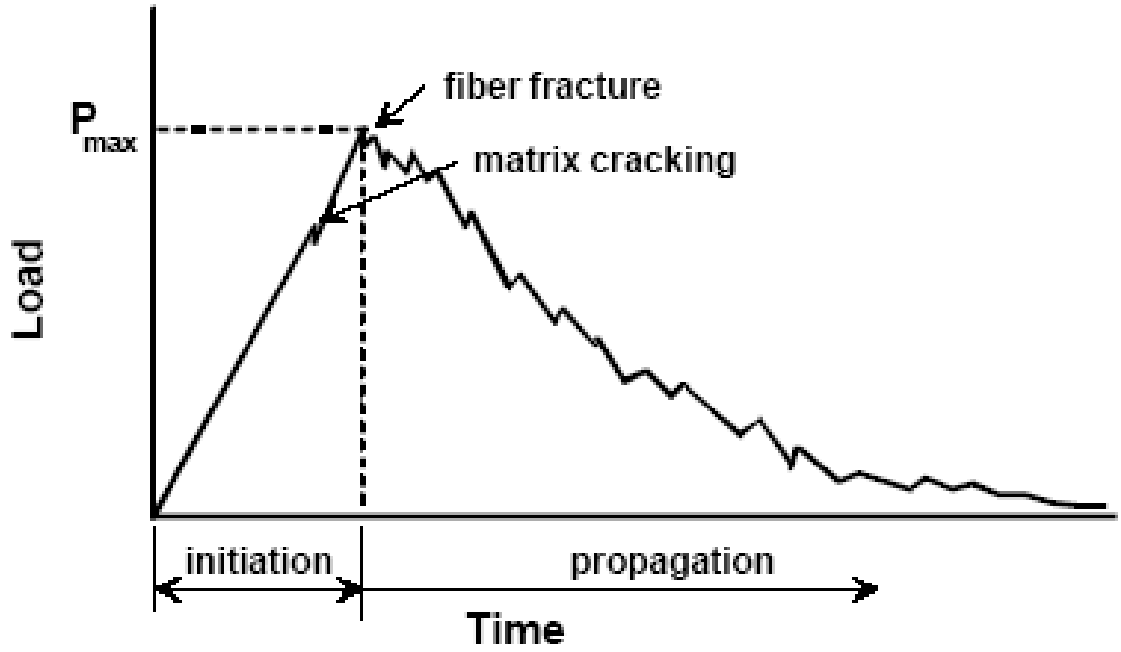

Figure 1-7 Typical load-time trace for drop-weight impact test on composites [3]

In order to achieve speed above 30m/s, a projectile is propelled through a device (gun) having a cylinder (barrel) slightly longer than its diameter. A compressed gas or a burning powder has been used as propellants as shown in Fig. 1-8.

Projectiles fired from a gas gun are accomplished by pressurizing a chamber containing a plastic diaphragm restricting gas flow (usually nitrogen) into the barrel. When a predetermined pressure is reached, the diaphragm is burst by electrical heating and the projectile is accelerated. Gas guns are generally used for high velocity testing at typical speeds ranging from 30m/s to 250m/s. however, velocity as high as 600m/s have been achieved with more sophisticated systems [3].

Ballistic velocities of 300m/s or more is usually accomplished through the use of a burning powder gun [9]. The projectile is propelled using a powder that is explosive upon ignition. Velocity is controlled using a pre-determined amount of charge. Extreme velocity as high as 3000m/s can be obtained [10].

There are a lot of applications dealing with the impact on composite materials because the phenomena of impact are occurring in these applications with directions to use the composite materials. Fig. 1-9 shows some of these applications.

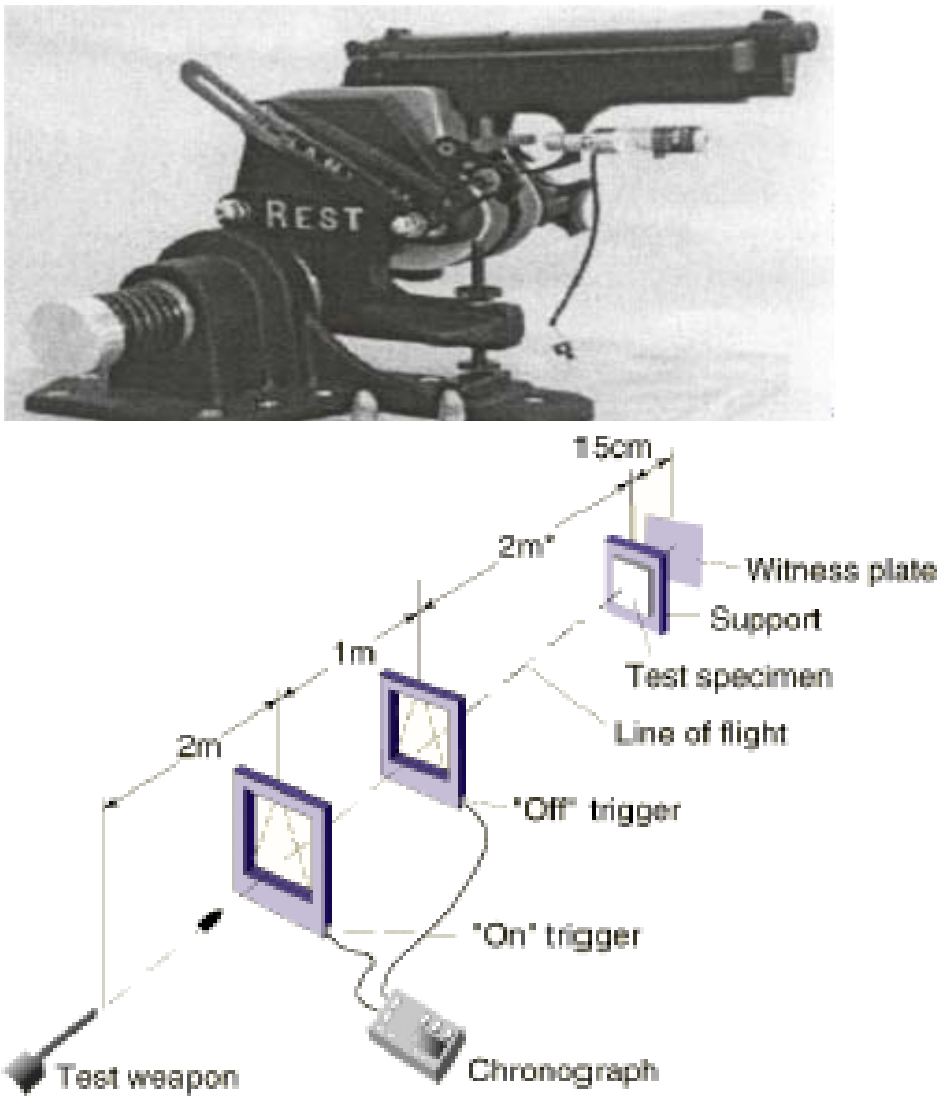

Figure (1.8) A 9mm Beretta handgun mounted in a Ransom Rest with laser for accuracy [3].

Military applications (maryu@arl.army.mil)

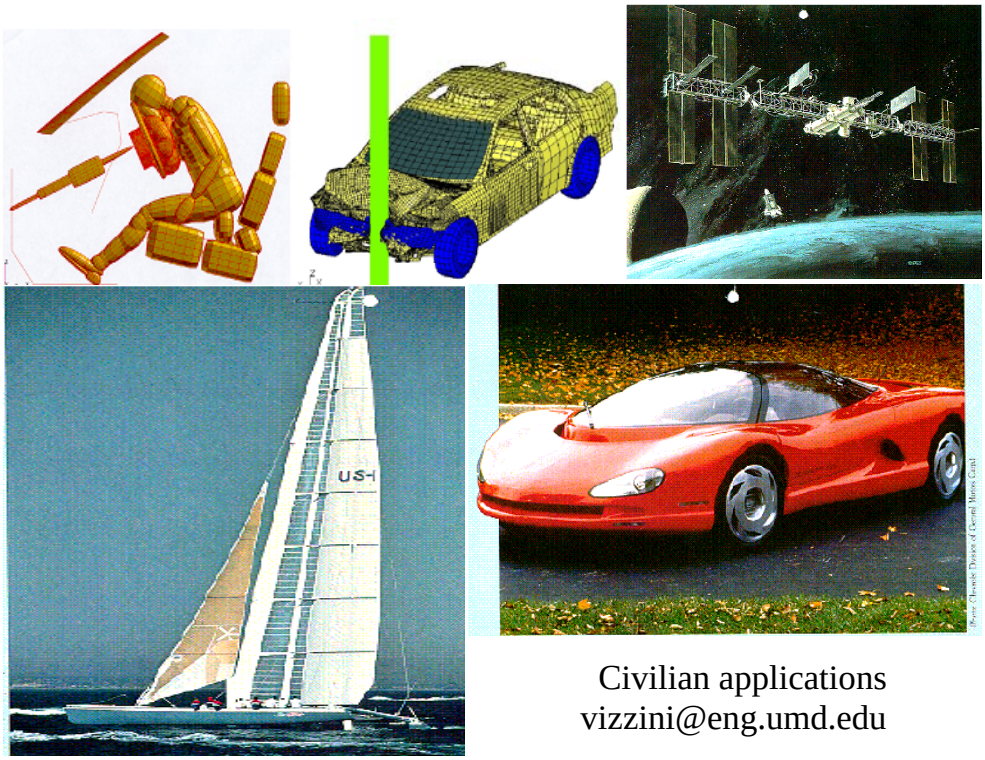

Civilian applications
vizzini@eng.umd.edu

Figure 1-9 Some applications of the impact on composite materials.

1.4 Layout of the Thesis

This thesis is organized into five chapters. Chapter 2 mainly provides a literature review of impact on composite materials. The review was based on the velocity range of the impact into two main ranges, which is the low velocity range of impact, and the high and ballistic ranges of impact velocity. The methods used by the authors are listed as well as the effect of different parameters on the impact through the earlier works. The results of this work are discussed reaching to the way that the presented work can be run on it, and then the aim of the work was listed in the end of the chapter.

Chapter 3 deals with the theoretical modeling of the presented work. The simulation of the impact energy absorbed due to penetration of rigid projectile on laminate composite materials is derived. Different divisions of absorbed energies are considered based on the earlier knowledge for the deformation and fracture that occur in the composite targets. Through the model developed, the analytical and numerical tools are used with some new derivations to simulate the impact with all steps.

Chapter 4 aims at the experimental tests. Three types of fiber materials and two types of matrix materials are used. In addition of different types of raw materials, different types of fiber weaves are used to study the effects of the weave types and the arrangements of laminates. The composite materials are fabricated to make the specimens used for measuring the mechanical properties and for the impact tests. Standard tests are used to measure the mechanical properties of the matrices and the composite specimens. The ballistic impact tester is designed with an assembled new computerized velocity measuring device and the perforation time. Sets of impact tests are carried out to check the theoretical model and study the parameters, which unable to analyze them in the model.

The results of the models developed in chapter 3 and the tests detailed in chapter 4 are shown in chapter 5. The variation of the parameters studied analytically and experimentally are studied and discussed and compared with the earlier published works.

Chapter 6 summarizes the work, conclusions and suggestions for future work.

Chapter Two

Literature Survey

2.1 Introduction

Understanding the behavior of materials under very high strain rate loading conditions is vital to many areas of civilian applications ranging from explosive forming, welding, cutting, compaction, and hardening, to oil well exploration and micrometeorite impact on space stations; military applications are also numerous and range from armor and anti-armor structures/vehicles to ballistic designs. There are many other additional applications of high strain-rate deformation, such as machining, accidental impact of vehicles and crashworthiness studies, earthquakes and the associated damage to structures, and explosive devices. All these applications require a thorough knowledge of the mechanics of high strain rate deformation, and the dynamic response of materials under those conditions. A number of material systems ranging from metals, ceramics, polymers in both monolithic and composite forms are being used to achieve a combination of properties specific to each of those applications. However one well-known problem of the fiber composite materials is their susceptibility to damage, which may lead to premature structural failure under either low or high velocity impact.

Impact mechanics on composite target is influenced by many factors including (i) projectile (shape, mass, stiffness and velocity after impact). (ii) Target (ply mudulli, stacking sequence, ply orientation, conventional strength and fracture toughness), (iii) behaviors of fiber/matrix interface and (v) damage behavior (damage threshold, damage strain relation), etc [1].

There is a great need to analyze, understand and quantitatively characterize complex impact mechanisms and damage failure process of composite laminated structure under projectile impact.

2.2 Low velocity impact

To analyze the impact response problems, it is obvious that an accurate account of the contact behavior is one of the most important steps. The classical contact law between elastic spheres and an elastic half-space derived by Hertz [11] has been used by many authors for studying impact response of homogenous isotropic materials [12]. In studying impact response of laminated composites, however the problem becomes more complicated [13].

One may easily realize that Hertzian contact law, which was based on assuming a homogenous isotropic materials, may not be adequate in describing the contact behavior on laminated composite due to their anisotropic and non-homogenous properties. Moreover, most of the limited composites used are quite thin and cannot be represented by half-space in the existing analytical work [13,15], leading of limits were assumed known, and the responses of the laminates assumed elastic.

Tan and Sun [14] and Guan and Yang [15] gave the development history of the contact problem through the low velocity impact. These models with their developments were used by authors to evaluate the response and compared it with experimental results.

Theoretically and experimentally the impact force is increased with time as well as indentation [14] until it reaches the limits to absorb the kinetic energy of the projectile, then there will be a springback and the force will decrease [14-20]. The drop weight type of impact test was used, the projectile shapes were heavy spheres compared to the target mass [15-17]. Free falling was made to get the known amount of kinetic energy, or using long bullet-like steel mass, which had a spherical head and attached to thin rod to form a pendulum [18]. When composite beams are used as a target, horizontal cylinders were used as a falling impactor [17-21].

The shapes studied earlier were rectangular plates [12-15], circular plates [16] and beams [17-21] with different boundary conditions.

The damage processes of composite laminates due to impact were studied theoretically [12,15,17,21] and experimentally [12,19-28]. The damage modes were delamination, matrix cracking and plastic indentation. The authors showed that the damage area for low velocity impact is increased as the impact energies increase, and through the impact duration the stiffness will decrease.

Different types of composite materials were studied through the history of studying low velocity impact on composite materials. One of them is whisker-reinforced aluminal silicon carbide ceramic composite [19], which showed that the local contact tensile stress did not reach critical values that would initiate fracture around the contact area, and all fractures were caused by dynamic flexural stresses, but this type of composite materials showed that it has lowest Young modulus. Other available published works on the impact on the ceramics or Foam/ ceramics composite were presented by Lee et.al [21], Craft et.al [22] and Markaki et.al [23,24]. They established that higher impact force are developed at a given drop weight in panels made of stiffer cores.

The other interesting results were the energy for dynamic penetration of laminates which was similar to that in the static case for different boundary conditions and the energy observed for simply supported condition was considerably lower than that for clamped end condition, also the impact at higher yield a highly localized damage [29]. For this similarity between the static indentation and the low velocity impact was used to study the indentation of sandwich beam with functional graded core by Apetre et.al [30]. The assumptions of the exponential variation of Young's modulus with keeping Poisson's ratio constant were used for the core. Results indicate that the contact stiffness of the core increases causing the contact stresses to increases. However values of maximum strain are reduced considerably due to grading of the core properties.

The composite targets, which are the fiber-reinforced matrix composites, were studied for unidirectional fibers reinforced composite [12,14,15,20,29]. The

experimental results of impacting graphite-epoxy composite followed the 1.5 power for Hartzian contact law very well. A linear relation was found between the permanent indentation and the maximum indentation at unloading independent of the size of indenters [14].

Guan et.al [15] developed the contact law by reducing the contact stiffness in their finite element solution due to damage and their results approaches more closely the experimental results, the delamination for their model was caused the reducing in the stiffness of the composite plate as well as the matrix cracking which was treated from experimental static indentation test of the plate.

Cairnes et.al [16] treated the thick circular laminated composite plate, subjected to lateral loading statically and with low velocity impact. Their analytical analysis agrees well with test data with the limitation of the analytical methods compared with numerical techniques, which was used by Levent [17].

Choi and Hong [18] used finite element method also for their analysis with modified Hertzian contact law to evaluate the impact load history, deflection, dynamic strain and compared favorable with the experimental tests. They considered the higher order shear deformation and large deflection effects.

Kiesling et.al [20] embedded a super elastic nitnol to the graphite epoxy composite and their test results showed that the nitnol additives give an increase to the absorbed energy of about one third more than composite plate without additives and increasing delamination area.

Ubels et.al [26] studied the impact damage of stiffened composite plate experimentally and showed that with increasing impact load the transferred shear and delaminated sublaminates became the ultimate failure mechanism.

Other studies treated different side cases as the impact on the composite tubes [31], influence of injection and holding pressure, molding temperature and fiber bundle size on resin transfer molding due to compression strength after impact [27], and the water used as damper to absorb the kinetic energy due to impact [28].

The numerical methods for solving three dimensional impact problems were not available packages with especial computer specifications [32]. Circular disk of

carbon epoxy laminate under low velocity impact damage was numerically studied by Moura et.al [33] using interface 3-D finite elements to simulate onset and growth of the bending crack and delamination.

2.3 High velocity impact

Although some of the high and ballistic velocity impact damage mechanics are similar to those at low velocity, the response of a structure composite is different and more complex. Furthermore, it is also more difficult to test at high and ballistic velocities.

Since the contact time between the projectile and the composite is considerably less at ballistic velocities, the impact loading induced localized response with no global deformation. This concept was demonstrated by looking at delamination in beams of various lengths impacted at low and high velocities [34,35]. It was found that the damage size decreases with increasing the length of beam for low velocity impact. At high velocity, however, the level of damage was independent of the length of beam.

Since the high velocity impact energy is dissipated over a smaller region, an additional damage mechanism is presented at high velocities known as the shear plug. Due to the stresses created at the point of impact, the material around the perimeter of the projectile is sheared and pushed foreword causing a hole or “plug”, slightly larger than the diameter of the projectile [34].

The fiber properties have the major effect for absorbing energy due to high velocity impact, the experimental results indicated that the rate of energy absorption of the panel increases drastically with the fiber modulus, but the very high modulus material tends to exhibit poor impact resistance due to its low working strain. Aramid fiber seems to exhibit the best combination of high modulus while steel maintaining reasonable high breaking strain [36]. While the absorbed energy was found to be a linear relation with the thickness of the composite laminate insuring that the weight efficiency of the fiber composite is greater than the metallic target

like steel [37]. For this important effect of the fiber mechanical properties, and the fabrication of hybrid composites from multi types of layered fibers was used [37]. The technique of interlaminate hybridization was found to enhance delamination under impact loading. Delamination was found to be an effective energy absorbing in hybrids. The impact energy absorption capability depends on which side face the impact direction. In general, the unsymmetric hybrids have better impact properties than their alternating sequence counterparts. In most cases, failure in these materials involved perforation, delamination and some tearing of the more brittle layers in conjunction with deflection of the tougher layers, provided the tougher side faced the impact direction. When the more rigid side was struck first, this stiff layer was perforated with a lesser degree of plastic deformation.

There were works on the hypervelocity impact reaching to 10km/s [10,38]. The perforation hole size increases as the projectile mass increases but was not proportional to the projectile size. The results show that the hole size decreases and the gauge pressure increases as projectile velocity increases.

The other important parameter affecting the high velocity impact is the projectile masses; Cantwell and Morton [39] studied this effect experimentally for low and high velocity impact. They found that varying the mass of the impinging projectile has a significant effect on the initiation and development of damage in composite structure.

When the kinetic energy of impactor is greater than ballistic range, the perforation takes place. Now the ballistic limit of velocity will be the additional parameters added to the parameters study in the high velocity impact. Ballistic velocity is the impact velocity that gives the ability for full penetration without remaining energy. The energy required achieving target perforation and ballistic limit remaining invariant of specimen geometry [40,41]. To avoid the perforation especially for the designing of personal body armor, aramid or spectra fiber composite was used, for this application the repeated impact was used to know the striking velocity [40]. The ballistic limit was increased with Areal density [42,43] and

the striking velocity decreased with the number of repeated impact, while the delamination zone was increasesd.

Different composite modes were used in the perforation studies which included ceramic spheres embedded by matrix [43], multi-layered metallic plates [44], pure cloth specimen [45], and woven fiber composites [46]. The fracture cone occurred for the ceramic composites while cone radius varied according to the sphere radius and energy dissipation was through the breaking up of the ceramic spheres and failure of the backing composite by shearing, fiber cutting and extensive delamination [43].

Kasano and Abe [44] derived a new analytical model for production of the perforation characteristics of unbounded multi-layered composite plates based on the conservation of momentum. Their model was based on the plugging the target through the impact, the plugs will fly in velocities less than the resting velocity of the projectile but values depend on their masses (thickness of the plug's layer). The model gave good agreements with the tests of impact perforation of multilayered aluminum targets.

For the perforation of PE fabric, the two kinds of perforation modes, that is, cutting of yarns and pullout of yarns are observed depending on the textile structure[45]. While for woven fiber composite, the ballistic impact was increased with increasing the thickness of the laminate, further the satin wave laminates exhibited higher ballistic limit than the plain weave [46].

The additions of the higher modulus additives to the composite were studied. These additions were in the cases of cord Kevlar thread by stitching machine [46], tensioned Kevlar over wind [47] or added layers of super elastic nitnol[34,35]. Small amount of these additives gave large percentage of the absorbed energy and increased the impact resistance.

The study of the woven fabric reinforced composites gave the important issues through the few recent years because the high developments of the roving techniques and the good mechanical properties of the woven fiber in the addition to the easier fabrications for these types of composites and their structures [48]. The

target may be a two-dimensional weave [45-52], and the three-dimensional weave[53,54]. The behavior for the weave was assumed to be isotropic [49,50], and in the other as an orthotropic [51]. The tests were showed that the woven composites must be assumed orthotropic to give the closer agreement to the tests [52]. It was found that the delamination area-taking place through the impact had a circular shape, while it has an elliptical shape in unidirectional fiber composite. Other parameters were found to be effective on the ballistic response in the addition of the area of delamination, which are the isotropy of the ballistic response; determine measuring the Feret Ratio or the Circular Shape Factor. Feret Ratio is the ratio of the minor to major Feret diameter, which is a basic measurement of region elongation. The Feret Ratio approaches one for an isotropic region or fine plain weave composite and goes to 0 for strongly elongated one (for unidirectional composite, which has, very high ratio of longitudinal to lateral modulus). The circular shape factor is a measurement of the circle based on the region area and perimeter. It is one for perfect circle and as the perimeter grows faster than the area for any other shape, it goes to 0 as the region get less circular [52].

The major damage modes of impacted 3-dimensional woven composite were found to be indentation, matrix failure and fiber breakage with axial and braider fiber yarn pullout, while the delamination does not occur [53,54].

There is a large amount of works dealing with the impact applications on composite structure, as an example; impacting a model section of aircraft structure [55,56], Personal body armors [57-61], concrete and building structure [62], and the impact on the thorax [63]…etc.

2.4 Concluding Remarks

From the literature review the following remarks can be stated:

1.There is no analytical model was found of treating the mechanical properties and stiffness matrices of laminated woven fibers composites.

2. There is no analytical solution was found of high velocity impact on layered fiber composite with including the different types of absorbing energies.
3. For the working of hybrid composite materials there are no conclusions about improving the mechanical and impact properties using hybrid arrangements of the composite layers.

2.5 Objectives and Approaches

The overall goal of this work is to understand the high velocity impact response of fiber composite materials and the energy absorbed due to impact for different fibers and matrices, and with different weave patron and hybrid arrangements.

The study focuses on the types of energy absorbed and conservation. The approach is to develop an analytical and computational methods to characterize the plate impact response, and then compare with available experimental data. For the same reasons the experimental work deals with the fabrication of the composite materials specimens, testing to evaluate the mechanical properties and design and building the impact rig and test the specimens under the high velocity impact.

Specific objectives of the present research are as follows.

- Developing an analytical solution to the plate impact problem of layered orthotropic system in elastic delamination, and penetration regimes. The energy conservation equation is used in this analysis; Conducting numerical simulation and analysis in order to study types of energy absorptions through the composite.

- Studying different types of fibers such as E-glass, Carbon and Kevlar with different weave patrons, and different matrices such as polyester and epoxy. Testing these materials in order to measure the mechanical properties of these raw materials.

- Designing and fabricating composite plate specimens for different fibers and matrices in hybrid arrangements and test specimens to obtain the mechanical properties

- Measuring the overall mechanical properties that may be used in the present model for the composite materials fabricated.

- Designing and building an impact rig using special powder gun manufactured for this purpose, with new computerized measuring device for penetration time and velocity measurements.

- Executing the impact tests for the fabricated specimens with different impact velocities and impactor shapes, and studying the hybrid arrangement for the composite and their effect on the impact resistance. The effects of fiber weave patrons and the mesh size on the impact mechanics of the composites will also be studied.

Chapter Three

Theoretical Analysis

3.1 Introduction

The analytical solution for impact on composite material target made of laminated oriented unidirectional and woven fibers based on matrix is presented. Therefore the analysis of material properties for unidirectional laminates is used to develop material properties of woven fiber composite. Types of observed energies due to impact are developed and evaluated.

3.2 Elastic properties of lamina

A lamina or laminated plate consists of several laminas each with a fiber oriented at a particular angle. This is generally made of stacking several thin layers of fibers at the desired locations and angles in a matrix and consolidating them to give the required thickness. The fiber orientation in each thin layer can be arranged in a specific manner so as to achieve the required properties of the structural member [64].

The elastic properties of fiber composites are functions of the elastic properties of fiber and matrix and of their relative volumes in the composites material.

3.2.1Unidirectional lamina

Analysis of the composite cylinder assemblage (CCA)[2] gives closed form results for the effective properties E_{11}, ν_{12} and G_{12} and closed bounds for properties E_{22} and ν_{21} and for the assumptions of transfers of isotropic fibers and isotropic matrix, as

$$E_{11} = E_m V_m + E_f V_f \quad \ldots(3.1)$$

$$\nu_{12} = \nu_m V_m + \nu_f V_f \quad \ldots(3.2)$$

$$G_{12} = G_m \left(\frac{V_f}{1/(G_f - G_m) + V_m / 2G_m} \right) \quad \ldots(3.3)$$

$$E_{22} = \frac{E_m E_f}{E_m V_f + E_f V_m} \quad \ldots(3.4)$$

$$\nu_{21} = \frac{E_{11}}{E_{22}} \nu_{12} \quad \ldots(3.5)$$

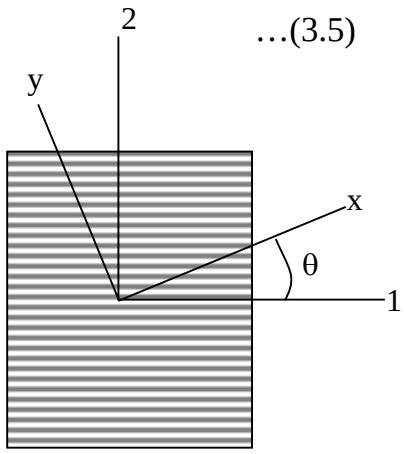

For angle ply lamina [64]

$$E_{xx} = \left[\frac{m^4}{E_{11}} + \left(\frac{1}{G_{12}} - \frac{2\nu_{12}}{E_{11}} \right) m^2 n^2 + \frac{n^4}{E_{22}} \right]^{-1}$$

$$E_{yy} = \left[\frac{n^4}{E_{11}} + \left(\frac{1}{G_{12}} - \frac{2\nu_{12}}{E_{11}} \right) m^2 n^2 + \frac{m^4}{E_{22}} \right]^{-1}$$

$$G_{xy} = \left[\frac{1}{G_{12}} + 4 \left(\frac{1 + 2\nu_{12}}{E_{11}} + \frac{1}{E_{22}} - \frac{1}{G_{12}} \right) m^2 n^2 \right]^{-1} \quad \ldots(3.6)$$

$$\nu_{xy} = E_{xx} \left[\frac{\nu_{12}}{E_{11}} - \left(\frac{1 + 2\nu_{12}}{E_{11}} + \frac{1}{E_{22}} - \frac{1}{G_{12}} \right) m^2 n^2 \right]$$

$$\nu_{yx} = \frac{E_{yy}}{E_{xx}} \nu_{xy}$$

3.2.2 Random oriented discontinuous fiber composite

For the same fiber aspect ratio and same volume fraction of that to determine the prosperities of unidirectional fiber composite the isotropic properties of the random oriented discontinuous fiber composite are given by[64]

$$E = \frac{3E_{11} + 5E_{22}}{8}$$
$$G = \frac{E_{11} + 2E_{22}}{8} \qquad \ldots(3.7)$$

3.2.3 Woven fibers composite lamina

There is no mathematical modeling for the mechanical properties of woven fiber reinforced composite, and because it is important for the present work then an approximate one was derived here using the approximation that the woven fibers are constructed from two orthotropic unidirectional fiber plies with the effect of bent yarn through the weave.

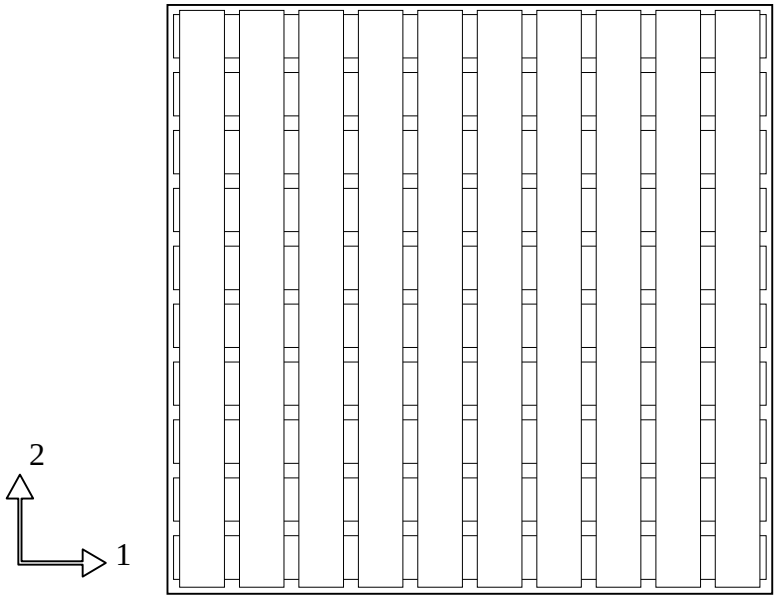

Figure 3-1 The composite plate of two orthotropic unidirectional fibers is considered as an infinite-end satin woven fibers composite.

Using the lamina stress-strain relations then for this laminate for the present plate of two orthotropic layers

$$A_{ij} = \sum_{k=1}^{N} (Q_{ij})(z_k - z_{k-1})$$

then

$$[A] = h\begin{bmatrix} \dfrac{Q_{11}+Q_{22}}{2} & Q_{12} & 0 \\ Q_{12} & \dfrac{Q_{11}+Q_{22}}{2} & 0 \\ 0 & 0 & Q_{66} \end{bmatrix}$$

$$[a] = [A]^{-1} = \frac{1}{h}\begin{bmatrix} \left(\dfrac{2(Q_{11}+Q_{22})}{\{(Q_{11}+Q_{22})^2 - 4Q_{12}^2\}}\right) & \dfrac{-4Q_{12}}{\{(Q_{11}+Q_{22})^2 - 4Q_{12}^2\}} & 0 \\ \dfrac{-4Q_{12}}{\{(Q_{11}+Q_{22})^2 - 4Q_{12}^2\}} & \dfrac{2(Q_{11}+Q_{22})}{\{(Q_{11}+Q_{22})^2 - 4Q_{12}^2\}} & 0 \\ 0 & 0 & \dfrac{1}{Q_{66}} \end{bmatrix} \quad \ldots(3.8)$$

For unidirectional fiber composite

$$Q_{11} = \frac{E_{11}}{1-\nu_{12}\nu_{21}},\ Q_{22} = \frac{E_{22}}{1-\nu_{12}\nu_{21}},\ Q_{12} = \frac{\nu_{21}E_{11}}{1-\nu_{12}\nu_{21}}\ \&\ \ Q_{66} = G_{12} \quad \ldots(3.9)$$

then

$$a_{11} = a_{22} = \frac{2(Q_{11}+Q_{22})}{h\{(Q_{11}+Q_{22})^2 - 4Q_{12}^2\}}$$

$$= \frac{2(E_{11}+E_{22})(1-\nu_{12}\nu_{21})}{h\{(E_{11}+E_{22})^2 - 4\nu_{21}^2 E_{11}\}} = \frac{2(1-\nu_{12}\nu_{21})\left(1+\dfrac{\nu_{12}}{\nu_{21}}\right)}{hE_{11}\left\{\left(1+\dfrac{\nu_{12}}{\nu_{21}}\right)^2 - 4{\nu_{21}}^2\right\}}$$

$$a_{12} = a_{21} = \frac{-4Q_{12}}{h\left\{(Q_{11}+Q_{22})^2 - 4Q_{12}^2\right\}}$$
$$= \frac{-4\nu_{21}E_{11}(1-\nu_{12}\nu_{21})}{h\left\{(E_{11}+E_{22})^2 - 4\nu_{21}^2 E_{11}\right\}} = \frac{-4(1-\nu_{12}\nu_{21})\nu_{21}}{hE_{11}\left\{\left(1+\frac{\nu_{12}}{\nu_{21}}\right)^2 - 4{\nu_{21}}^2\right\}} \quad \ldots(3.10)$$
$$a_{66} = \frac{(Q_{11}+Q_{22})^2 - 4Q_{12}^2}{hQ_{66}\left\{(Q_{11}+Q_{22})^2 - 4Q_{12}^2\right\}} = \frac{1}{hG_{12}}$$

Then an infinite-end satin woven fibers composite properties are

$$(E_1)_\infty = (E_2)_\infty = \frac{1}{ha_{11}} = \frac{\left\{\left(1+\frac{\nu_{21}}{\nu_{12}}\right)^2 - 4{\nu_{21}}^2\right\}}{2(1-\nu_{12}\nu_{12})\left(1+\frac{\nu_{21}}{\nu_{12}}\right)} E_{11}$$
$$(G_{12})_\infty = \frac{1}{ha_{66}} = G_{12} \quad \ldots(3.11)$$
$$(\nu_{12})_\infty = -\frac{a_{12}}{a_{11}} = \frac{2\nu_{21}}{\left(1+\frac{\nu_{21}}{\nu_{12}}\right)} = \frac{2\nu_{12}\nu_{21}}{(\nu_{12}+\nu_{21})}$$

For woven fibers of finite-end satin, the properties will be decreased due to fibers bent, assuming that there is a multiplication factor which when multiplied by the infinite-end satin woven fibers composite properties gives the properties of the woven fibers of finite-satin then

$$(E_{11})_w = (E_{22})_w = W_E (E_{11})_\infty = W_E \frac{\left\{\left(1+\frac{\nu_{21}}{\nu_{12}}\right)^2 - 4\nu_{21}{}^2\right\}}{2(1-\nu_{12}\nu_{12})\left(1+\frac{\nu_{21}}{\nu_{12}}\right)} E_{11}$$

$$(G_{12})_w = W_G\, G_{11} = W_G (G_{12})_\infty \qquad \ldots(3.12)$$

$$(\nu_{12})_w = (\nu_{21}) = W_\nu\, (\nu_{12})_\infty = W_\nu \frac{2\nu_{12}\nu_{21}}{(\nu_{12}+\nu_{21})}$$

where W_E, W_G and W_ν are new factors called the woven multiplication factors for E_{11}, G_{12}, and ν_{12} respectively. These factors can be evaluated from the evaluation of these properties experimentally which is done in the tensile tests of the 0, 90 composite plates and the woven fibers composites formed, all details are seen in the next chapter of the experimental work.

Now because of the homogenous orthotropic behavior of the woven fiber lamina, then the mechanical properties of angle ply woven lamina stay covered by expressions [64]

$$E_{xx} = E_{yy} = \left[\frac{m^4+n^4}{E_{11}} + \left(\frac{1}{G_{12}} - \frac{2\nu_{12}}{E_{11}}\right)m^2n^2\right]^{-1}$$

$$G_{xy} = \left[\frac{1}{G_{12}} + 4\left(\frac{2(1+\nu_{12})}{E_{11}} - \frac{1}{G_{12}}\right)m^2n^2\right]^{-1} \qquad \ldots(3.13)$$

$$\nu_{xy} = E_{xx}\left[\frac{\nu_{12}}{E_{11}} - \left(\frac{2(1+\nu_{12})}{E_{11}} - \frac{1}{G_{12}}\right)m^2n^2\right]$$

$$\nu_{yx} = \frac{E_{yy}}{E_{xx}}\nu_{xy}$$

3.3 Impact analysis

3.3.1 introduction

Up to this date, the research of impact of woven hybrid composites has been experimental and Numerical. In order to understand the mechanisms in the woven hybrid composite under low, high and ballistic velocities for impact, and the energy transfer between the impactor and the composite, analytical models are needed.

3.3.2 Constitutive relations

A laminated composite plate of length **a**, breadth **b** and thickness h with n arbitrarily oriented layers is considered. The plate axes and the layer details are illustrated in Fig. 3-2.

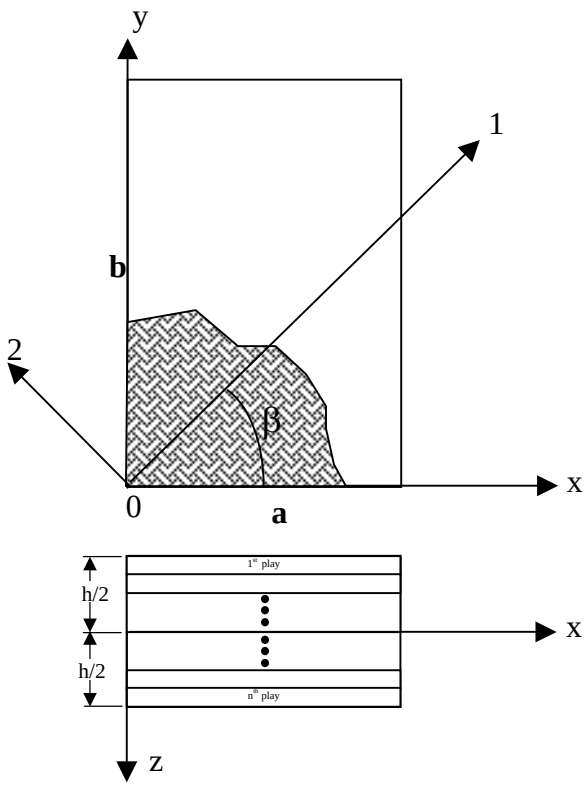

Figure 3-2 Plate axis and layer details.

The x–y plane coincides with the middle plane of the plate and the z-axis is oriented along the thickness direction. The displacements u, v and w at any point (x, y, z) in the laminate are given by

$$\begin{aligned} u(x,y,z) &= u^0(x,y) + z\theta_x(x,y) \\ v(x,y,z) &= v^0(x,y) + z\theta_y(x,y) \\ w(x,y,z) &= w^0(x,y) \end{aligned} \qquad \ldots(3.14)$$

Where u^0, v^0 and w^0 denote the mid-plane displacements and θ_x and θ_y denote the rotations along the x and y axes, respectively. Considering first order shear deformation, the strain components in a lamina are expressed as

$$\begin{aligned} &\varepsilon_x = \frac{\partial u}{\partial x} = \varepsilon_x^o + z\,k_x, \varepsilon_y = \frac{\partial u}{\partial x} = \varepsilon_y^o + z\,k_y, \\ &\gamma_{xy} = \frac{\partial u}{\partial y} + \frac{\partial v}{\partial x} = \gamma_{xy}^o + zk_{xy}, \\ &\gamma_{xy}^o = \frac{\partial w}{\partial x} + \theta_x, \gamma_{yz}^o = \frac{\partial w}{\partial y} + \theta_y \end{aligned} \qquad \ldots(3.15)$$

Where ε_x^o , ε_y^o and γ_{xy}^o are mid-plane strains, k_x, k_y and k_{xy}, are the plate curvatures and γ_{xz}^o and γ_{yz}^o are the transverse shear strains, respectively.

The strains in the i^{th} lamina at a distance z from the mid-plane in the matrix form are given by

$$\begin{bmatrix} \varepsilon_x \\ \varepsilon_y \\ \gamma_{xy} \\ \gamma_{xz} \\ \gamma_{yz} \end{bmatrix} = \begin{bmatrix} \varepsilon^0_x \\ \varepsilon^0_y \\ \gamma^0_{xy} \\ \gamma^0_{xz} \\ \gamma^0_{yz} \end{bmatrix} + z \begin{bmatrix} k_x \\ k_y \\ k_{xy} \\ k_{xz} \\ k_{yz} \end{bmatrix} \quad \ldots(3.16)$$

Here k_{xz} and k_{yz} are considered as zero.

The stresses at any point in the k^{th} lamina are

$$\begin{aligned} &\{\sigma\} = \left[\overline{Q}_{ij}\right]_k \{\varepsilon\},\ i,j = 1...6, \\ &\{\sigma\} = \left[\sigma_x\ \sigma_y\ \sigma_z\ \tau_{xz}\tau_{tz}\tau_{xy}\right]^T, \{\varepsilon\} = \left[\varepsilon_x\ \varepsilon_y\ \varepsilon_z\ \gamma_{xz}\gamma_{tz}\gamma_{xy}\right]^T \end{aligned} \quad \ldots(3.17)$$

$[Q_{ij}]_k$ is the off-axis stiffness of the k^{th} lamina. Here, ε_z is zero. The elasticity matrix of the composite plate is given by

$$\left.\begin{aligned} &\left[A_{ij}, B_{ij}, D_{ij}\right] = \sum_{k=1}^{n} \int_{zk-1}^{zk} \left[\overline{Q}_{ij}\right]_k \left(1, z, z^2\right) dz, \qquad i,j = 1,2,6 \\ &\textit{and} \\ &\left[A_{sij}\right] = \sum_{k=1}^{n} \int_{zk-1}^{zk} \alpha \left[\overline{Q}_{ij}\right]_k dz, \qquad i,j = 4,5 \end{aligned}\right\} \ldots(3.18)$$

α is the shear correction factor considered as 5/6. And the stresses in the fiber direction 1–2 in the k^{th} lamina were found by multiplying the transformation matrix as given with the stresses determined at different points of the lamina in the x–y coordinates [64].

$$\begin{Bmatrix} \sigma_1 \\ \sigma_2 \\ \tau_{12} \end{Bmatrix}_k = \begin{bmatrix} m^2 & n^2 & 2mn \\ n^2 & m^2 & -2mn \\ -mn & mn & m^2 - n^2 \end{bmatrix} \begin{Bmatrix} \sigma_x \\ \sigma_y \\ \tau_{xy} \end{Bmatrix}_k \quad \ldots(3.19)$$

Here, m and n denote cosine and sine of the angle β made by the fibers with the x-axis in each lamina. The lamina stresses along material axes in each ply were applied to the failure criterion to check for ply failure.

3.3.3 Energy Balance:

Based on the conservation of the total energy, the part of the kinetic energy of the projectile is absorbed by the plate, and assumed to be classified into four types which are: -

1- The strain energy due to dynamics of plate's theory (Contact energy) U_c .
2- Strain energy in the large deflection penetration zone U_{Ld} .
3- Delamination strain energy U_{del}.
4- Friction energy U_F.

The energy balance according to this classification for the impact becomes

$$\frac{1}{2} M_p V_{pi}^2 = + U_c + U_{Ld} + U_{del} + U_F + \frac{1}{2} M_p V_{po}^2 \quad \ldots(3.20)$$

3.3.3.1- Strain energy due to deformation of plate

The equation of motion for the laminated composite plate subjected to dynamic load (impact) is [64]

$$D_{11}\frac{\partial^4 w}{\partial x^4} + 4D_{16}\frac{\partial^4 w}{\partial x^3 \partial y} + 2(D_{12} + D_{66})\frac{\partial^4 w}{\partial x^2 \partial y^2} + 4D_{26}\frac{\partial^4 w}{\partial x \partial y^3} + D_{22}\frac{\partial^4 w}{\partial y^4} + \rho h \frac{\partial^2 w}{\partial t^2} = q \quad \ldots(3.21)$$

where

w(x,y) is the deflection along the z direction. q(x,y,t) is the intensity of transverse distributed load per unit area acting on the thin plate.D_{11}, D_{16}, D_{12}, D_{66}, D_{26}, D_{22} are the flexural rigidity coefficients of the laminated plate.

For especially orthotropic laminates ($D_{16} = D_{26} = 0$), the governing differential equation becomes.

$$D_{11}\frac{\partial^4 w}{\partial x^4} + 2(D_{12}+D_{66})\frac{\partial^4 w}{\partial x^2 \partial y^2} + D_{22}\frac{\partial^4 w}{\partial y^4} + \rho h\frac{\partial^2 w}{\partial t^2} = q(x,y,t) \qquad \ldots(3.22)$$

The force for this plate is dynamics impact force, which is obtained from the modified Hertzian contact theory.

Contact Law

The relationship between the impact force P and contact deformation α is given by Hertz Contact Law [12]

$$q = nw_m^{1.5} \qquad \ldots(3.23)$$

where the contact deformation is the distance between the center of the projectile's nose and the mid-surface of the beam and n is the modified constant of the Hertz Contact Law proposed by Tan and Sun[14].

$$n = \frac{4}{3}\sqrt{R_p}\left[\frac{1}{(1-\nu_p)/E_p + 1/E_{c22}}\right] \qquad \ldots(3.24)$$

where R_p, ν_p , E_p are the local radius, Poisson's ratio, and Young's modulus of the projectile, respectively. E_{c22} is the transverse modulus normal to the fiber direction in the surface ply facing the projectile.

The solution of plate problems via the analysis method is limited in that the boundary conditions are restricted, e.g., simple supports, etc [63]. If these conditions are more complex, the analysis becomes increasingly tedious and even impossible. In such cases numerical and approximate methods are the only approaches that can be employed. In the engineering application of the theory of plates are usually dealing with inaccurate input data. In the first place, the external loads are known only with a certain degree of accuracy. In addition, the material properties, such as the modulus of elasticity, the Poisson's ratio, ν, and the D_{ij} (for composites) can contain considerable inaccuracies.

Furthermore, the actual boundary conditions are merely approximations of the theoretical ones. Consequently, even an "exact" solution only approximates the real behavior of a plate. The error caused by the inherent inaccuracy of the input is called error of data.

Employing approximate methods, an additional inaccuracy is introduced in the computation, which is called the error of calculation. Naturally, this must be smaller than the error of data. As a rule, it is desirable that the errors of calculation have less than 5% discrepancy in comparison with the exact solution [5]. For many plate problems of considerable practical interest, analytic solutions to the governing differential equations cannot be found. Fortunately, numerical treatment of differential equations can yield approximate results, acceptable for most practical purposes. Among the numerical techniques presently available, the finite difference method is one of the most general. In applying finite difference method, the derivatives in the differential equation under consideration are replaced by difference quantities at some selected points, referred to as nodes or pivotal points, or simply as points of division. The numerical solution is thus obtained from differential equations, which are applicable to the actual continuous structure.

The numerical solution by finite differences generally requires replacing the derivatives of a function by difference expressions of the function at the nodes. The differential equation governing the displacement is applied in a difference form at each node, relating the displacement at the given node and at nodes in its vicinity to

the external applied load. This usually provides a sufficient number of simultaneous equations for the displacements to be determined. The finite-difference coefficients of the equations applied at nodes on, or close to, the boundary have to be modified, compared with the coefficients used at interior points, in order to satisfy the boundary conditions of the problem. Therein lies one of the difficulties of the method of finite differences and a disadvantage in its use compared with the finite-element method. Nevertheless, the finite difference method can be conveniently used for a variety of problems, and, when it is used, the number of simultaneous equations required (for a comparable degree of accuracy) is generally only about a half or a third of the number of the equations needed in the finite-element method [65].

$$D_{ij} = \frac{1}{3}\sum_{k=1}^{n}\left[\overline{Q}_{ij}\right]\left(h_k^3 - h_{k-1}^3\right) \text{ Flexural stiffness matrix} \qquad \ldots(3.25)$$

Then the solution of the dynamic of plate equation (3.22) is by using the finite difference method, the Details of the solution is derived in appendix A, this solution was required for the equivalent elastic wave speed and the natural frequency to optimize the best time and distance increments, the details of finding the natural frequency for rectangular clamped plates (CCCC plates) is shown in appendix B.

The strain energy for these cases was evaluated numerically from the integration of strain energy through the plate area using [64]

$$U_c = \int_0^b\int_0^a \left[D_{11}\left(\frac{\partial^2 w}{\partial x^2}\right)^2 + 2D_{12}\frac{\partial^2 w}{\partial x^2}\frac{\partial^2 w}{\partial y^2} + D_{22}\left(\frac{\partial^2 w}{\partial y^2}\right)^2 + D_{66}\left(\frac{\partial^2 w}{\partial x \partial y}\right)^2 \right] dxdy \qquad \ldots(3.26)$$

3.3.3.2 Strain energy due to deformation of delamination zone, (assumed deformation shape formulation)

Assumptions

i- Delamination occurs at all layers.

ii-The delaminations areas are approximately circular and this area covers the large deformation zone.

Consider the large deformation circular zone shown in Fig 3-3.

For layer i

$$\frac{y_i}{r_i} = \frac{y}{d/2} \qquad \ldots(3.27)$$

r_i: hole radius of layer i through penetration

y_i : height of cone penetrate the layer i

R_i: radius of curvature of layers i in the delamination zone, which is assumed to be constant.

$$r_i = a - R_i \sin(\phi/2)$$

Then

$$R_i = \frac{a - r_i}{\sin(\phi/2)}$$

$\phi/2$: half cone angle of the impactor.

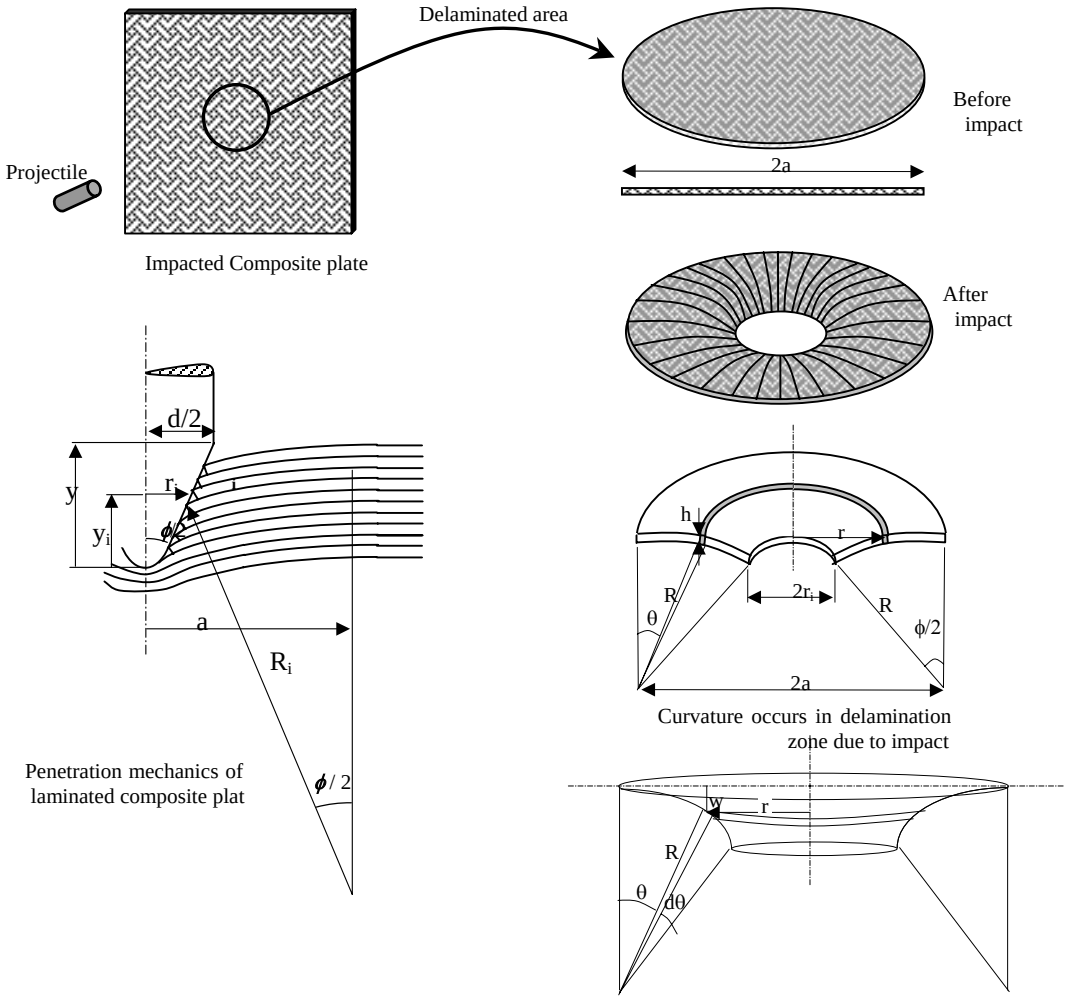

Figure 3-3 Schematic drawing represent the impact delaminated large deformation and penetration zone.

Consider a washer element in the ply i (deformed ply) has a radius r then

$$r = a - R_i \sin(\theta)$$

Using the volume constancy of the delamination area after and before the penetration, then

$$\pi a^2 h = \int_0^{\phi/2} 2\pi r h R_i \, d\theta$$

$$a^2 = \int_0^{\phi/2} 2\left(a - \frac{a - r_i}{sin(\phi/2)} sin(\theta)\right) \frac{a - r_i}{sin(\phi/2)} d\theta$$

$$a^2 = 2\left(\frac{a - r_i}{sin(\phi/2)}\right)\left(\frac{a\phi}{2} + \frac{a - r_i}{tan(\phi/2)}\right)$$

Multiply by $\sin^2(\phi/2)$ and rearrange the equation

$$a^2\left(sin(\phi/2) - \phi - 2\,cot(\phi/2)\right) + a\left(r_i\phi + 4r_i\,cot(\phi/2)\right) + 2r_i\,cot(\phi/2) = 0$$

$$a = \frac{-2r_i\phi - 4r_i\,cot(\phi/2) \pm \left[\{r_i\phi + 4r_i\,cot(\phi/2)\}^2 - 4\{sin(\phi/2) - \phi - 2cot(\phi/2)\} \times 2r_i\,cot(\phi/2)\right]^2}{2[sin(\phi/2) - \phi - 2cot(\phi/2)]}$$

…(3.28)

The equation (3.28) has two unknowns which are the delamination radius “a” and the hole radius of the ply “r_i”, then a second equation is needed to calculate the unknowns which is the failure criteria of the delamination zone.

3.3.3.3 Energy observed due to delamination itself

The failure criterion for delamination is given by [15]: -

$$F_{delam} = \left(\frac{\sigma_n}{S_n}\right)^2 + \left(\frac{\sigma_s}{S_s}\right)^2 \qquad \text{…(3.29)}$$

Where σ_n and σ_s are the normal and shear interface stresses, respectively, and S_n and S_s are the corresponding strength, delamination occurs when $F_{delam} \geq 1$.

From curvature of plate shown in Fig. 3-3.

$$R_i = \frac{a - r_i}{sin(\phi/2)}$$

The strain can be calculated using $\kappa_\theta = \frac{1}{R_i}$.

For Cartesian coordinates,

$$x = r\,cos(\beta) \qquad r = \sqrt{x^2 + y^2}$$

$$y = r\,sin(\beta) \qquad \beta = tan^{-1}\frac{y}{x}$$

Now that

$$\kappa_x = \frac{-\partial^2 w}{\partial x^2},\ \kappa_y = \frac{-\partial^2 w}{\partial y^2},\ and\ \kappa_{xy} = \frac{-\partial^2 w}{\partial x \partial y}$$

And in polar coordinates

$$\kappa_r = \frac{-\partial^2 w}{\partial r^2},\ and\ \kappa_\theta = -\frac{1}{r^2}\frac{\partial^2 w}{\partial \theta^2}$$

From geometry

$$w = R_i(1 - cos(\theta))$$
$$r = a - R_i\,sin(\theta)$$

I.e. $R_i = \left(\frac{a-r}{sin(\theta)} \right)$ and $\theta = sin^{-1}\left(\frac{a-r}{R_i} \right)$

$$dr = -R_i \, cos(\theta) d\theta$$

$$\frac{\partial w}{\partial r} = \frac{(1 - cos(\theta))}{sin(\theta)}$$

$$\frac{\partial^2 w}{\partial r^2} = 0$$

$$\frac{\partial w}{\partial \theta} = (a-r)\left(csc(\theta)cot(\theta) + csc^2(\theta)\right)$$

$$\frac{\partial^2 w}{\partial \theta^2} = (a-r)\left(sec^3(\theta) + esc(\theta)tan^2(\theta) - 2\,csc^3(\theta)cot(\theta)\right)$$

Using step by step chain rule

$\frac{\partial w}{\partial x} = \frac{\partial w}{\partial \theta} . \frac{\partial \theta}{\partial x}$ And $\frac{\partial w}{\partial y} = \frac{\partial w}{\partial \theta} . \frac{\partial \theta}{\partial y}$

$$\frac{\partial \theta}{\partial x} = \frac{-2x(1/2)}{\sqrt{x^2 + y^2} R_i \sqrt{1 - \left(\frac{\sqrt{x^2 + y^2}}{R_i} \right)^2}}$$

$$\frac{\partial\theta}{\partial y}=\frac{-2y(1/2)}{\sqrt{x^2+y^2}R_i\sqrt{1-\left(\frac{\sqrt{x^2+y^2}}{R_i}\right)^2}}$$

This gives

$$\frac{\partial\theta}{\partial x}=\frac{-x}{r\sqrt{R_i^2-r^2}} \text{ and } \frac{\partial\theta}{\partial y}=\frac{-y}{r\sqrt{R_i^2-r^2}}$$

Then

$$\frac{\partial w}{\partial x}=\frac{-x}{r\sqrt{R_i^2-r^2}}(a-r)\left(csc(\theta)cot(\theta)+csc^2(\theta)\right)$$

And

$$\frac{\partial w}{\partial y}=\frac{-y}{r\sqrt{R_i^2-r^2}}(a-r)\left(csc(\theta)cot(\theta)+csc^2(\theta)\right)$$

$$\frac{\partial^2 w}{\partial x^2}=\frac{\partial}{\partial\theta}\left(\frac{\partial w}{\partial x}\right).\frac{\partial\theta}{\partial x} \text{ and } \frac{\partial^2 w}{\partial y^2}=\frac{\partial}{\partial\theta}\left(\frac{\partial w}{\partial y}\right).\frac{\partial\theta}{\partial y}$$

$$\frac{\partial^2 w}{\partial x^2}=\frac{x^2}{r^2\left(R_i^2-r^2\right)^2}(a-r)\left(csc(\theta)cot(\theta)+csc^2(\theta)\right)=-\kappa_x$$

$$\frac{\partial^2 w}{\partial y^2}=\frac{y^2}{r^2\left(R_i^2-r^2\right)^2}(a-r)\left(csc(\theta)cot(\theta)+csc^2(\theta)\right)=-\kappa_y$$

$$\frac{\partial^2 w}{\partial x \partial y} = \frac{\partial}{\partial \theta}\left(\frac{\partial w}{\partial x}\right).\frac{\partial \theta}{\partial y}$$

$$\frac{\partial^2 w}{\partial x \partial y} = \frac{xy}{r^2\left(R_i^2 - r^2\right)^2}(a-r)\left(csc(\theta)cot(\theta) + csc^2(\theta)\right) = -\kappa_{xy}$$

From plate bending theory

$$\begin{Bmatrix} \varepsilon_x \\ \varepsilon_y \\ \gamma_{xy} \end{Bmatrix} = \begin{Bmatrix} \varepsilon_x^o \\ \varepsilon_y^o \\ \gamma_{xy}^o \end{Bmatrix} + z\begin{Bmatrix} \kappa_x \\ \kappa_y \\ \frac{1}{2}\kappa_{xy} \end{Bmatrix}$$

With assumption of zero mid-span strain

$$\begin{Bmatrix} \varepsilon_x \\ \varepsilon_y \\ \gamma_{xy} \end{Bmatrix} = z\begin{Bmatrix} \kappa_x \\ \kappa_y \\ \frac{1}{2}\kappa_{xy} \end{Bmatrix}$$

$$\begin{Bmatrix} \varepsilon_x \\ \varepsilon_y \\ \gamma_{xy} \end{Bmatrix} = \frac{-z(a-r)\left(csc(\theta)cot(\theta) + csc^2(\theta)\right)}{r^2\left(R_i^2 - r^2\right)^2}\begin{Bmatrix} x^2 \\ y^2 \\ \frac{1}{2}xy \end{Bmatrix}$$

For ply

$$\begin{Bmatrix} \sigma_x \\ \sigma_y \\ \sigma_{xy} \end{Bmatrix} = [\overline{Q}] \begin{Bmatrix} \varepsilon_x \\ \varepsilon_y \\ \varepsilon_{xy} \end{Bmatrix}$$

For interface and assuming plane strain problems

$$\begin{Bmatrix} \sigma_x \\ \sigma_y \\ \tau_{xy} \end{Bmatrix} = [D] \begin{Bmatrix} \varepsilon_x \\ \varepsilon_y \\ \gamma_{xy} \end{Bmatrix} \quad \ldots(3.30)$$

$$\text{Where } [D] = \frac{E_m(1-\nu_m)}{(1+\nu_m)(1-2\nu_m)} \begin{bmatrix} 1 & \frac{\nu_m}{1-\nu_m} & 0 \\ \frac{\nu_m}{1-\nu_m} & 1 & 0 \\ 0 & 0 & \frac{1-2\nu_m}{2(1-\nu_m)} \end{bmatrix} \quad \ldots(3.31)$$

ν_m and E_m are Poisson's ratio and elasticity modulus of matrix respectively. Substitute equation (3.31) in equation (3.30) and rearrange, it gives

$$\begin{Bmatrix} \sigma_x \\ \sigma_y \\ \tau_{xy} \end{Bmatrix} = \frac{E_m(1-\nu_m)}{(1+\nu_m)(1-2\nu_m)} \begin{Bmatrix} \frac{-z(a-r)\left(csc(\theta)cot(\theta)+csc^2(\theta)\right)}{r^2\left(R_i^2-r^2\right)^2} \end{Bmatrix} \begin{bmatrix} 1 & \frac{\nu_m}{1-\nu_m} & 0 \\ \frac{\nu_m}{1-\nu_m} & 1 & 0 \\ 0 & 0 & \frac{1-2\nu_m}{2(1-\nu_m)} \end{bmatrix} \begin{Bmatrix} x^2 \\ y^2 \\ \frac{1}{2}xy \end{Bmatrix} \quad \ldots(3.32)$$

From maximum principal stress and shear stress

$$\sigma = \frac{\sigma_x + \sigma_y}{2} + \sqrt{\left(\frac{\sigma_x - \sigma_y}{2}\right)^2 + \tau_{xy}^2} \quad \text{and} \quad \tau = \sqrt{\left(\frac{\sigma_x - \sigma_y}{2}\right)^2 + \tau_{xy}^2}$$

Substitute in equation (3.29), it yields another equation containing radius r_i and delaminations radius a. Solve with equation (3.28) to get the delaminations ***a*** and the hole radius of ply i due to penetration. The same steps can be repeated for all penetrated plies.

The strain energy for the deformation of large deformation zone is

$$U_{Ld} = 4\sum_{i=1}^{n}\int_0^{\pi/2}\int_0^a \left[D_{11}\left(\frac{\partial^2 w}{\partial x^2}\right)^2 + 2D_{12}\frac{\partial^2 w}{\partial x^2}\frac{\partial^2 w}{\partial y^2} + D_{22}\left(\frac{\partial^2 w}{\partial y^2}\right)^2 + D_{66}\left(\frac{\partial^2 w}{\partial x \partial y}\right)^2\right] r\,dr\,d\theta \qquad \ldots(3.33)$$

While the delamination energy is

$$U_{del} = \pi D\sum_{i=1}^{n}\int_0^a \left(\frac{\partial^2 w}{\partial r^2} + \frac{1}{r}\frac{\partial w}{\partial r}\right)^2 r\,dr \qquad \ldots(3.34)$$

3.3.3.4 Friction energy

This observed energy is required to calculate the friction coefficient between the impactor and the plies. The friction process is very difficult due to delaminations, change in area of the contact, and load with time and thermal effect on the friction. Also after delaminations there are other losses in energies due to friction in delaminations of plies.

The friction coefficients between the composite and the projectile material are measured using friction disk with the details shown in the next chapter.

The assumptions used in the friction work are that the friction is independent on the heat generation through the penetration. This assumption is fair especially because the penetration time is very small to transfer heat through the surfaces. The Friction due to delamination is small with low movement compared with the friction due to penetration which vary clear in the geometry of the penetration and friction, and because the delamination energy was considered, then the friction through the delamination was considered through the analyses of the delamination. Then the analyses of frictional energy is based on the variation of penetration loads through the penetration.

Using the momentum equation for the projectile

$$m(Vi - Vr) = \int_0^{tp} (q - F\cos(\phi/2) - \mu F \sin(\phi/2)\, dt \qquad \ldots(3.35)$$

The energy absorbed for friction is

$$U_F = \int_0^{h/\cos(\phi/2)} F ds \qquad \ldots(3.36)$$

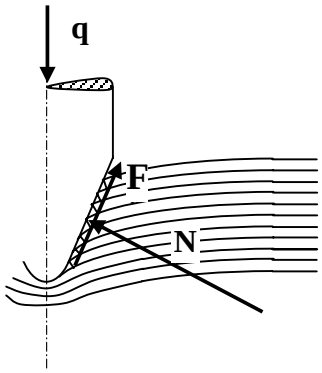

Figure 3-4 the normal force and friction through the impact penetration load

Chapter Four

Experimental Work

4.1 Introduction

The impact mechanics on a composite laminate plate is complicated because of the many modes of the absorbing energies. The analysis of the different types of energies absorbed due to impacting rigid projectile on composite materials have been given in the previous chapter. This chapter well concentrates on the experimental aspects of this problem. Specifically, it examine the rate of kinetic energy observed and the rest energy kept in the projectile after impact.

Three fold purposes are planned to be investigated through this chapter. First, to outline the general steps, currently designed to fabricate the rectangular models of commercial composite material available in industrial use. The manufactured models exhibited certain orthotropic properties, and manufacturing the required specimens, which are used for evaluating the mechanical properties and for being tested in the present impact tester.

Second, to evaluate the mechanical properties for the composites used, specially, the composite materials which are made from different fiber materials, namely; E-glass, Kevlar, and Carbon, and for different fibers geometries which are random, unidirectional, and woven with different weave patterns (plain weave, crowfoot satin weave & 8-end satin weave). The matrices used are polyester and epoxy.

Third, the gun impact mechanics tester design and layout with its new-presented computerized measuring device for projectile velocity and penetration time and the set up of the impact test for the specimens to evaluate the kinetic energy of the projectile before and after impact and the time duration through the perforation.

4.2 Fabrication of laminated plates test specimens

4.2.1 Background

It is well known that the laminated composites consist of layers of at least two different materials that are bonded together. Lamination is used to combine the best aspects of the constituent layers in order to achieve more useful material. This definition is quite fit with the class of laminated fibrous composites (composed of fibers in matrix) in which the final composite product results from the layer staking [66]. Here, layers of fabric – reinforced material are the woven, random and unidirectional fibers built up with the different fiber materials and different textile geometry, different strength and stiffness depend on these conditions; Thus, the strength and stiffness of the laminated fiber – reinforced composites can be tailored to specific design requirements of the structural element being built. Examples of such elements include, Polaris missile cases, fiberglass boat hulls, aircraft wing panels and body sections.

The primary reinforced agents used in production of composites at the present time, are E-glass, carbon, aramid, and other natural fibers. The typical resin matrixes include polyester, phenolic, epoxy, and so many other chemical compounds. The first application of fiberglass composites was conceived and developed in the Wright – Patterson Co. in Ohio 1943, for light airframe structures [66].

The design based on a balsa wood core with fiberglass reinforced (FR) skins. These skins were made of five plies of 3mm thick glass fabric impregnated with 42-45% weight polyester resin. As a result of continued research and development with respect to both the material themselves and their production techniques, the (FR) composites have experienced greatly increased commercially availability and

become competitive with other materials in more specialized big markets because of its relative ease, inexpensive and flexibility to meet the environmental demands [66].

In the present work, the demand is focused to construct laminated composite models of rectangular plates which exhibit certain degree of "Orthotropic" in order to check the capability of the new model and study the parameters resulting from changing material and geometry of fibers and the material of matrices, in addition to the effect of adding layers of stiffened layer on the mechanical and impact properties of manufactured composite plates.

The characteristics of the desired end product (such as size, shape, and quality) are determined basically by two factors: the physical / chemical properties of the prepared raw material (fiber and saturated resin), and the method by which the building blocks are combined and modeled. Using the hand lay– up method, the apparent factors like the worker skillness and the chemical treating of the matrix as reacted with the additive agents. Comparing with other processing method, those of high; quality methods those of high quality live the Bag- molding and the "Thermoset Matched " "Die- Molding" process [66], the conventional hand lay- up method, used in the present work, satisfied thoroughly the mentioned demands easily, with minimum equipment investment and less start- up leaf time.

4.2.2 Fiber reinforcements and matrix resins

As mentioned earlier, the fibrous composite laminates fabricated mainly from two main constituents, which are the fibers reinforcements, and the unsaturated matrix resin. It is important to remember that the inter ply layer, or the adhesive layer between any two successive layer is the resin itself with some adding thickness for distinguishing this interply layer. The followings demonstrate the physical and chemical specification of these two constituents.

(A) The fiber reinforcements

The fiber materials used as reinforcements in the present work are E-Glass, Carbon, and Kevlar aramid fibers. Now the compositions, forming, and properties are listed below.

I) E-Glass

Glass is amorphous material obtained from the molting (melt) state by cooling the liquid at the rate such that no ordered regions (known as crystals) are formed. Chemically, glass is essentially composed of a silica network. However, pure silica, or quartz, requires very high temperature before it can be melted and drawn into fibers. Therefore, other chemical components are added to decrease the glass viscosity to levels suitable for melting, homogenizing, removal of gassseous inclusions, and fiberizing. The type and amount of modifiers alternate the physical properties of the resultant glass to varying degree.

Although a number of glass compositions have been developed, only a few are used commercially to create continuous glass fibers. The four main glasses used are high alkali (A-glass), electrical grade (E-glass), a modified E-glass that is chemical resistant, and high strength S-glass.

The type used in the present work is E-glass, which is the material most widely used as a reinforced medium for plastic as well as for textile fiberglass product applications. The representative chemical compositions of these four types of glass are given in Table 4-1 and the inherent properties are given in Table 4-2.

Table 4-1 Glass composition [2]

	Material, percentage weight (%)							
Glass type	Silica	Alumina	Calcium oxide	Magnesia	Boron oxide	Soda	Calcium fluoride	Minor oxides
E-glass	54	14	20.5	0.5	8	1	1	1
Commercial fiberglass used in the present work								
A-glass	72	1	8	4	-	14	-	1
ECR-glass	61	11	22	3	-	0.6	-	2.4
S-Glass	64	25	-	10	-	.3	-	0.7

Table 4-2 Inherent properties of glass fibers[2]

Glass type	Specific gravity	σ_{ult} (MPa)	E_t (GPa)	α (10^{-6}/K)	Dielectric constant(a)	Liquidus temperature ^oC
E-glass	2.58	3450	72.5	5.0	6.3	1065
Commercial fiberglass used in the present work						
A-glass	2.50	6043	69.0	8.6	6.9	996
ECR-glass	2.62	3625	72.5	5.0	6.5	1204
S-Glass	2.48	4590	86.0	5.0	5.1	1454

II) Carbon fibers

A fiber that is produced by the pyrolysis of organic precursor fibers, such as rayon, polyacrylonitrile (PAN), and pitch, in an inert environment. Carbon fibers typically carbonized in the region of 1315 ^oC and assay at 93 to 95% carbon. There are some types of carbon fibers (which their properties are available in [2]), the commercial type was used in the present work is P-55 carbon-high modulus fiber which its properties are shown in Table 4-3.

Table 4-3 Mechanical properties of P-55 carbon-high modulus fiber [2].

Product name	Manufacturing	Precursor type	Density (Kg/m^3)	σ_{ult} (GPa)	E_t (GPa)
P-55	Union Carbide	Pitch	2000	1.73	379

III) Kevlar

The predominate organic reinforcing fiber used in advanced composites since the early 1970s has been aramid or aromatic polyamide, known as Kevlar. Kevlar 49 fabric with the mechanical properties shown in Table 4-4 is used in the tests.

Table 4-4 Mechanical properties of Kevlar 49 used in the presented work [2]

Material	Density Kg/m^3	Filament diameter (μm)	E_t (GPa)	σ_{ult} (GPa)	ε_{break} (%)	Available yarn count, No. Filaments
Kevlar 49	1440	12	131	3.6	2.8	≈150

(B) The unsaturated matrix resin:

Two types of matrixes are considered in the tests, are polyester resin and epoxy resin.

I) Polyester resin

It is a chemical compound of reactive polymers (glycol's or "phthalic" anhydride with the acid "malice" anhydride). The compound stays stable liquid for months or even years, as long as the carbon double – bonds in the poly –molecular structure, is kept conservative. In his patents, sixty years ago, Ellis [67] discovered that the adding of a reactive monomer (usually referred to "peroxide" catalyst or "styrene") then an exothermic reaction (rejecting heat) or "curing" will be set up involving the conversion of double – bond into single – bond through cross – linkage polymerization process. The added catalyst initiates and shares the polymer network within certain duration time, called the "gel time" of the process. A typical catalyst, frequently used in practice, is the MEKP, refereed to methyl ethyl ketone proxide. In order to decrease the unprofitable much gel time, during the lay – up procedure, an "accelerator" agent may be employed for this purpose, like the "cobalt – naphthenate" as being used for a general – purpose polyester resin.

The new product is, hence, the "saturated" polyester resin. Depending on the mole ratio of the phthalic / maleic, and the mass percentage of the catalyst / accelerator agents, the mechanical properties of the resin will be cited. Other glycol compounds and additive agents produce wide variety of resin type for broad range of applications. Recently, the polyester resin, as refereed to "Palatal P50T" [67], is found commercially used and officially approved in German standards under DIN 16946.

II) Epoxy resin

Epoxy resins are used extensively in composite materials for a variety of demanding structural applications. All epoxy resins contain the epoxide (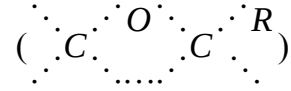), where R represents the point of attachment to the remainder of the resin molecule. The epoxy used in the present work is epoxy Laida[2].

(C) Fabric forms and materials used:

The geometrical aspect of the fibers used in the present work has the detail shown in Table 4-5, the selection of different fiber materials aims to study the effect of each on the properties and impact, also the using of different fabric forms and weights are to study the fabric effect and to determine the woven facture defined in the theoretical part of this work. The matrix types and their density are tabulated also.

Table 4-5 Materials used in the presented tests

(A) Fibers

Fiber material	Weave	Construction tows/cm	Mass/area kg/m^2
E-glass	Plain	2.5*2.5	0.500
	Plain	12.5*12.5	0.260
	5-end satin	5*5	0.280
	Random	-	0.450
Carbon	Plain	7*7	0.170
	3-end satin	5*5	0.210
Kevlar	3-end satin	7*7	0.230

(B) Matrixes

Polyester	ρ= 1268 kg/m^3	Epoxy	ρ= 1430 kg/m^3

4.2.3 Mould preparation

There are two groups of samples molded, matrix samples, and layered fiber composite plates samples. The matrix samples were made to verify the mechanical properties of matrix specially because the environment conditions and process of molding are very important parameters affecting the properties, because of that there is no offered properties can be used directly, then the Tensile, Bending, and Torsion tests were done. Composite plates samples were made for using different fibers and matrix material to verify the mechanical properties and to use them as targets in the high velocity impact tests.

(A) Matrix samples:

For production the samples of tests (Tensile, Bending), made one sample for each test was made from pure epoxy with standard dimensions and then used these samples were used to make the moulds.

The moulds used are produced from paste of panes rolled out at pane and then formed the shape of each sample on it as shown in Fig. 4-1.

Figure 4-1 matrix sample produced from paste of panes rolled out at pane and then formed the shape of tensile and bending tests.

The tensile test specimens have been produced according to (D638) as shown in Fig. 4-2a. The tensile test specimens produced for pure epoxy. The tensile test

specimens were produced using a mould shown in Fig. 4-1, After solidification grinding processes were carried out for each specimen to get the standard dimensions [Fig. 4-2b].

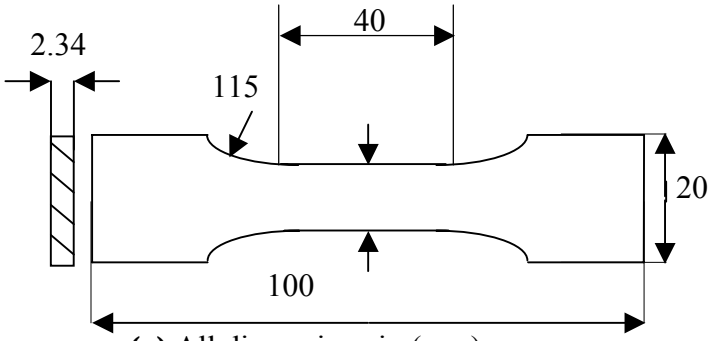

(a) All dimensions in (mm).

Figure 4-2 Matrix tensile specimens.

To produce the samples are for the compression a plastic pipes with a diameter (D=10mm, L= 24mm) as shown in Fig. 4-3. The compression test specimens have been produced according to (ASTM-D695M-89), where the length to diameter ratio is approximately 2:1.

Figure 4-3 Matrix compression specimens.

Flexural test specimens have been produced according to (ASTM D790-89) with length to depth ratio equal to 32:1, depth (3.2mm), a width (25mm) and a length (127mm) as illustrated in fig. 4-4 then are specimen produced using a mould shown in Fig. 4-1. After solidification, grinding process was used to get the standard shape shown in Fig. 4-4.

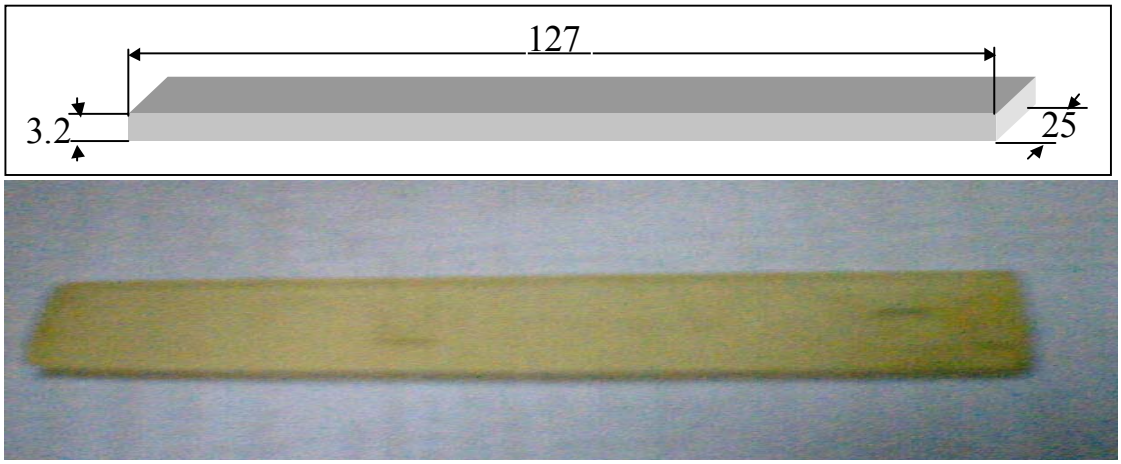

Figure 4-4 Matrix Flexural test specimens

Torsion test specimens are produced as a prismatic bar with a width 8mm, depth 6mm and length 130mm as shown in Fig. 4-5.

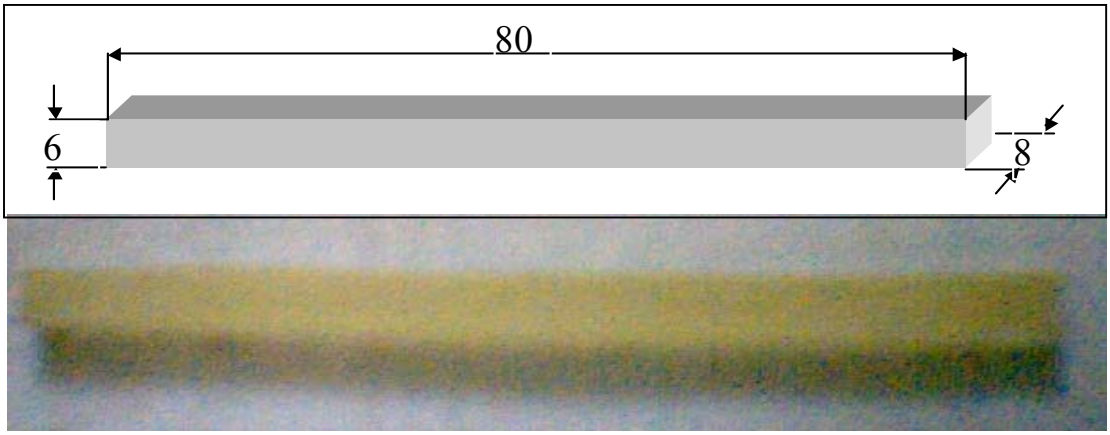

Figure 4-5 (a) Dimensions for torsion test specimen, (b) Photograph for pure and reinforced epoxy torsion test specimens.

(B) Composite plate samples

Plate strip specimens used in this investigation are fabricated from the fiber matrix plies, and symmetrical lay – up were prepared by using a 30*30cm ceramic open mold with x-ray photo sheet painted with wax film to avoid abrasive and inshore flattening as shown in the schematic arrangement of Fig 4-6. The molder applies a pigments “release” material to the mold, as the First step in making any open mold product. Without such material, the part will permanently bond to the mold surface.

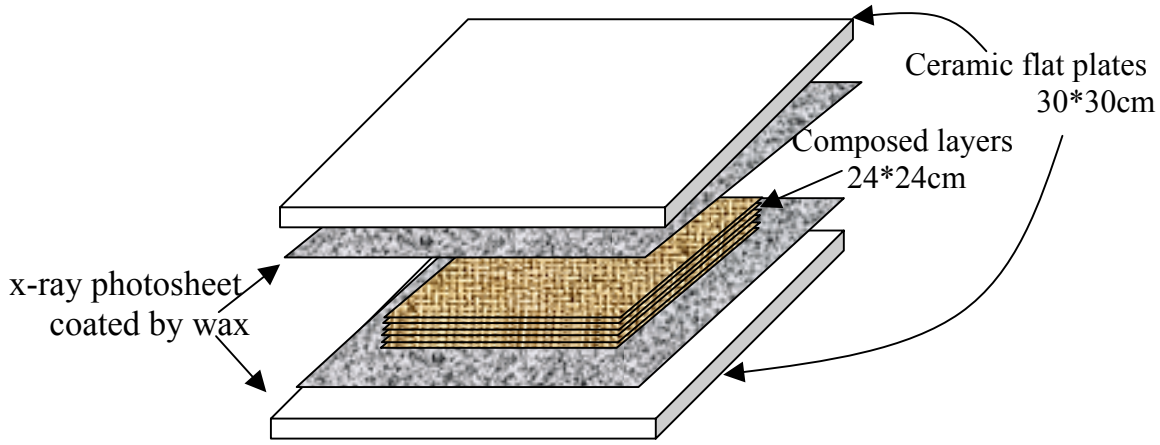

Figure 4-6 Schematic of mold of test specimen

Secondly, a pre – measured unsaturated polyester and catalyst (or matrix) are then thoroughly mixed together, and for ensuring complete air removal and wet out, it should cover the base surface completely especially at the end edges.

The Third step is the application of fiber in the resin layer, these woven or chopped fiber layer are put in the resin layer and with using brushes and rollers the fiber layer would saturated by resin, then another fiber sheet would be put and repeat the process until the end layer, the x-ray photo sheet coated with wax will cover the composite and with rolling over all layers to ensure complete air removal. When using polyester resin, the curing step of the specimens, which is a change of properties of the thermosetting resin by chemical reactions, this process forming a strong three- dimensional network thus, the cross- link structure is known as curing.. The curing step related to a curing temperature, and curing time; thus, the

specimens are cured according to the manufacture's recommendations, in a dryer oven for the recommend time and temperature according to are 8hr and 70 ^{0}C respectively[68].

The pressure applied through the forming of the specimens is optimized by trial and error to give approximate 60% fiber volume fraction, which is calculated from the mass fraction, the composite volume is equal to the summation of fiber and matrix volumes

$$V_c = V_F + V_M$$

Or

$$1 = v_F + v_M$$

where V and v represent the volume and volume fraction respectively, and subscripts C, F and M represent the composite, fibers and matrix respectively.

Form $V = m / \rho$ then

$$m_c / \rho_c = m_F / \rho_F + m_M / \rho_M$$

Where m and ρ are the mass and density respectively. The density of composite plate can be calculated from $\rho_c = m_c / V_c$, the mass of plate was measured using three digital electronic balance type.

The mass of fiber can be measured by multiplying the area of all layers times the mass per unit area (see Table 4-7) and the density of the fiber is from Tables (4-2 to 4-4), then the volume fraction of fiber will be calculated using

$$v_F = V_F / V_c = (m_F / \rho_F) / (V_c) \qquad \ldots(4.1)$$

Manual scissors, rotating grinding, and manual grinding are used to cut the plies for the lay-up. For the tensile specimens the patterns are necessary.

III) Test samples:

Three types of composite sample are used which are the tensile test specimens, friction disk specimens, and impact test specimens. Tensile tests are conducted according to the (ASTM D412) standard. The test specimens, shown in Fig 4-7 with strain gauge located at the center normal to the length to measure the lateral strains, any composite where stretches for two direction (principle, and 30^{o}) to evaluate the required tensile material properties.

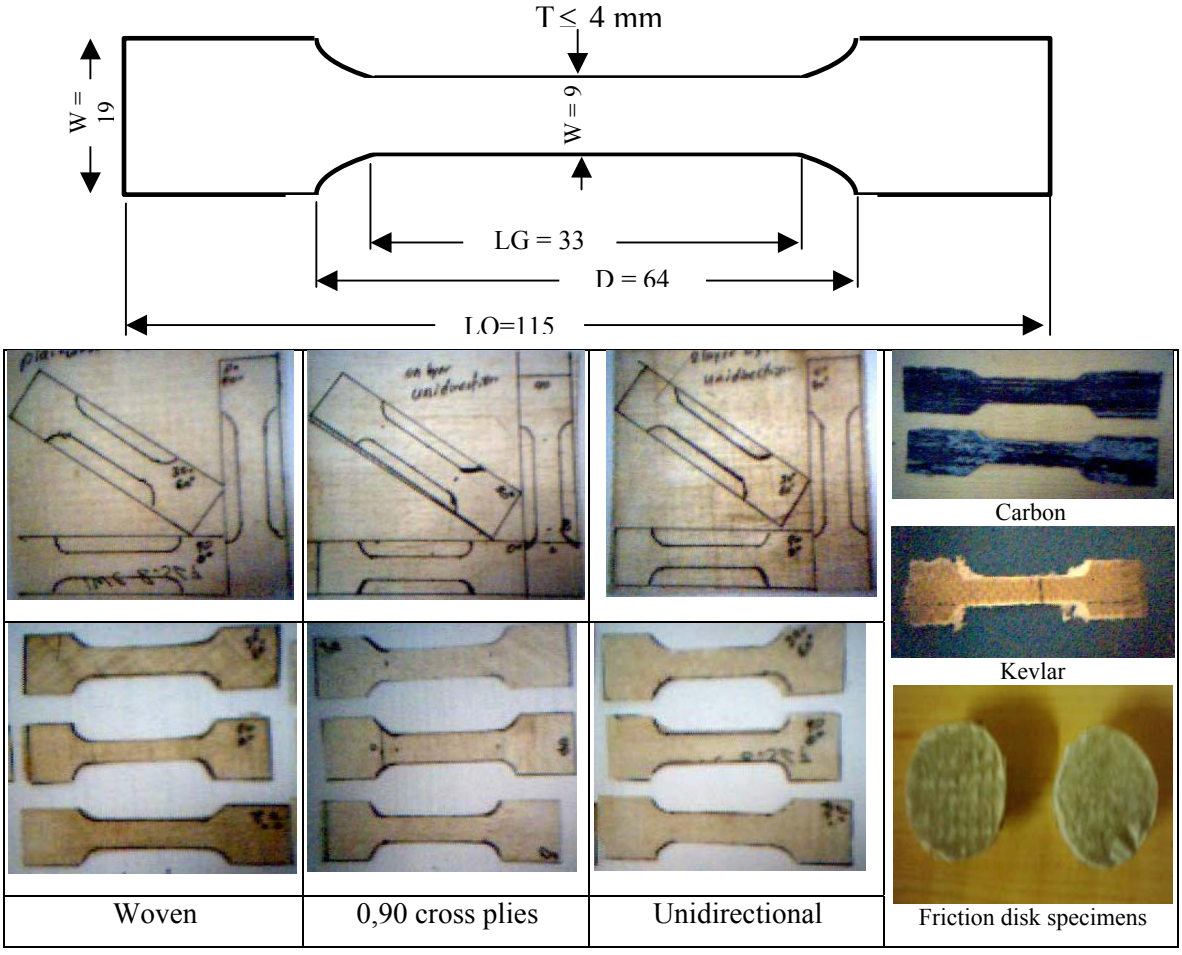

Figure 4-7 Some Specimens used for testing properties

4.3 Tests for mechanical properties

The mechanical properties for matrixes are measured using four tests (tensile, compression, bending, and torsion), while the mechanical properties of composites are measured using tensile and friction tests.

4.3.1 Tensile and compression tests:

The tensile and compression testing devices used are PHYWE, model D-3300, which has a maximum load 30kN that displayed by a digital display of a strain gage and measuring displacement using a dial gage as shown in Fig. 4-8. During tensile and compression tests a digital camera is used in order to record the force and displacement values in each moment to get more accuracy.

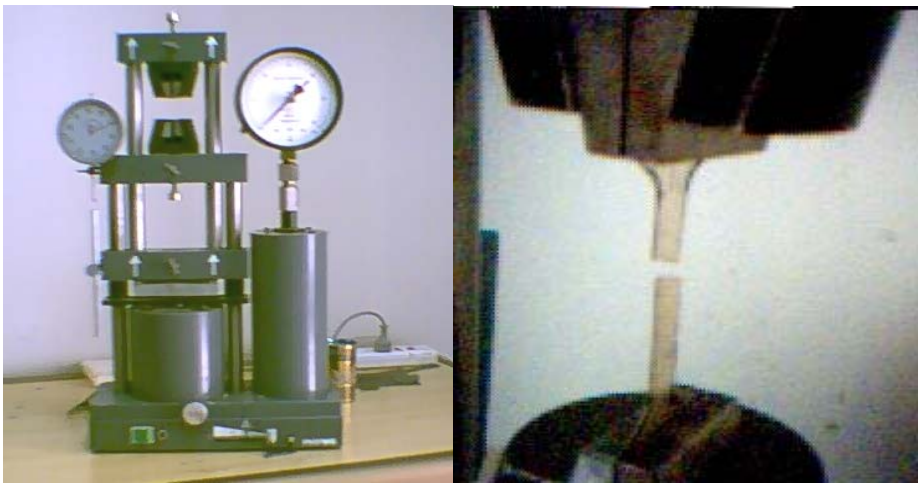

Figure 4-8 Tensile Testing device and fixation mechanism.

The tensile test was used for matrix and composite. The stress and strain normal to the load axis are $\sigma_L = F / A$, and $\varepsilon_L = \delta / LG$, while the lateral strain is recorded from strain gauge directly. The strain gauge used is Omega using quarter Bridge {Fig. 4-9} and 120Ω strain gauge prop was used. Then the Poisson's ratio can be determined using $\nu_{12} = -\varepsilon_T / \varepsilon_L$, the modulus of elasticity ($E_{11}=E_{22}$) and the ultimate tensile stress (σ_{ult}) are evaluated from the stress strain curves.

Figure 4-9 Micro Strain meter used in tensile tests.

For composite specimens the modulus of rigidity can be measured after knowing E_{11}, E_{22}, and ν_{12} and from E_{xx} evaluated from the tensile test of 30^0 specimens with m= cosθ, and n=sinθ and from elasticity relation for orthotropic lamina[64]

$$E_{xx} = E_{yy} = \left[\frac{m^4 + n^4}{E_{11}} + \left(\frac{1}{G_{12}} - \frac{2\nu_{12}}{E_{11}} \right) m^2 n^2 \right]^{-1} \quad \ldots(4.2)$$

The unique unknown is G_{12}, which can be calculated.

For using results for woven composite and the 0,90 composite the new woven multiplication factors W_E, W_G, and W_ν can be calculated from equation (3.12).

4.3.2 Friction test

Friction test is done using with friction disk apparatus type Sanderson which is shown in Fig. 4-10. Friction disks are in contact with a steel disk by pressing the disks at steel disk using a normal force at each side. The knowing of the values of Friction coefficient between the composite and steel is very important because of its need for the present theoretical work.

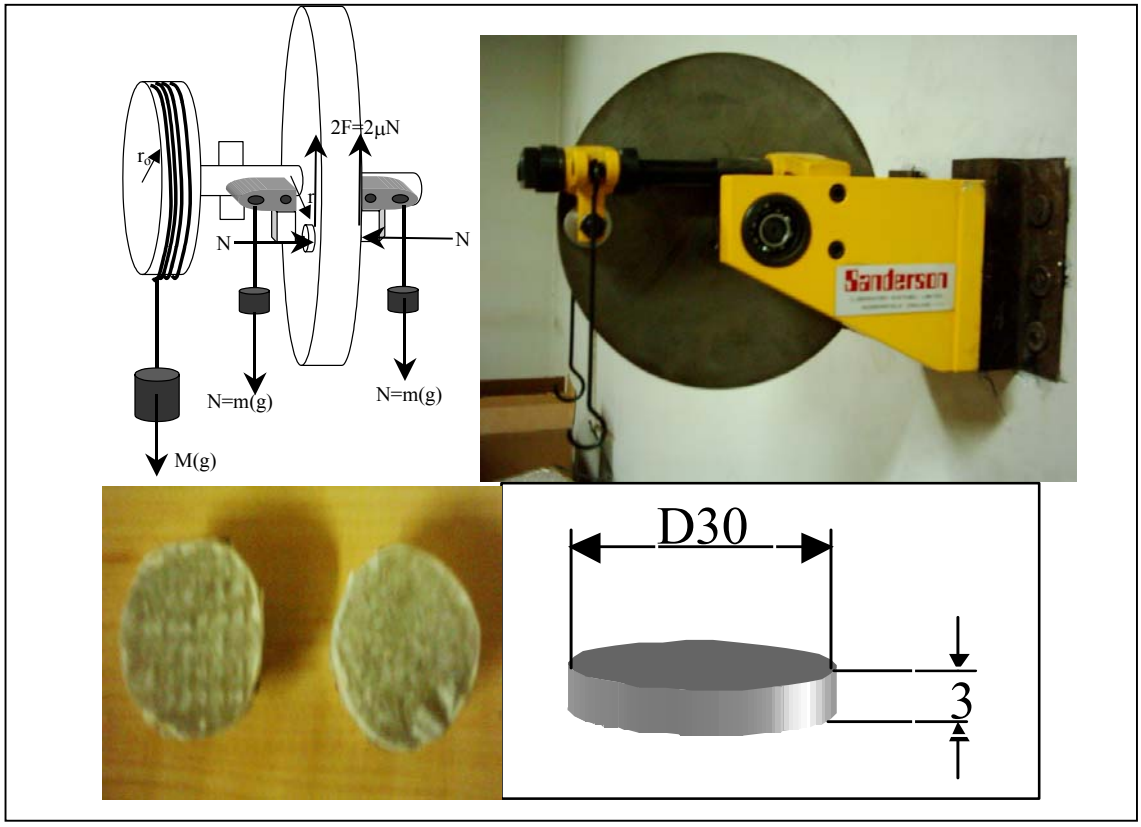

Figure 4-10 Friction testing device, the force equilibrium, and specimens

Weights are used to give impeding motion then the force equilibrium give relation ship

$$2\mu m g r = M g r_o$$

then

$$\mu = \frac{M g r_o}{2 m g r} \qquad \ldots(4.3)$$

The assumption that the type of fiber does not effect the coefficient of friction allow the ability of using one pair of the specimens for every matrix.

4.3.3 Torsion testing device: -

Torsion tests are carried out using Gunt Hamburg model WP500 device as shown in Fig. 4-11.

Torsion testing device is used for tests of pure matrix (epoxy and polyester) to find modulus of rigidity and maximum shear stress by displaying the torque directly from digital display of a strain gage for each twisting angle.

Figure 4-11 Torsion testing device

For rectangular shafts [Fig. 4-12], however, with longer side d and shorter side b, it can be shown by experiment that the maximum shearing stress occurs at the center of the longer side and is given by: -

$$\tau_{max} = \frac{T}{k_1 db^2} \qquad \ldots(4.4)$$

Where k_1 is a constant depending on the ratio d/b and given in table (4.6) below[69]: -

Table (4.6). Table of k_1 and k_2 values for rectangular sections in torsion [69]

d/b	1.0	1.5	1.75	2	2.5	3	4	6	8	10.0	∞
k_1	.208	.231	.239	.246	.258	.267	.282	.299	.307	.313	.333
k_2	.141	.196	.214	.299	.249	.263	.281	.299	.307	.313	.333

The essential difference between the shear stress distributions in circular and rectangular members is illustrated in Fig. 4-12, where the shear stress distribution along the major and minor axes of a rectangular section together with that along a

"radial" line to the corner of the section are indicated. The maximum shear stress is shown at the center of the longer side, as noted above, and the stress at the corner is zero.

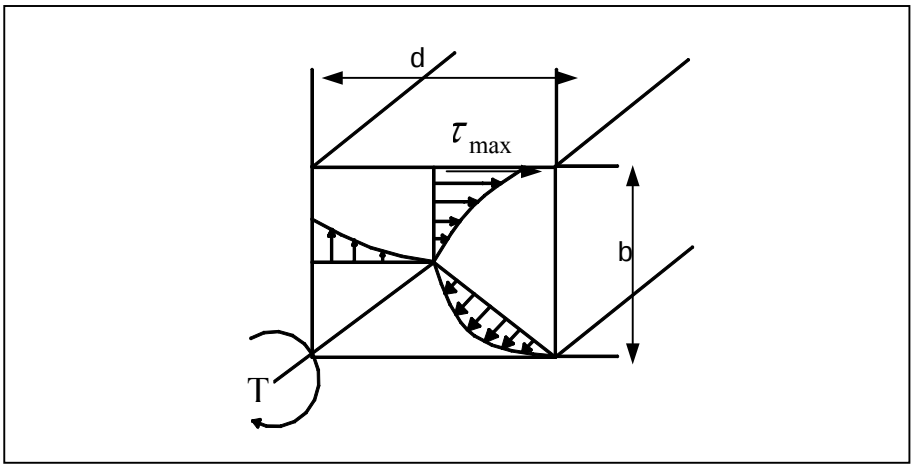

Figure 4-12 Shear stress distribution in a solid rectangular shaft.

$$\frac{\theta}{L} = \frac{T}{k_2 d b^3 G}$$

k_2 being another constant depending on the ratio d/b and also given in Table 4-5. In the absence of Table 4-5, however, it is possible to reduce the above equation to the following forms: -

$$\tau_{max} = \frac{T}{db^2}\left[3 + 1.8\frac{b}{d}\right] = \frac{T}{db^3}\left[3d + 1.8b\right] \qquad \ldots(4.5)$$

And

$$G = \frac{42TLJ}{\theta A^4} = \frac{42TLJ}{\theta d^4 b^4} \qquad \ldots(4.6)$$

where A is the cross section area of the section (=db) and $J = (bd/12)\left(b^2 + d^2\right)$.

4.3.4 Bending testing

Flexural testing device used is Sanderson type as shown in Fig. 4-13. Flexural testing specimen is being tested as a simply supported beam or built in beam that is loaded at any span from central point and can measure the deflection using a dial gage, which is fixed to the flexural testing device.

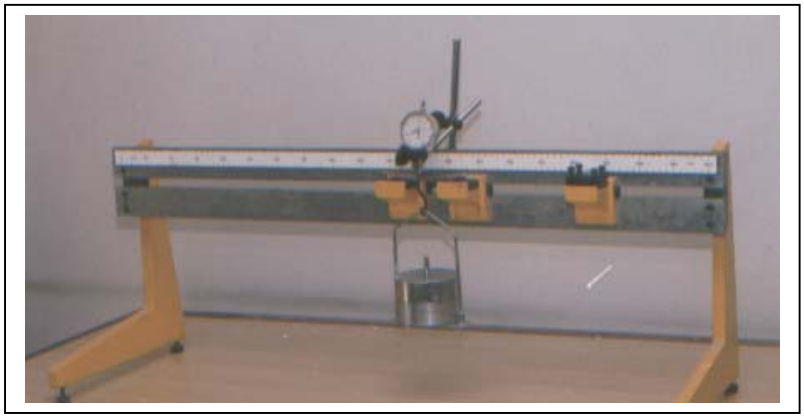

Figure 4-13 Flexural testing device.

Flexural strength can be defined as the ability of material to bent under an applied load. The study of flexural strength is very important especially for brittle materials that have low elastic bounds. For a beam that is shown in Fig. 4-14, the stress (σ) at a distance (y) from the neutral axis is related to the bending moment (M) and the second moment of area (I) of the beam section by $\sigma/y = M/I$ with three point loading,

$$M = \frac{FL}{4}.$$

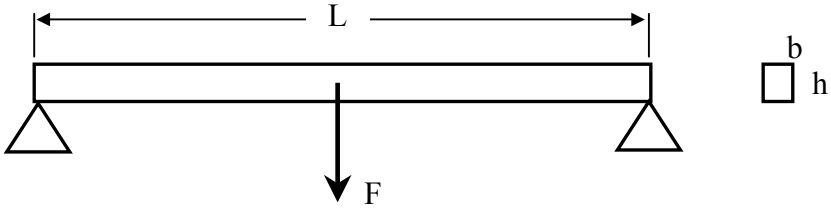

Figure 4-14 Bending test

The modulus of elasticity from the bending of the matrix material is

$$E = \frac{FL^3}{48yI} \qquad \ldots(4.7)$$

4.4 Impact Testing

The famous ballistic testing is the National Institute of Justice (NIJ) standards (MIL-STD-662E, NIJ Standard 0108.01) as shown in Fig. 4-15.

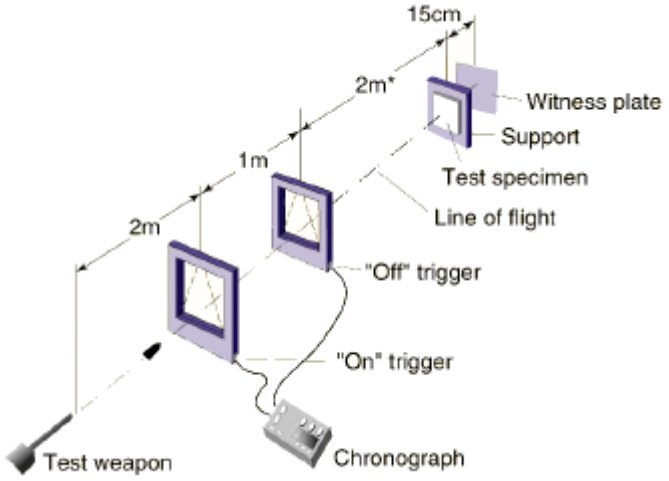

Figure 4-15 Ballistic testing {National Institute of Justice (NIJ) standards}[35]

These standards are widely used by government agencies and armor manufacturers for product acceptance testing. The energy absorption values for various hybrid configurations can be obtained using these standards. Due to the exploratory nature of the ballistic research, these test standards were chosen because they enable the user to gain an understanding of the aspects of how to improve the ballistic impact resistance of various systems without requiring a large amount of costly test samples. Also, these standards test for the maximum degree of damage a particular projectile. Testing according to these standards does, however, have their limitations. Because they are based on a limited amount of data points, it is difficult to acquire results with a good statistical significance. Also, the standards lack a method for obtaining dynamic information that may help to explain the impact event. Damage characterization is limited to energy absorption values and post impact inspection [35].

For tests with fully penetration (perforation), a second chronograph was used after the target to measure the resting velocity and evaluating the observed energy that was equal to the difference between the incidents and resting kinetic energies [9].

The new development through the building ballistic test of this work is the design and building a computerized chronograph not only to measure the after and before impact velocities but also to measure the approximate penetration time using the simplest method, specially, that the techniques used to measure the penetration time were very complex and expensive, additionally these techniques were covered with securities due to their military applications, and pointed to their with a fuzzy view through the searches.

The ballistic testing rig used in this work is shown schematically in Fig. 4-16

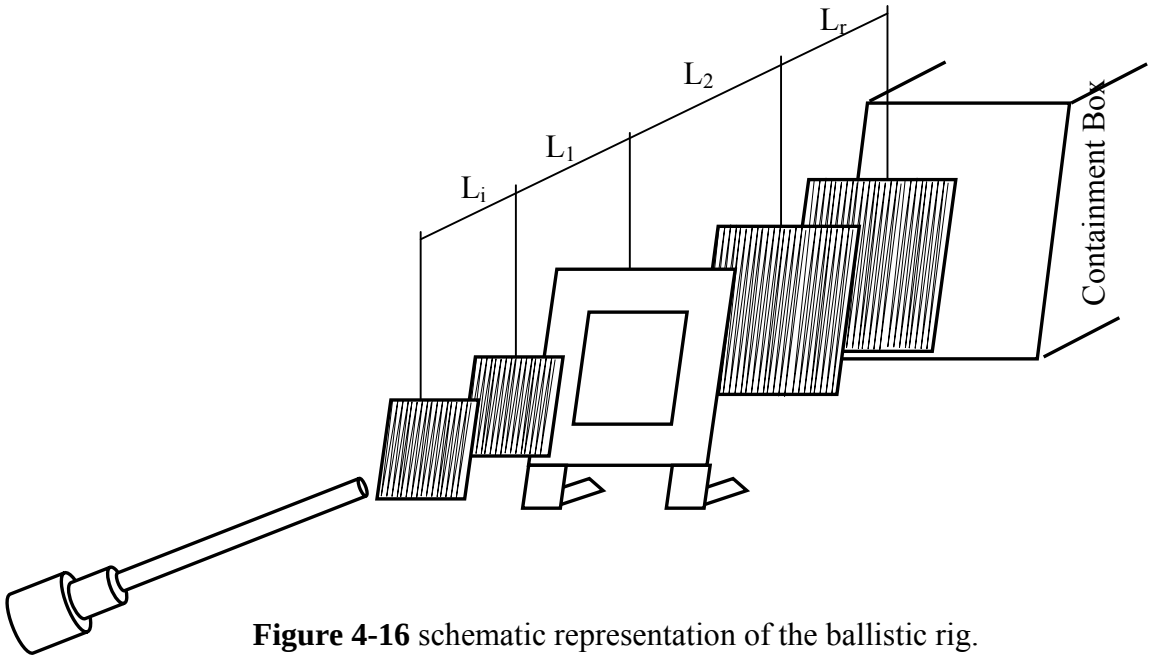

Figure 4-16 schematic representation of the ballistic rig.

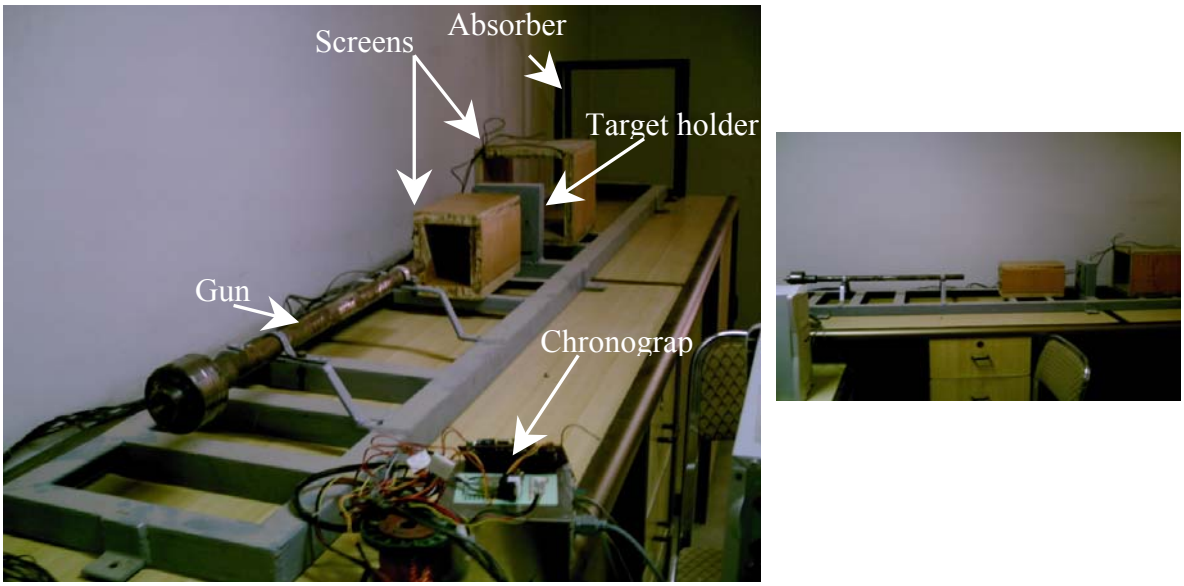

Figure 4-17 Photographic view of the present impact rig.

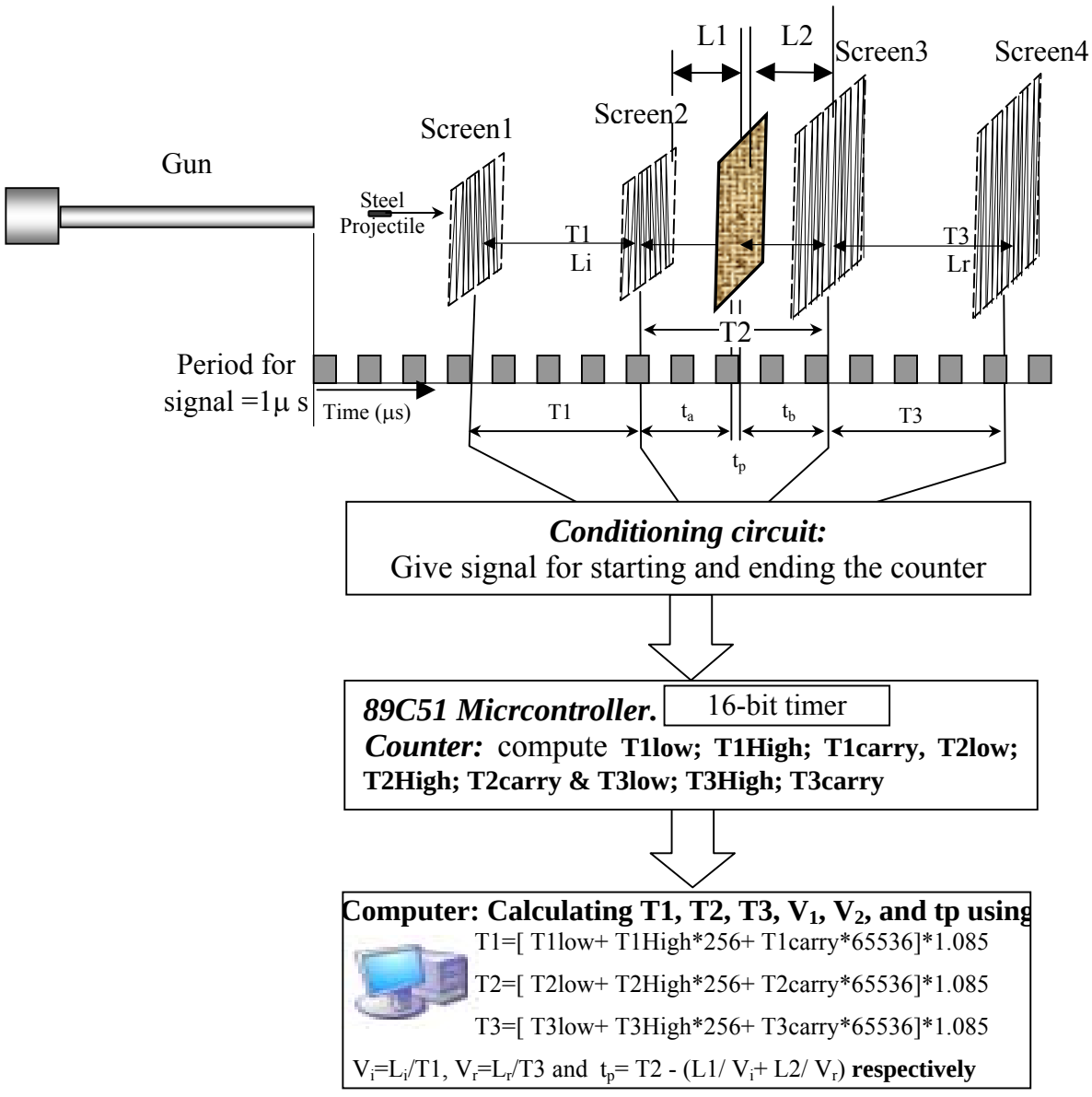

Figure 4-18 Block diagram represent the velocity measurement device.

Basically the rig consisted of 3*0.3m rigid frame constructed from 2*(1/8)" L beams to insure the rigidity as shown in Fig. 4-17. Two rigid clamped were welded to the front of the frame on which a gun barrel (7.85 mm), nominal bore and 750mm length was mounted. The composite chronograph was fixed behind the gun and the target holder was welded in location between the second and the third screen of the chronograph.

4.4.1 The Launching Gun

The Launching Gun used for tests was constructed and designed earlier by Salah [70]. Briefly, the basic design feature are, a smoothbore gun barrel of 7.85mm nominal internal diameter and 750mm length giving L/D ratio of approximate 95.5. The smooth bore enable the use of the gun to propel rigid projectile of any head shape. Moreover, the cartridge housing situated at the end of the gun was constructed so as to accommodate many kinds of powder gun cartridge. This capability enable accelerating the projectile to velocity rang from (60m/s to 900m/s). Finally, the materials and dimensions were chosen so as to withstand internal pressure as high as 3000bars resulting from detonation of the powder gun charge.

The main construction items of the gun are:-

(a) The gun barrel: A long cylinder made of special treated alloy steel with 27mm outer diameter and 7.85mm bore, one of the barrels end was threaded externally to be fastened to the envelope housing.

(b) The cartage envelope: a steel cylinder of 27mm outside diameter and 55mm length, the inside configuration was machined so as to envelop the two types of cartridge used in this work

(c) The envelope housing: A hollow steel structure with an internal thread at one end through which it is fastened to the gun barrel. The other end is specially

designed to be securely joined to the breach while the inside bore holds the cartridge envelope.

(d) The breech: made to be joined to the envelope housing at one end and to carry the firing pin at the other.

(e) The firing pin: with conical head configuration suited for the capsule initiated cartridges.

The gun is mounted on two clamps and firmly secured by bolts and nuts. The lower parts of these clamps are welded to a steel structure that is fixed to the test rigs base.

4.4.2 Experimental Setup

The test specimens are rigidly clamped between two steel frames. Bolts at the corners and mid-sections of the steel frame are tightened to insure a rigid mount on all four edges of the test specimen. A 10 mm of material is clamped around the perimeter of the test specimens. These two steel frames were attached to a support structure. The test specimen is perpendicular to the line of flight of the bullet at the point of impact.

4.4.3 Velocity measurements

The basic criterion of the velocity- measuring unit is to measure the time interval that takes the projectile to cross a pre- determined distance Fig. 4-18 shows a block diagram of the unit that has provision for the measurement of the initial, as well as the post-perforation, velocities of the projectile.

Evidently, the unit consists of two identical measurement groups; each group is integrated from the following elements:

(a) Two wire grid break circuits (screen), as apparent in Fig. 4-17, (0.2 mm) diameter wire, with one end of the wire connected to appositive power supply, while the other is connected to earth, is wound in zigzag pattern around lines of nails fixed in a wooden frame. The wooden frames of the initial velocity measuring grids are of (100*100) mm dimensions while the un-predictable post-perforation deviation in the projectile's path necessitated larger frames (200*200) mm. However, the distance between two successive grids is kept (300) mm.

(b) Signal processing circuit, Fig. 4-19 shows the electronic circuit used for processing the electrical signal that is generated as the projectile cuts the wire grid breaks the circuits as it passes through it.

(c) Electronic digital clock circuit, a (4MHz) crystal quartz oscillator generates a series of equally timed pulses.

Basically, the projectile velocity may be obtained by dividing the distance between two consecutive wire grids by the time period taken to cross it.

Moreover, the use of wire grids provided means to register the projectiles post-perforation yaw and pitch angles and the real distance it traveled.

89C51 controller uses its 16 bit internal timer to measure three time intervals T1, T2, T3, and then sends the results to the computer through serial link (RS-232), the velocity can be then calculated by this equation:-

$$v = \frac{\text{displacement}}{\text{time}}$$

16-bit timer has two registers TL (lowbyte), TH (highbyte). Each frame contain 9 bytes as follows

T1low; T1High; T1carry

T2low; T2High; T2carry

T3low; T3High; T3carry

Time interval is calculated using this relation: -

T1=[T1low+ T1High*256+ T1carry*65536]*1.085

T2=[T2low+ T2High*256+ T2carry*65536]*1.085

T3=[T3low+ T3High*256+ T3carry*65536]*1.085

Circuit diagram of the chronograph is shown in Fig. 4-19

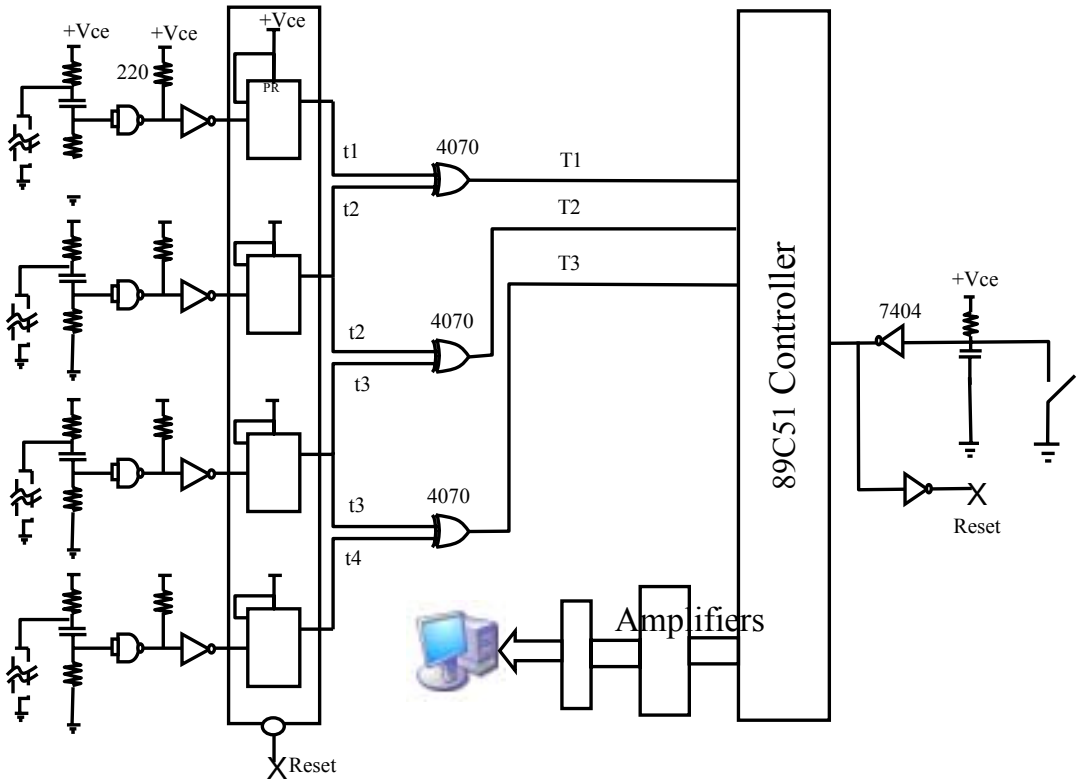

Figure 4-19 Electronic circuit of the velocity-measuring device.

For this circuit the time table is shown in Fig. 4-20

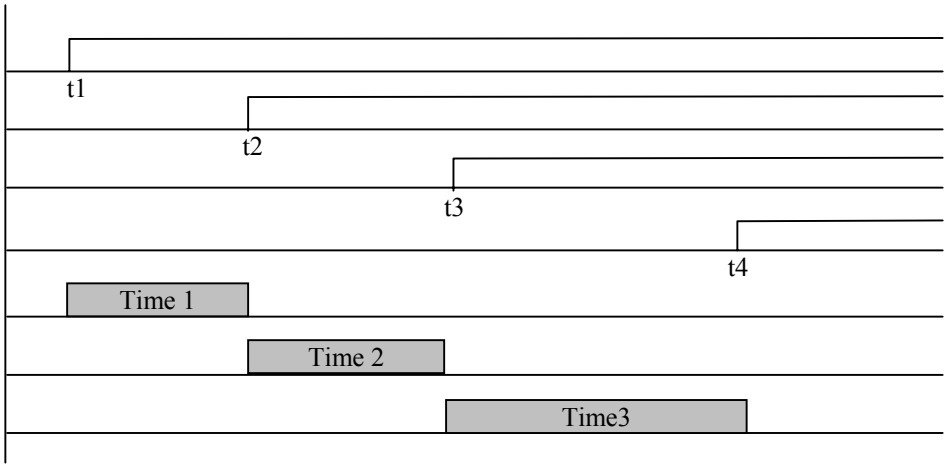

Figure 4-20 Timetable of output for the velocity-measuring device

Then the incident velocity and resting velocity will equal

$V_i = 0.3/(T1)$

$V_r = 0.3/(T3)$

To evaluate the approximate penetration time assuming that the velocity remaining constant through crossing the incident and resting screen then the time interval between the incident screen end and the target is then

$t_b = L1/V_i$

and the time interval just after impact to the start of the resting screen is then

$t_a = L2/V_r$

then the approximate penetration time becomes

$t_p = T2 - (t_b + t_a)$

A problem appears when practical implementations begin, the process of measuring the time requires sequential activation of the sensors, so if for some reason one of the sensors couldn't be activated this will lead the controller to enter an endless loop waiting the inactivated sensor to be activated, to avoid such problem, a time out solution had been used to wait for 65535 μsec.

4.4.4 The target holder

The universal holder used for normal impact of all targets used in this work consists of the following parts:

(a) A back steel plate whose dimensions are (120*120 mm). Four M6 bolts are welded to the four corners of the plate, and the plate has a (80mm) diameter hole centrally located. The back plate is held in its position within the rig through two L shaped steel supports welded to the backing plate at one side and screwed to the overall structure at the other.

(b) A clamping plate is made of steel with the same basic dimensions of the backing plate. The plate is further drilled with four (6mm) holes at each corner and an (80 mm) diameter central hole in a way that coincides with the corner- welded bolts and the central hole of the backing plate.

The targets are held in place by inserting them between the two plates. Tightening a nut at each corner bolt provides the clamping action needed to secure these targets, the holder assemble is fixed within the rig so as it's center-line coincides with the axis of the gun barrel.

4.4.5 The Frame

All of the rig's components were rigidly welded to a steel frame made of 2″ L beam to insure the rigidity. A steel hammer was used to strike the firing pin, thus blowing cut the cartridge charge.

4.4.6 Projectiles Material and Preparation

Projectiles are machined from steel shaft used in copier feeder with 70 to 73 BHN Five basic configuration projectiles are used in this work, namely the flat ended and the conical nosed with different cone angles, all types have the same shank diameter of (7.8) mm and of (20mm) total length. However, the flat ended projectiles weighted about (8.7g), all ends are ground so as to maintain high flatness surface. Meanwhile, the conical nosed projectiles are further machined to form the (60^0) apex angle thus the weight was reduced to about (7.5g)

4.4.7 The Cartridges:

Two main cartridge types are used according to the velocity range to which the projectile is accelerated. For velocity ranging from 100m/s to 350 m/s, four groups of commercially available cartridges, supplied by HILTI, of low explosive are used. The second type is the (7.62*54mm) sniper's gun cartridge supplied by Al-Yarmouk Company. The original ogival lead bullets are removed and replaced by the projectiles used in this work and by varying the amount of gunpowder; projectiles are accelerated up to (700m/s) velocity.

Chapter Five

Results and Discussions

5.1 Introduction

The results of the theoretical model and the experimental work are listed and discussed in this chapter. The parameters used in the model were studied to show their effects and limitations. The energy absorbed is divided into multi types as derived in Chapter Three. The numerical values for the energies are calculated to find the fraction of every type of these energies. Different types of composites are used to study the effect of composite properties on the absorbing energy and the fractions of their types.

The experimental results comprise the mechanical properties of the matrix and composites and the impact tests results. The mechanical properties of polyester and epoxy are measured to be used for the delamination model used in the theory. While the mechanical properties of composites are measured to be used in the elastic deformation, penetration, of the model.

The impact test results are listed for different composite materials, thicknesses, velocities of impact, and projectile shapes. Using the mechanical properties of the matrices and composites, the impact at the theoretical model is utilized, to check the model and formulate the comparison with the present experimental results.

5.2 Mechanical properties

5.2.1 Matrices

The mechanical properties of the matrices (epoxy and polyester) are found using the tensile, compression and torsion tests. The results of these tests are shown

in Figures 5-1 to 5-3, while their evaluated properties from these tests are listed in Table 5-1.

It has been shown that the epoxy resin used is equivalent to the epoxy casting resin, no filler at 25°C[2]. The polyester resin used is equivalent to the cast polyester neat resin [2]. It has been shown that the epoxy resin has more strength and higher modulus than the polyester resin, this behavior is known because of the chemical composition bond in the epoxy, which gives longer chains and network for its chemical structure. This explains the instability in the epoxy as shown in Fig. 5-1, while the polyester does not show that, but failure took place at the upper limit of the load.

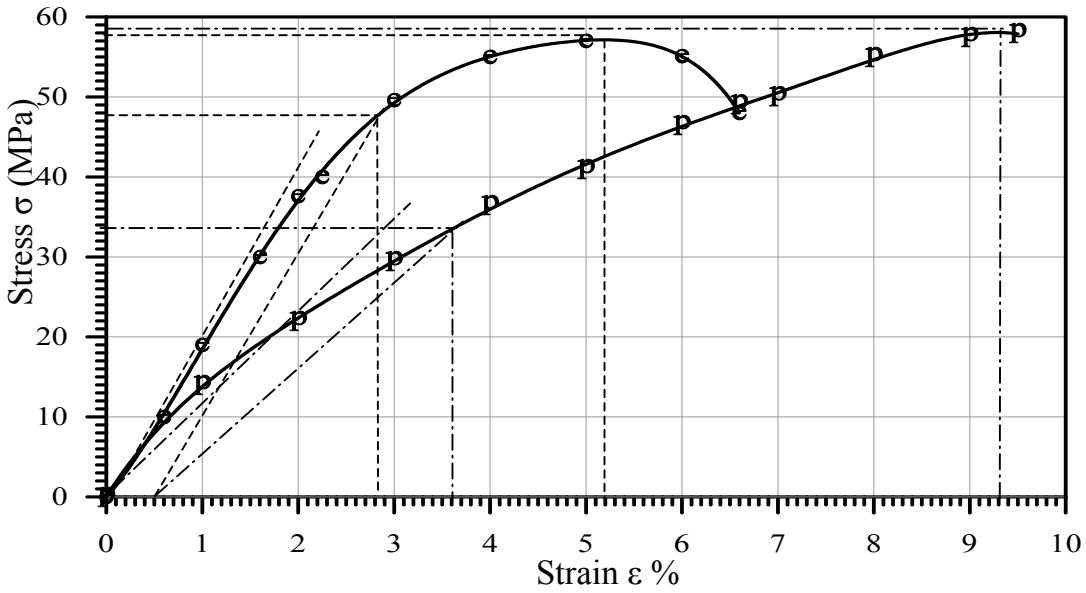

Figure 5-1 Experimental tensile Stress-Strain curves for polyester (p) and epoxy (e) tensile test (Tensile speed = 3mm/min).

The compression stress strain curves in Fig. 5-2 show that the epoxy resin has greater compression modulus and smaller ultimate compression strength than the polyester resin and these results are in agreement with published results [2].

Because of the assumption that the resins are isotropic, then the modulus of rigidity is beneficial to evaluate the Poisson's ratio for the resins and the ultimate shear strength. This is important to predict the ultimate tensile strength in the delamination failure criteria, which is used in the theoretical part of the thesis.

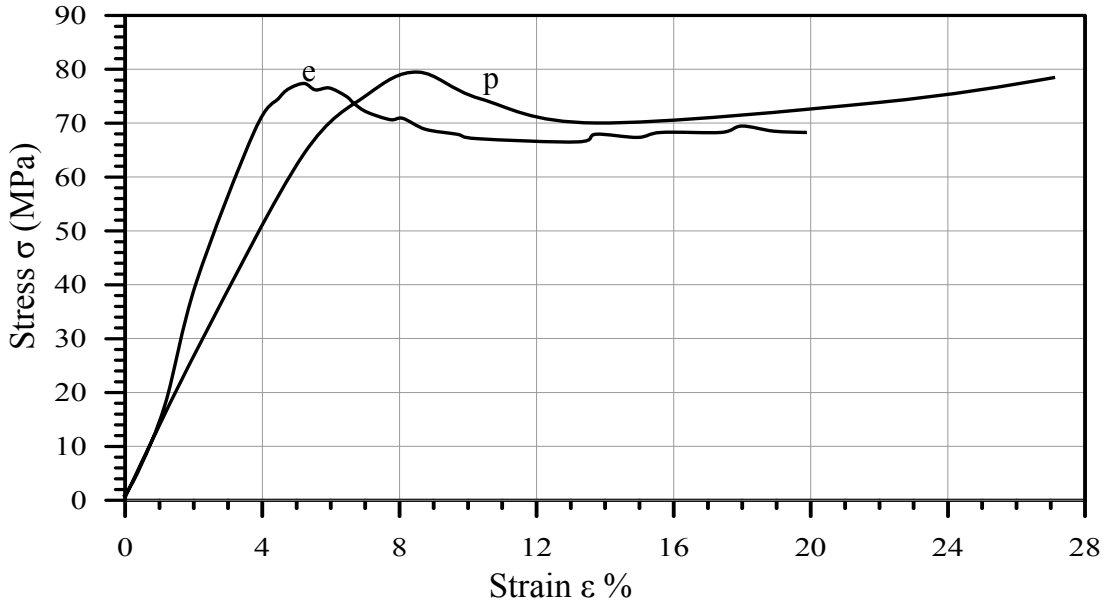

Figure 5-2 Experimental compression Stress-Strain curves for polyester (p) and epoxy (e), Compression test (Compression speed = 3mm/min).

Figure 5-3 shows the shear stress and the shear strain relations for the resins used. In general the ability of resin in the shearing load relative to tensile load is greater than the metallic materials. This appears clearly for the epoxy resin and less in the polyester resins.

The summary of the mechanical properties for the epoxy and the polyester are shown in table (5.1).

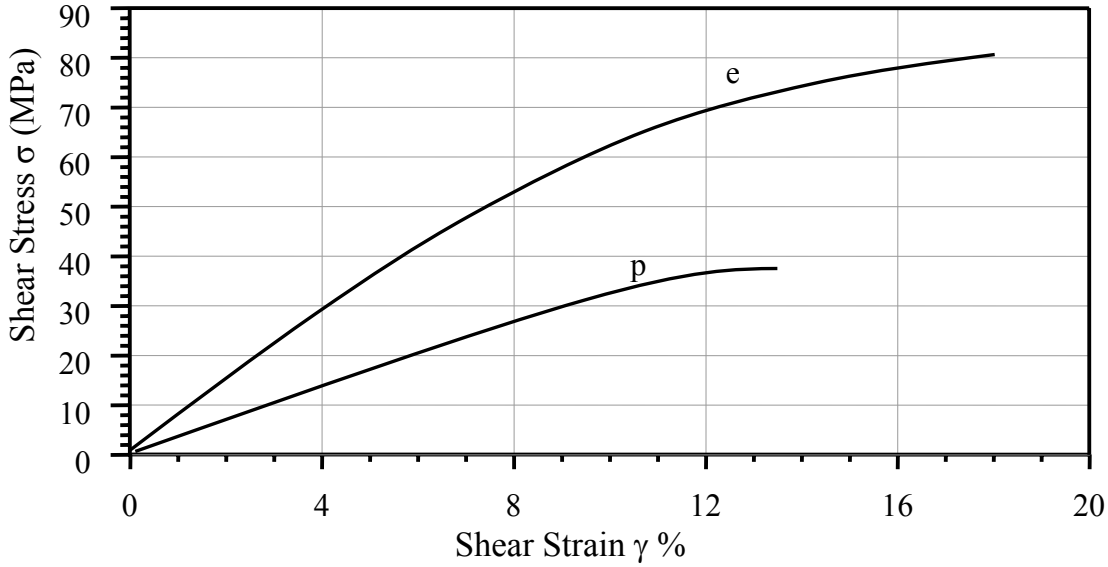

Figure 5-3 Experimental Shear Stress- Shear Strain curves for polyester (p) and epoxy (e), Torsion test.

Table 5-1 The measured mechanical properties for matrixes.

Test →	Tensile				Compression		Bending	Torsion			
Matrix ↓	E_t (MPa)	σ_{Yt} (MPa)	σ_{ult} (MPa)	ε_F (%)	E_c (MPa)	σ_{Yc} (MPa)	E_b (MPa)	G (MPa)	τ_{ult} (MPa)	γ_F (%)	ν
Polyester (p)	933	33.8	58.5	9.4	1276	79.2	1352	324	37.2	13.4	0.44
Epoxy (e)	1714	47.7	57.6	5.2	1875	76	2563	620	80.6	17.9	0.382

5.2.2 Composites

Two types of tests are used for evaluating the mechanical properties of the composites, which are the tensile tests and the friction test. The stress-strain curve for the tensile tests are shown in Figures 5-4 to 5-13. The figures (a) represent the tensile test in the direction of the fiber, with a strain gauge to measure the lateral strain and the Poisson's ratio. While the figures (b) represents the tensile tests in the (30^o) inclination angle with the fiber direction to evaluate the modulus of rigidity of the composites.

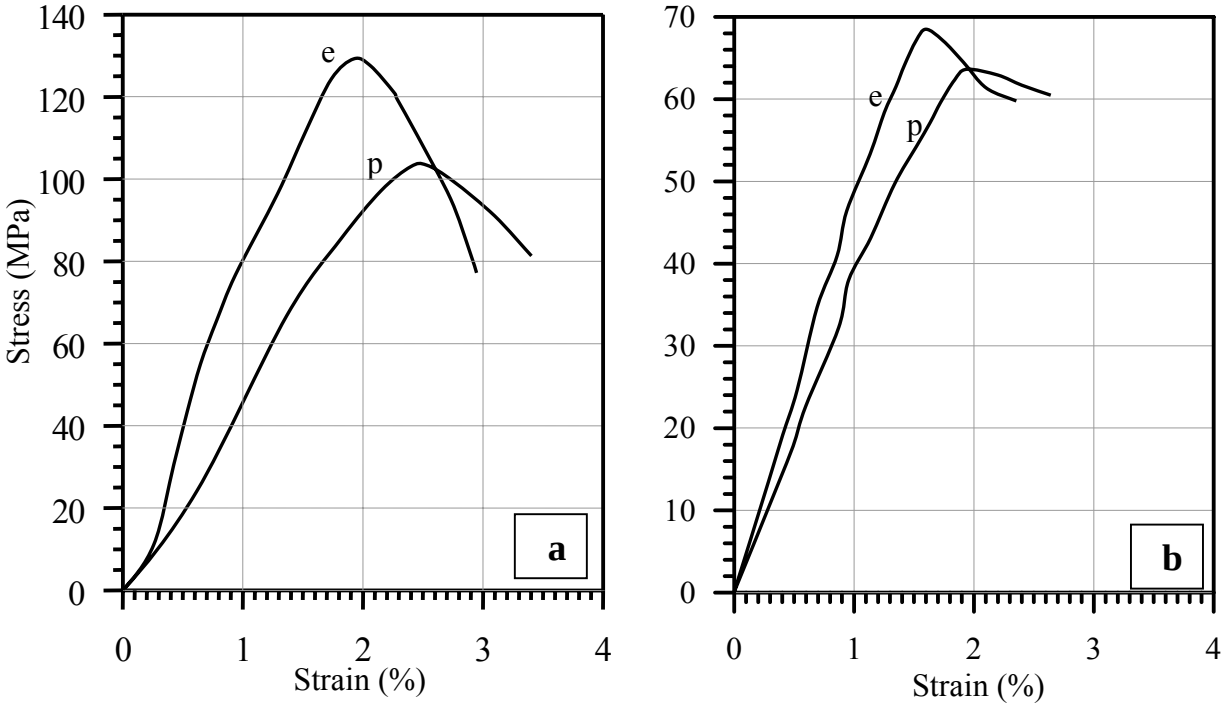

Figure 5.4 Tensile stress-strain curves for 0-90 carbon reinforced {polyester (p) and epoxy (e). a) 0^o, b) 30^o

It is clear that there is an effect of the mechanical properties of the matrix type on the overall properties for the composite ply. This effect is decreased as the properties of the fiber increase as in the stress strain curve for Kevlar reinforcement shown in Fig. 5-6.

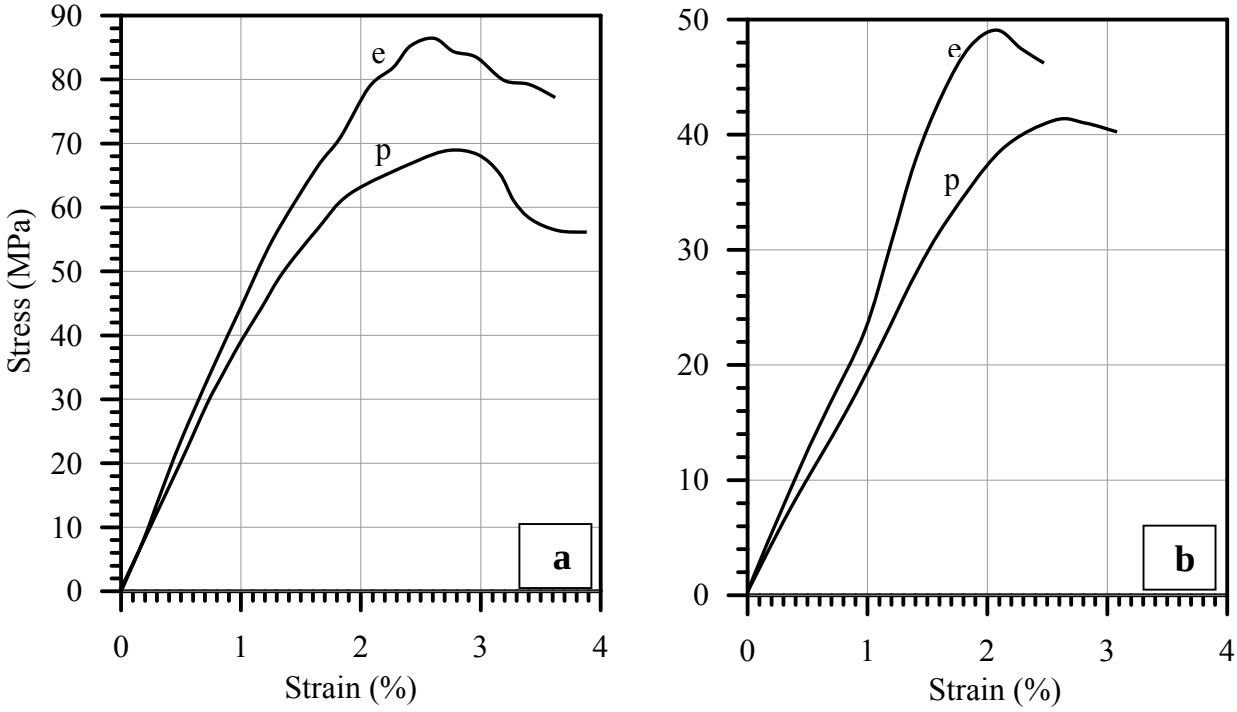

Figure 5-5 Tensile stress-strain curves for 0-90 E-glass reinforced {polyester (p) and epoxy (e). a) 0^o, b) 30^o

The evaluations of the weave factors derived in the theory are needed to measure the mechanical properties of the woven composite. The stress strain relations for the tensile tests of the different weave structure of the fibers are shown in figures {5-7 to 5-13}. The same effects of the matrix types are found as shown in Fig. 5-7, for this reason and because of the lower cost of the polyester resin it has been used for other types of woven fiber composites.

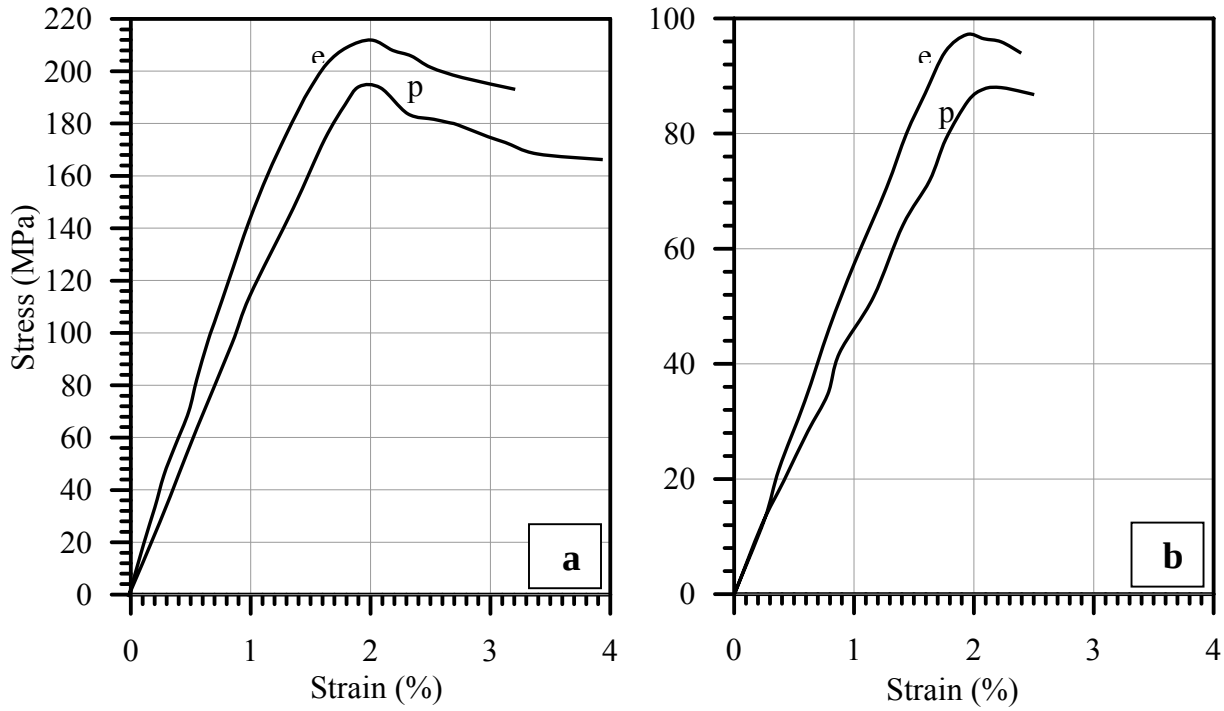

Figure 5-6 Tensile stress-strain curves for 0-90 Kevlar reinforced {polyester (p) and epoxy (e). a) 0^o, b) 30^o

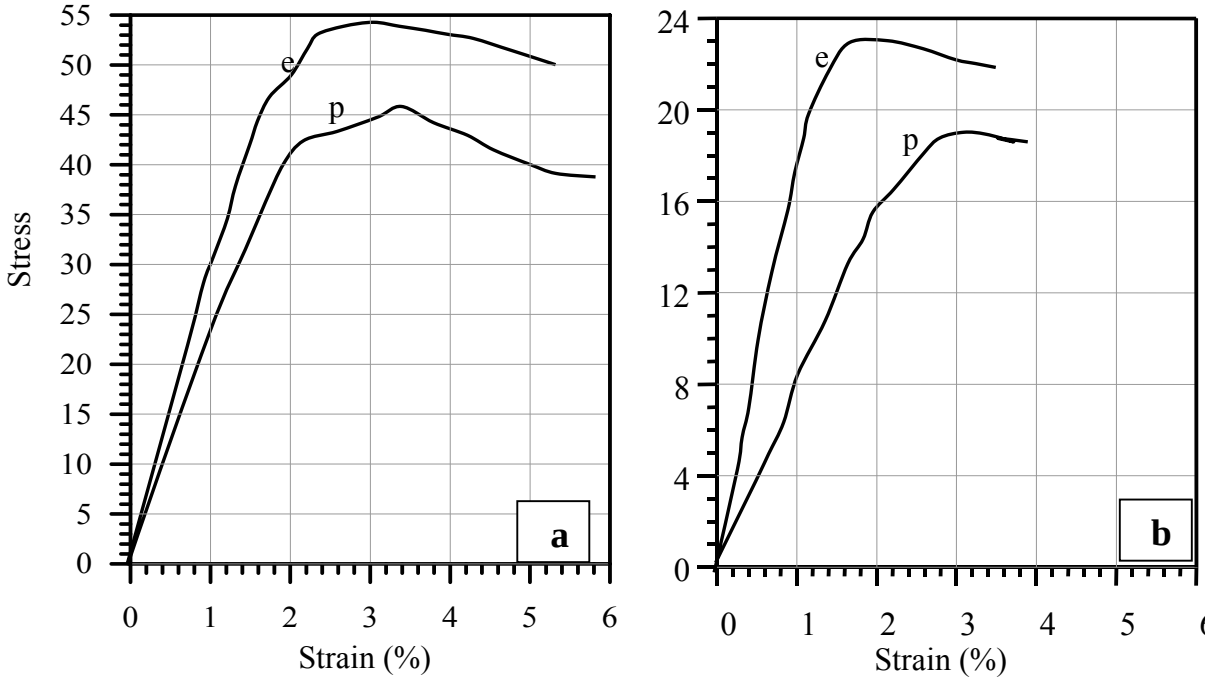

Figure 5-7 Tensile stress-strain curves for plain-woven E-glass fiber (2.5*2.5) reinforced {polyester (p) and epoxy (e)}. a) 0^o, b) 30^o

It was shown that the epoxy matrix not only gives higher properties than polyester but also give large woven factors. This is because of its higher properties.

The composite properties are affected directly with the fiber properties. This causes the largest properties for the Kevlar fiber composite shown in Fig. 5-13 and less for the carbon fiber composites {figures (5-11 and 5-12)} and the lowest in the glass fiber composites {figures (5-8 and 5-11)}.

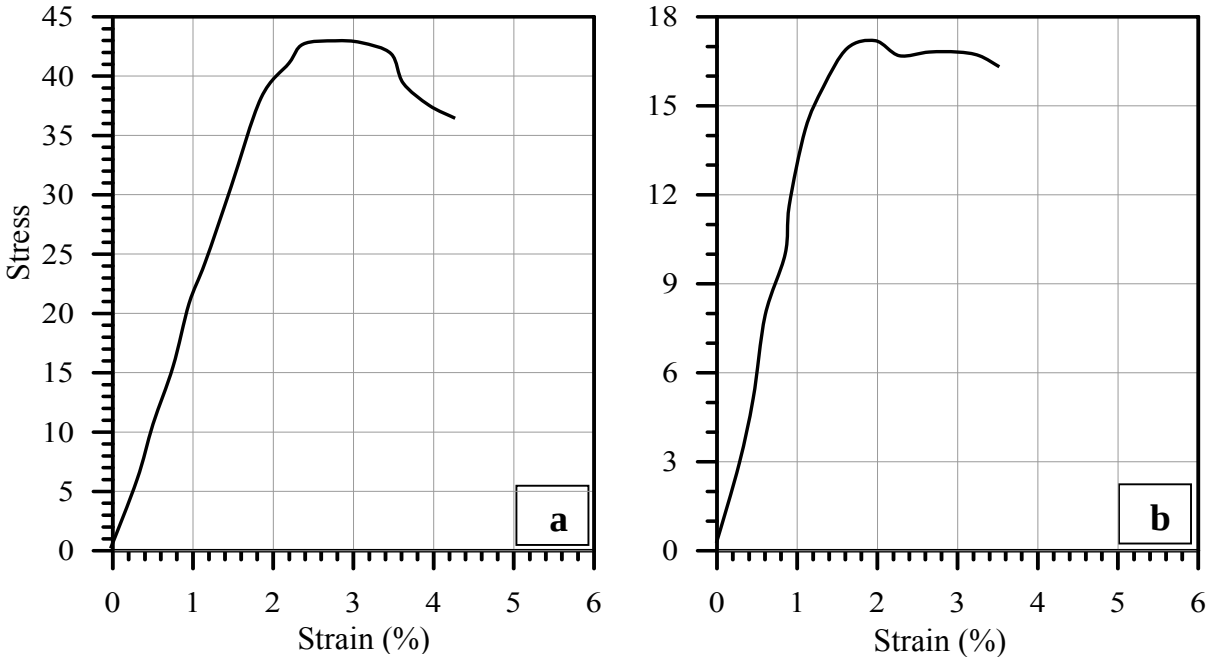

Figure 5-8 Tensile stress-strain curves for plain-woven E-glass fiber (12.5*12.5) reinforced polyester. a) 0^o, b) 30^o

The study of the woven style has an affecting factor on the fiber composite properties as shown in figures {5-7 to 5-10}, the meshing size effect is shown in Fig. 5-7 and Fig. 5-8. It has been shown that the greatest mesh size {Fig. 5-7} gives larger Young's modulus and higher tensile strength than the low mesh {Fig. 5-8}. This is due to the longer consolidation through the weave for the largest mesh size. In addition the largest mesh size gives lower number of the fiber bends.

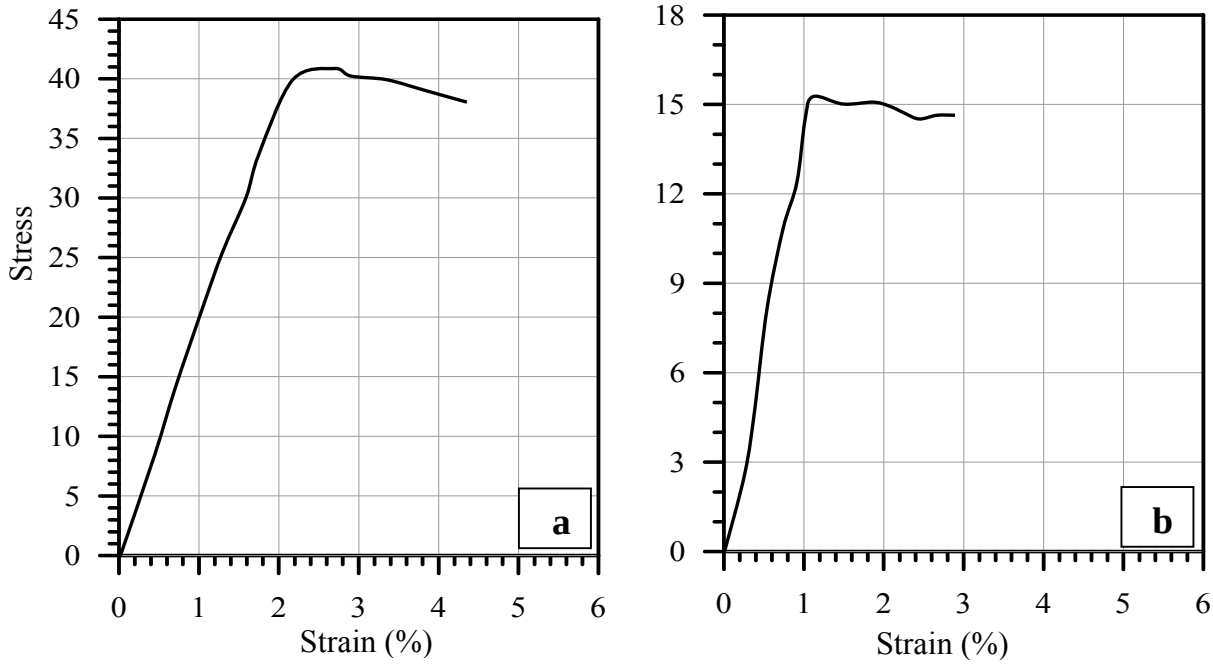

Figure 5-9 Tensile stress-strain curves for 5-end satin woven E-glass fiber (5*5)) reinforced polyester. a) 0^o, b) 30^o

The chopped random E-glass has the stress strain relation shown in Fig. 5-10, the random fiber was not needed to find its modulus of rigidity using inclination tensile test because of it isotropic behavior.

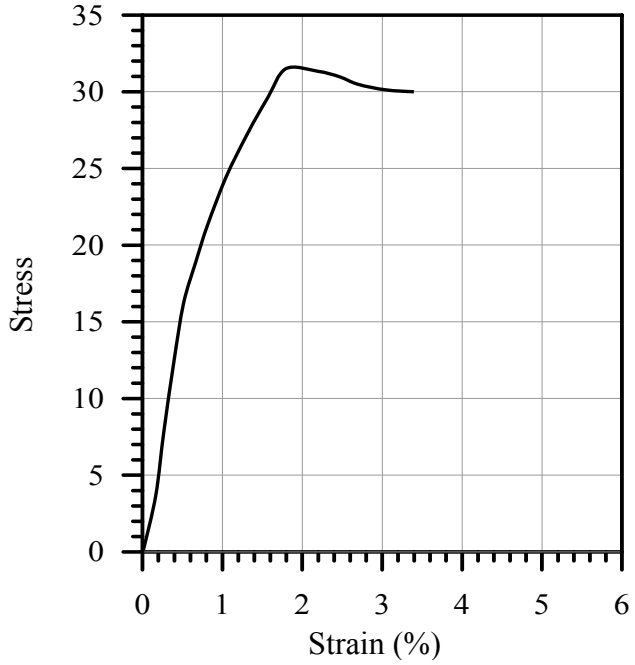

Figure 5- 10 Tensile stress-strain curves for random chopped E-glass fiber reinforced polyester

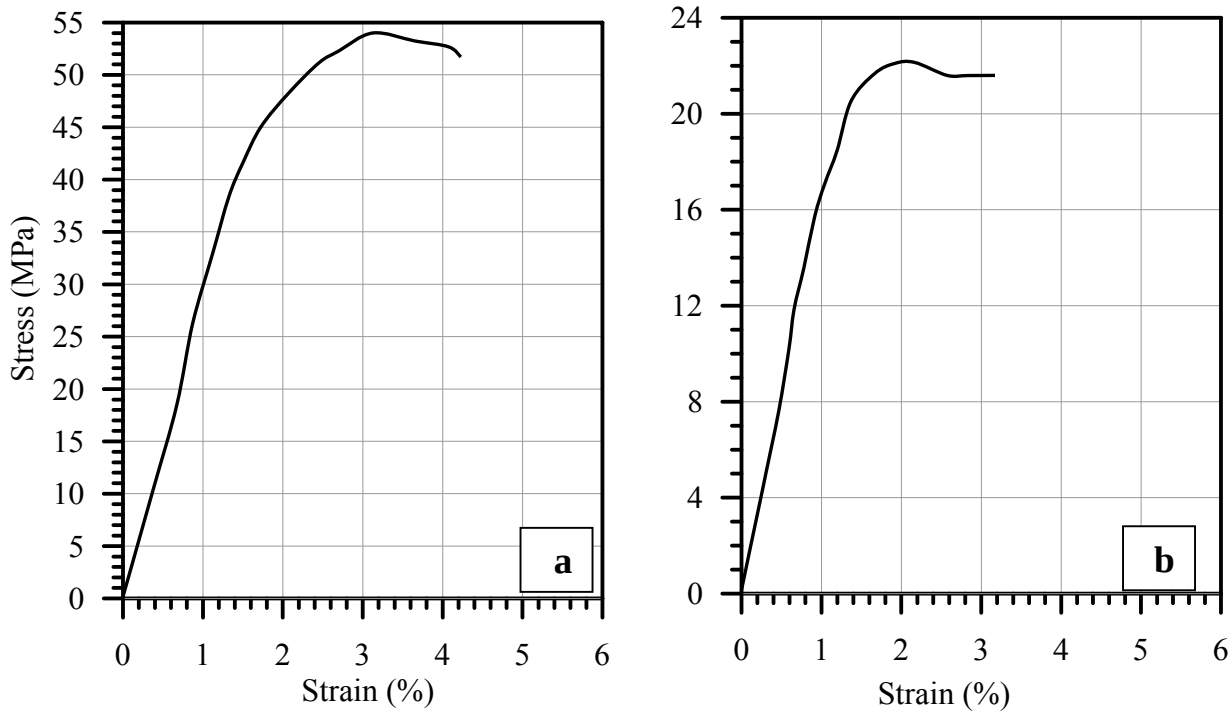

Figure 5-11 Tensile stress-strain curves for plain-woven carbon fiber reinforced polyester. a) 0^o, b) 30^o

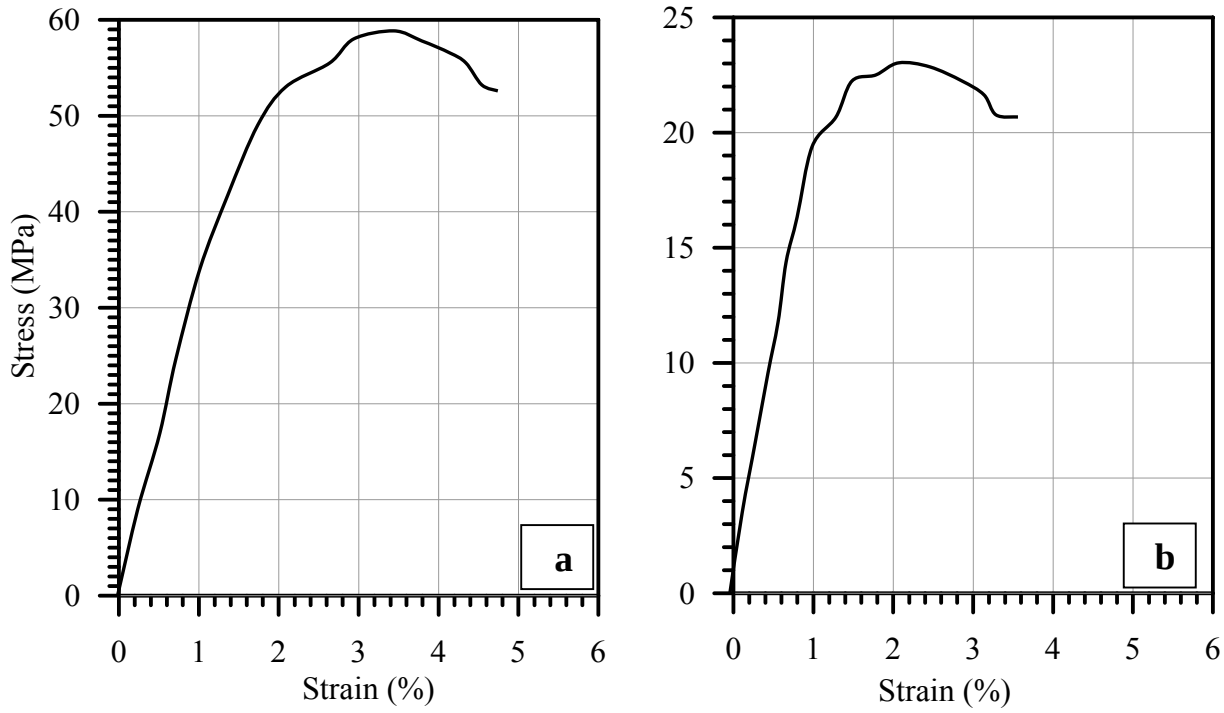

Figure 5-12 Tensile stress-strain curves for 5-end satin woven carbon fiber reinforced polyester. a) 0^o, b) 30^o

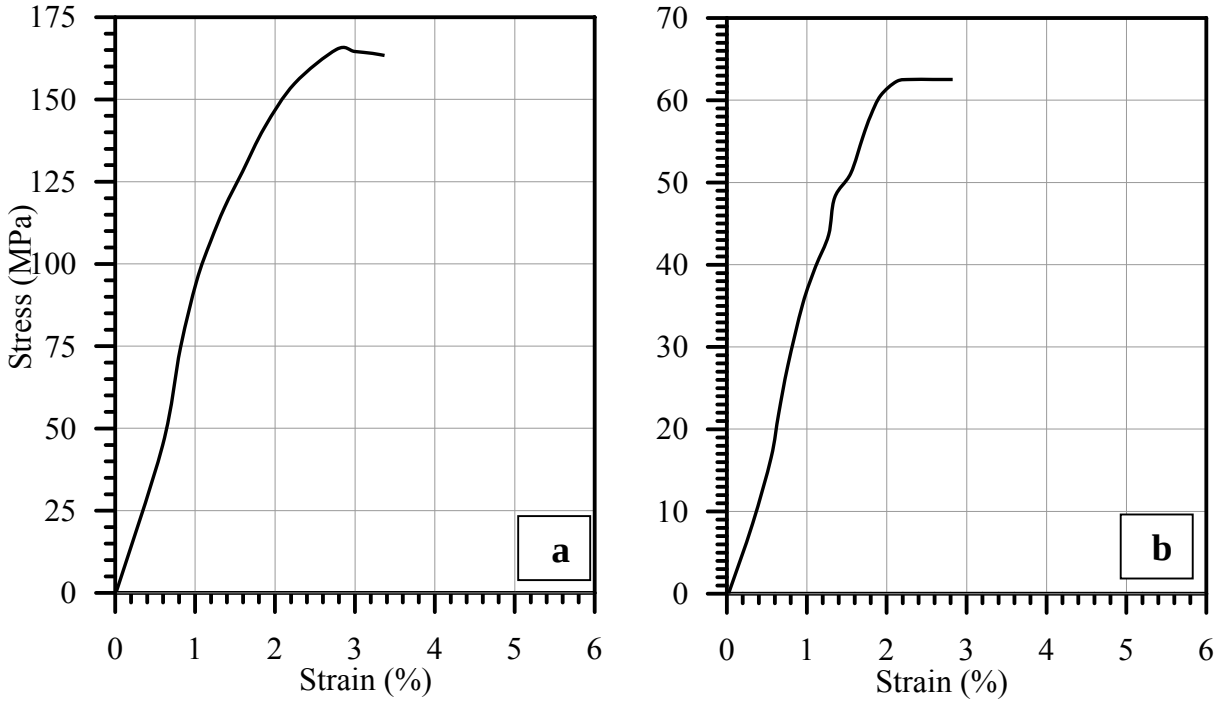

Figure 5-13 Tensile stress-strain curves for 3-end satin Kevlar fiber reinforced polyester. a) 0^o, b) 30^o

The results are summarized in Table 5-2

Table 5-2 The measured mechanical properties for the composites manufactured.

Composition		Woven composite ply					0-90 composite ply				Woven factors		
Fiber	Matrix	Style	σ_{ult} MPa	$E_1=E_2$ MPa	ν	G_{12} MPa	σ_{ult} MPa	$E_1=E_2$ MPa	ν	G_{12} MPa	W_{ult}	W_E	W_G
E-Glass	Epoxy	Plain (2.5*2.5)	53.94	2611	0.096	473	87	4183	0.103	573	0.79	0.62	0.83
E-Glass	Polyester	Plain (2.5*2.5)	46.61	2226	0.112	474	79	3957	0.095	564	0.75	0.59	0.84
E-Glass	Polyester	Plain (12.5*12.5)	43.45	2051	0.093	448	79	3957	0.095	564	0.72	0.55	0.79
E-Glass	Polyester	5-end satin (5*5)	41.08	2138	0.045	455	79	3957	0.095	564	0.74	0.52	0.81
E-Glass	Polyester	Random	32.39	3184	0.231	1293	79	3957	0.095	564	-	-	-
Carbon	Polyester	Plain (7*7)	54.6	3023	0.061	583	105	5098	0.044	925	0.77	0.52	0.63
Carbon	Polyester	5-end satin (5*5)	59.85	3512	0.085	550	105	5098	0.044	925	0.83	0.57	0.59
Kevlar	Polyester	3-end satin (7*7)	166.8	9517	0.043	852	194	11492	0.038	1498	0.91	0.86	0.57

5.3 Results of the Theoretical Model:

The theoretical model developed in this work using the conservation of energy is divide the absorbed energy into four branches which are elastic-dynamic deformation of plate (contact energy), strain energy of the penetration zone, delamination energy and friction energy. The details of the results for every type of these energies are presented.

The plates which are studied for the theoretical model has 80*80 mm^2 in area and the thicknesses are the remaining parameters studied throughout the work. The equation of motion for the composite plates requires the impact excitation force. So the modified contact Law was used. Fig. 5-14 shows the contact force verses the middle deflection of the plate. The contact law was independent of the thickness of the plate; therefore the figure contained the curves for composite used without reference to the thickness. Then this represents the contact stiffnesses for these materials. It has been shown that the contact stiffness is higher for the high modulus materials such as Kevlar composite. And because the modulus for the resting materials was in the same order then the contact stiffnesses for these materials were closely related together. This phenomenon gives the reason for using the Kevlar composite layer as a stiffened layer for the E-Glass composite laminate. The Plain 2.5*2.5 E-Glass reinforced Polyester composite is used for this purpose.

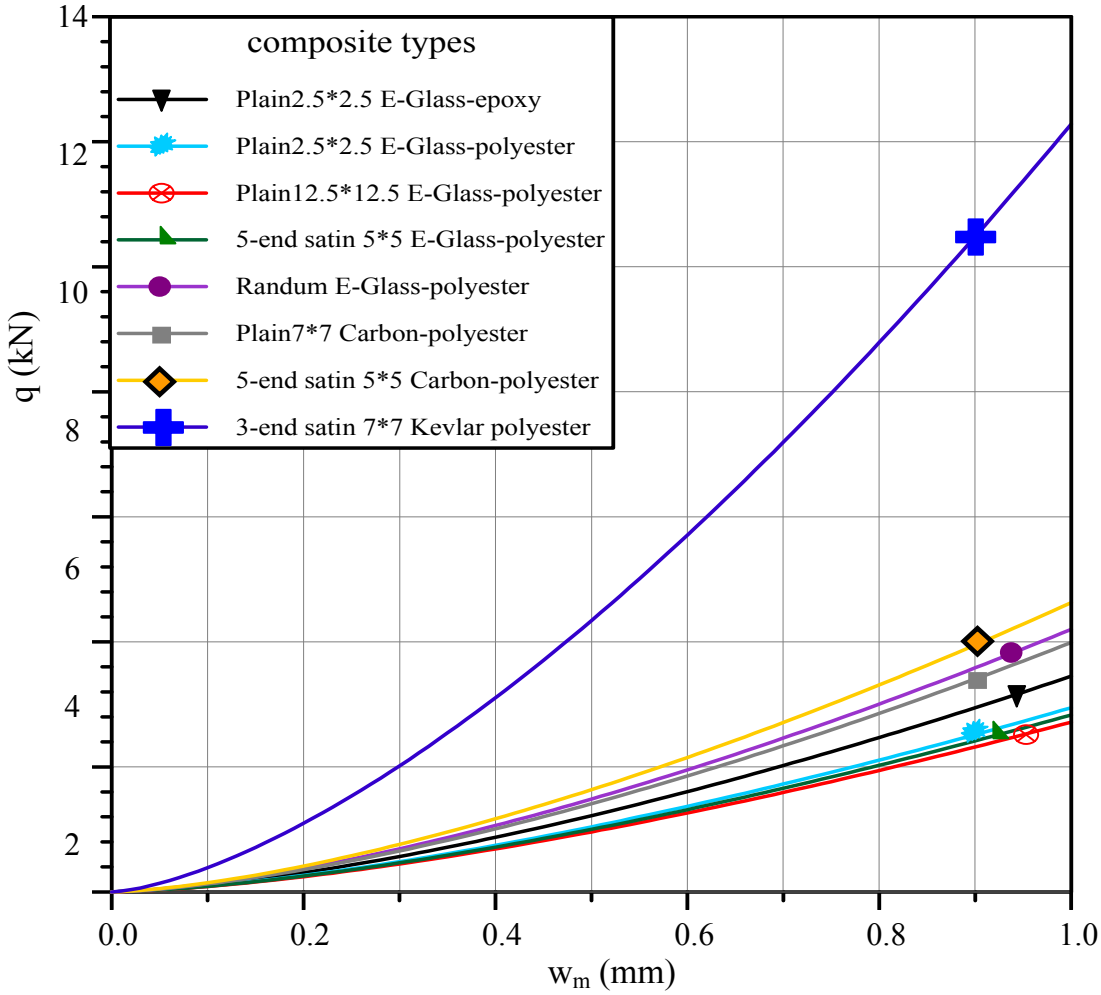

Figure 5-14 Contact force q verses plate middle deflection (w_m) for the composites used

The first mode natural frequency of the plate is determined for the materials studied for different thicknesses as shown in Fig. 5-15. Use of the first mode of fragments natural in the impact analysis is due to large deflection that occurs through the impact. The natural frequency increases with increasing the thickness and this gives the ability to use longer increment time for the finite difference simulation. It was shown that the natural frequency increased with increasing the modulus of elasticity because the stiffness for higher modulus material was higher.

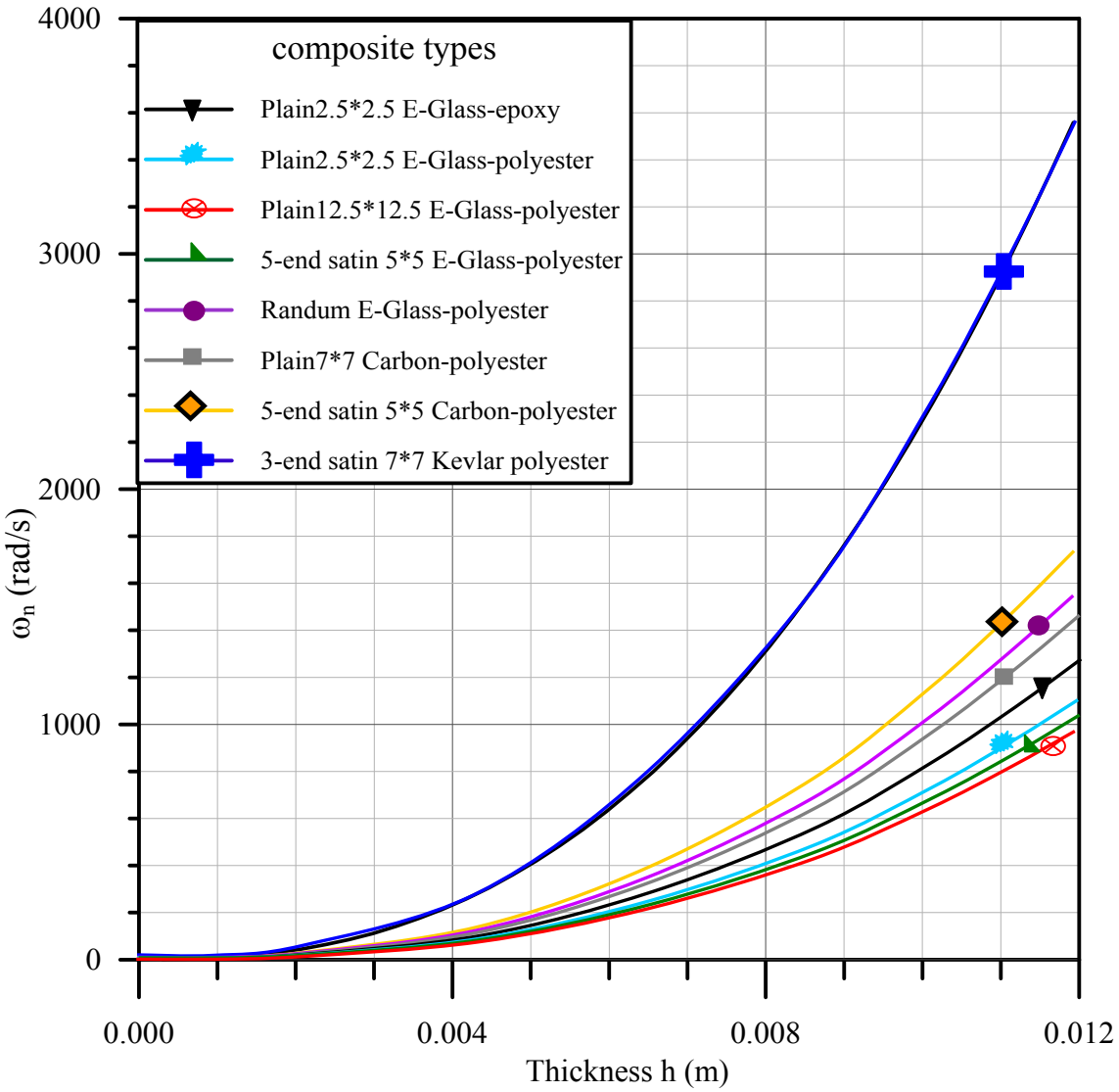

Figure 5-15 Natural frequency verses thickness of plates for the composite materials used.

The equivalent elastic wave speed for the composite materials is shown in Fig. 5-16. The elastic wave speed in proportional to the modulus of elasticity and inversely proportional to the density of the material, because of that it is shown that the Kevlar composite has higher wave speed then the other composites

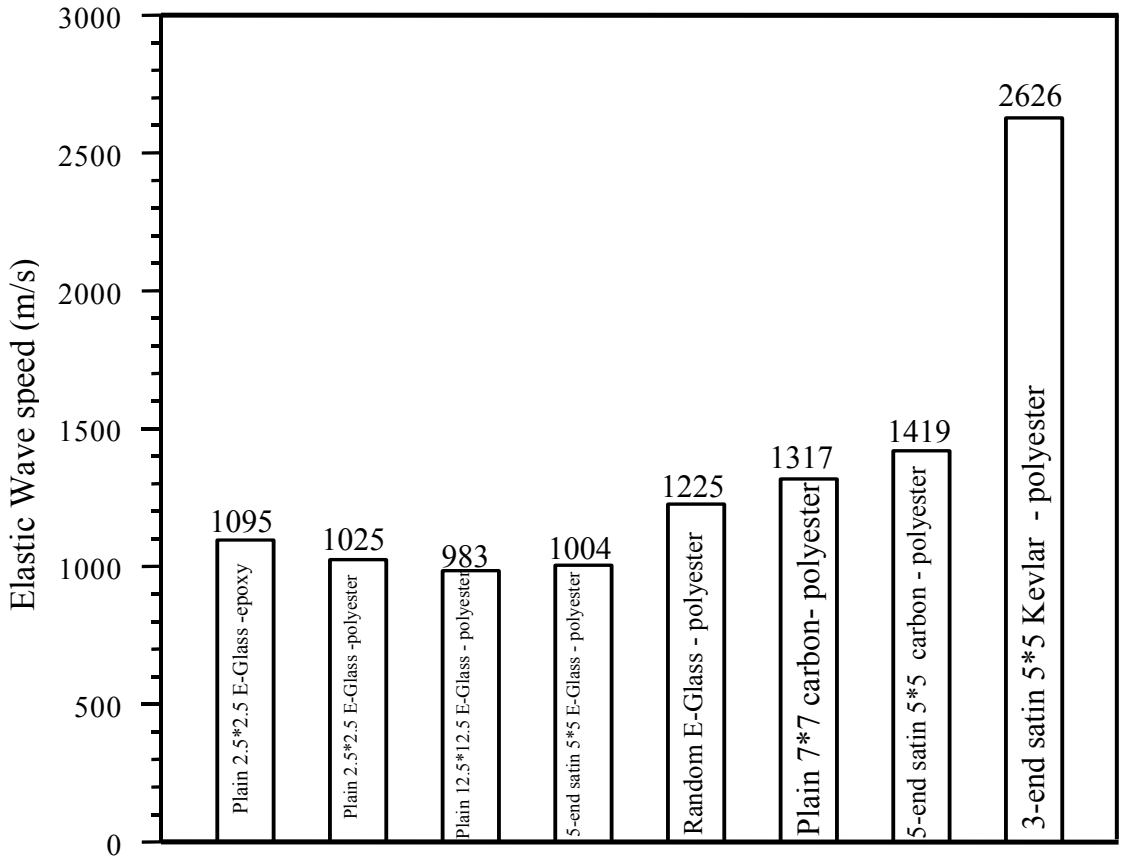

Figure 5-16 Approximate Elastic wave speed for the composite materials used.

From the elastic wave speed and the natural frequency of studied the materials the time increment for the finite difference solution of the dynamic equation was estimated using the domain and the details are given in appendix A. Through the solution of the (Matlab 6.5) program built for this purpose the time and displacement increment was calculated. The program gave the ability to draw the deflection that occurs at the end of the period of the elastic dynamic deformation which occurred when the maximum stresses calculated through the running of the program (through the contact force that penetrates the plate elastically) reaching the ultimate stress for the front layer for the composite plate. The results of the maximum force for different thicknesses of plate ranged from 1 to 10 mm and for

different incident velocities ranged from 50 to 600 m/s for the materials are shown in figures (5.17) to (5.24) for different thicknesses.

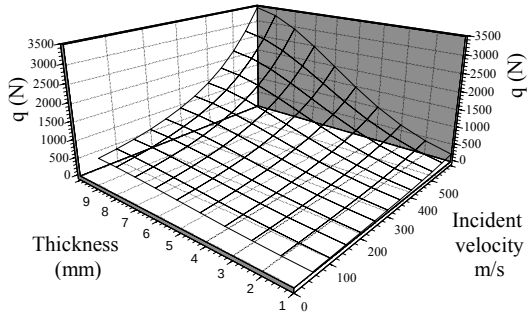

Figure 5-17 3-D force thickness velocity for Plain 2.5*2.5 E-Glass epoxy.

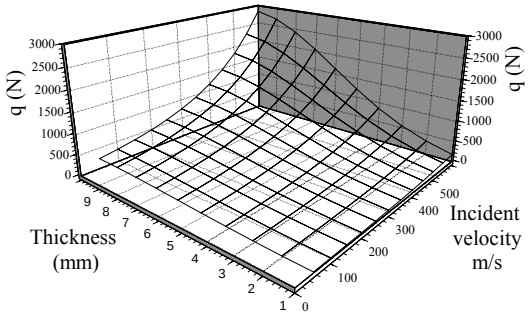

Figure 5-18 3-D force thickness velocity for Plain 2.5*2.5 E-Glass Polyester.

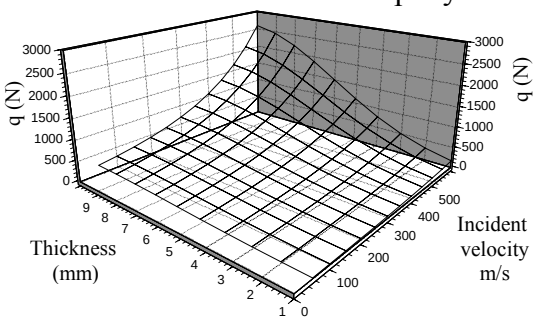

Figure 5-19 3-D force thickness velocity for Plain 12.5*12.5 E-Glass Polyester.

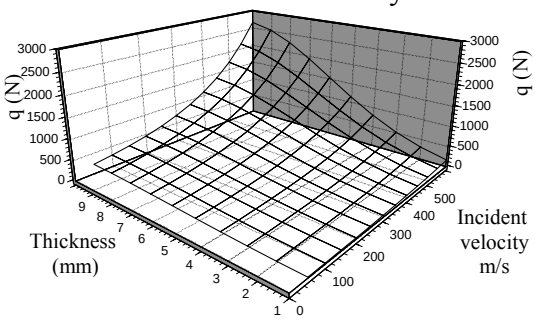

Figure 5-20 3-D force thickness velocity for 5-end satin 5*5 E-Glass Polyester.

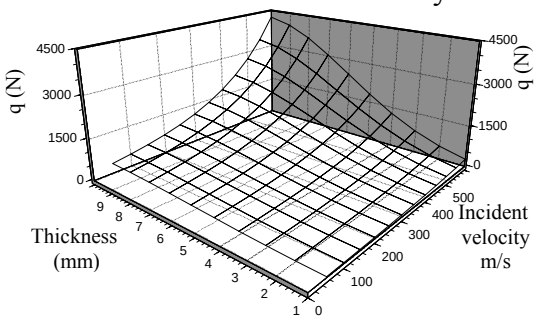

Figure 5-21 3-D force thickness velocity for Random E-Glass Polyester.

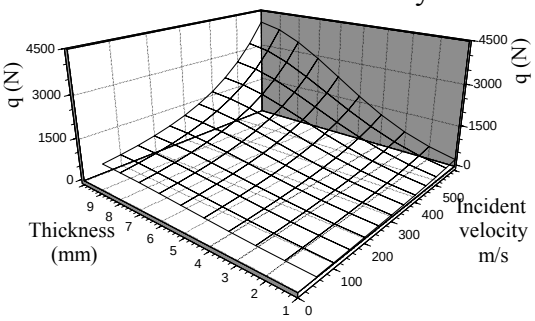

Figure 5-22 3-D force thickness velocity for Plain 7*7 Carbon Polyester.

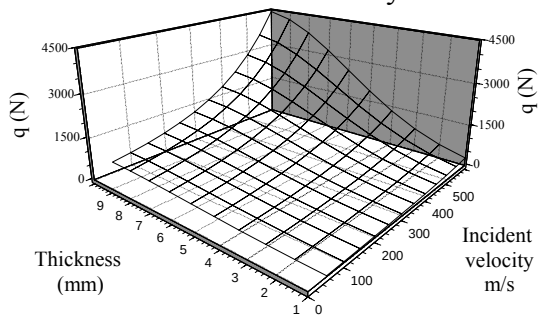

Figure 5-23 3-D force thickness velocity for 5-end Satin 5*5 Carbon Polyester.

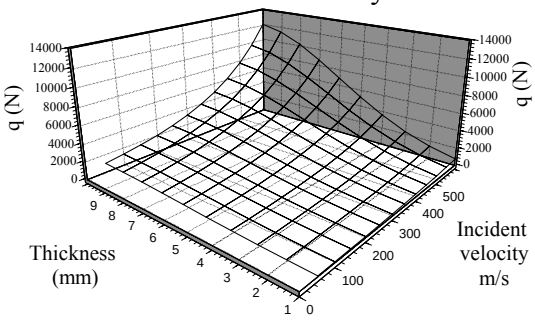

Figure 5-24 3-D force thickness velocity for 3-end Satin Kevlar Polyester.

The figures are plotted in the three dimensional forms where the vertical axis represents the maximum contact force before the failure penetration takes place, the left axis represents the variation in thickness and the right axis represents the variation in the incident velocity. It has been shown that the Kevlar composite carried the maximum value of maximum force due to impact as shown the largest value for q in its Fig. 5-24. The maximum force to be carried by the composite for the elastic impact zone increased with increasing the plate thickness because the resistance to the deformation due to contact is increased with the thickness, which was called, the stiffness.

It has been shown that the contact force increased with increasing the velocity of the projectile; this is because increasing the velocity means increasing its momentum. Consequently the of force and momentum the latter will increases.

Figure 5-25 shows the deformation shape of clamped two layers 3-end satin Kevlar reinforced polyester plate (80*80mm) impacted by 7.5g rigid impactor with V_i=100m/s and r_p=1mm. This ensures that the first mode natural frequency is in agreement with the choice of the optimally when the increment time for the finite difference and for showing the deformation shape occurs for the plate in the elastic zone.

It has been shown that the shape of the deformation is equivalent to the first mode shape for frequency of clamped composite plate [65]. The maximum deflection is located in the middle of the contact point with the impactor. And the special orthotropic for the woven style for the fiber is affected for the symmetry of the deformation through the two principal dimensions of the plate. The other phenomena can be shown is the polar symmetry that occurs near the contact point. This gives the reason and fixation of the presented assumption that the delamination area is circular for the woven composite plate subjected to lateral impact force.

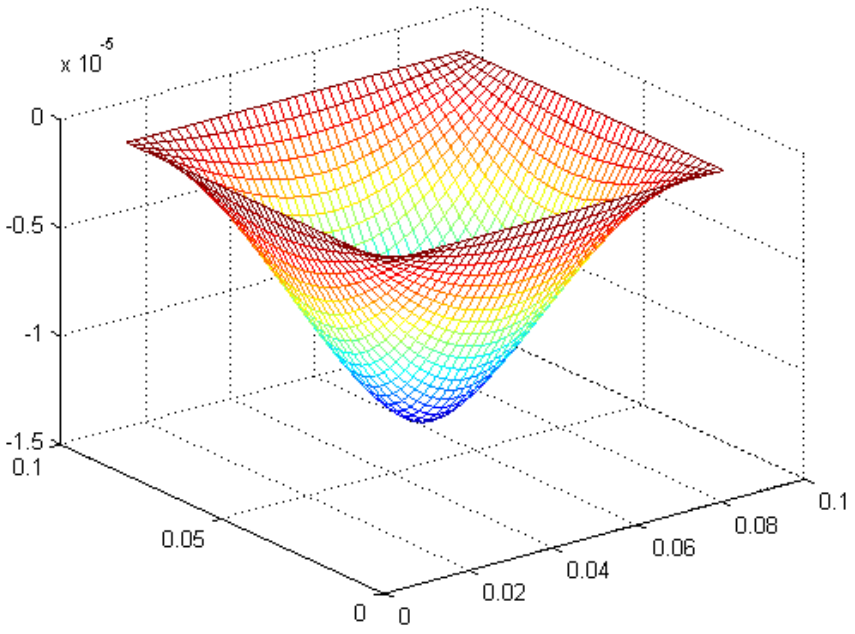

Figure 5-25 Maximum elastic deformation of clamped two layers 3-end satin Kevlar reinforced polyester plate (80*80mm) impacted by 7.5g rigid impactor with V_i=100m/s and r_p=1mm.

The contact energy absorbed through the impact of the contact force shown previously is shown in Figures 5-26 to 5-33 for the materials studied.

From all these results it has been shown that the Kevlar composite has higher contact energy absorbed because it carries a higher value for contact force as discussed earlier. The carbon fiber composite is the second for absorbing contact energy; the E-Glass composite was the third. The arrangement is the same for these materials for the mechanical properties as discussed earlier.

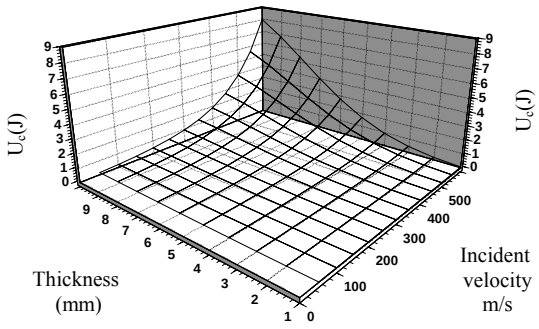

Figure 5-26 3-D Contact energy (U_c)~ thickness- velocity for Plain 2.5*2.5 E-Glass epoxy.

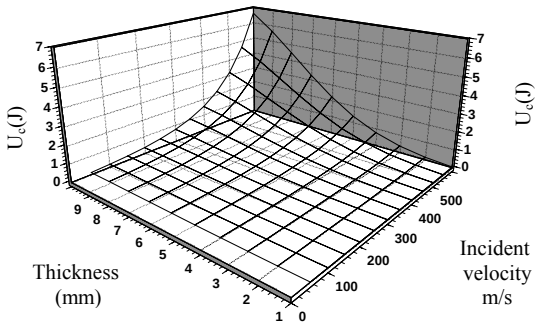

Figure 5-27 3-D Contact energy (U_c)~ thickness- velocity for Plain 2.5*2.5 E-Glass Polyester.

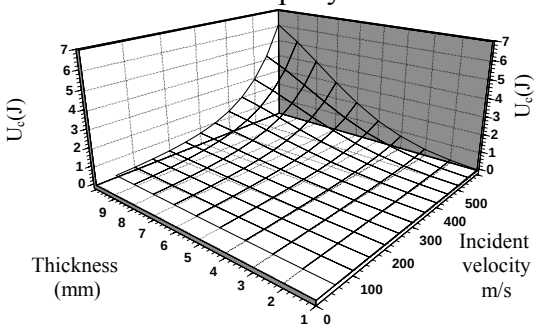

Figure 5-28 3-D Contact energy (U_c)~ thickness- velocity for Plain 12.5*12.5 E-Glass Polyester.

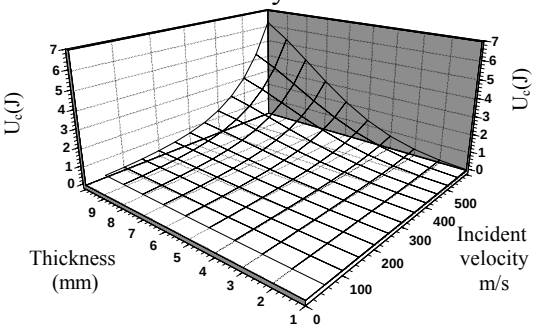

Figure 5-29 3-D Contact energy (U_c)~ thickness- velocity for 5-end satin 5*5 E-Glass Polyester.

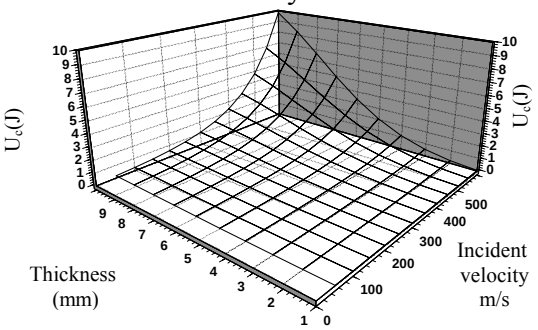

Figure 5-30 3-D Contact energy (U_c)~ thickness- velocity for Random E-Glass Polyester.

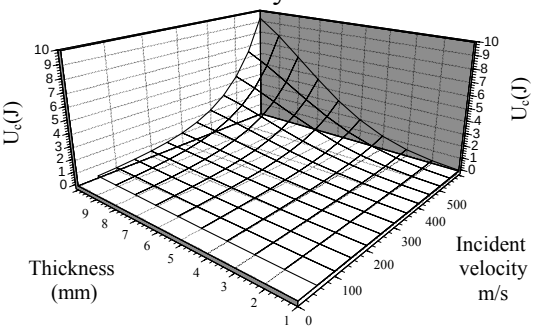

Figure 5-31 3-D Contact energy (U_c)~ thickness- velocity for Plain 7*7 Carbon Polyester.

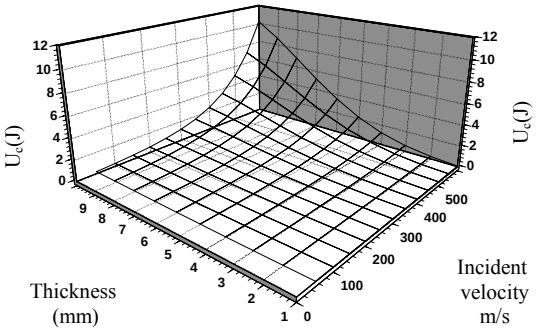

Figure 5-32 3-D Contact energy (U_c)~ thickness- velocity for 5-end Satin 5*5 Carbon Polyester.

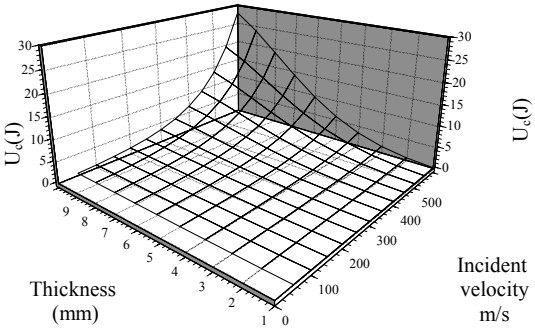

Figure 5-33 3-D Contact energy (U_c)~ thickness- velocity for 3-end Satin Kevlar Polyester.

The comparisons of the contact force and energy for different materials with constant thickness (4mm) and with constant incident velocity (250m/s) are shown in Fig. 5-34 and Fig. 5-35 respectively for contact force. And for the energy is shown in Fig. 5-36 and Fig. 5-37.

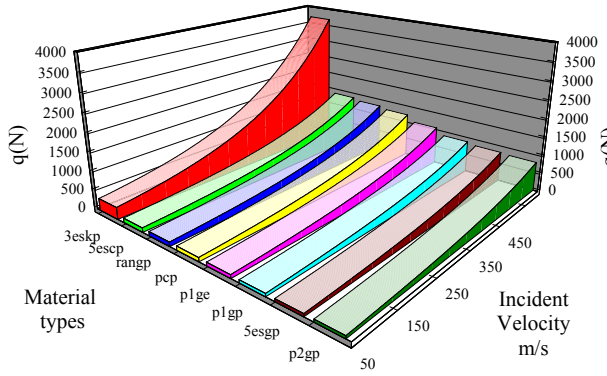

Figure 5-34 contact force for materials used for plate with 4mm thickness for different incident velocities.

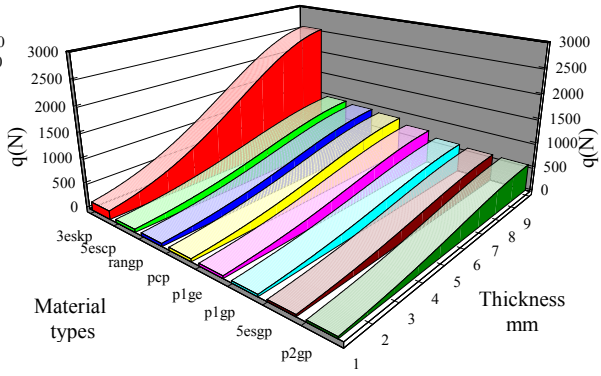

Figure 5-35 contact force for materials used for plate for different thickness with 250m/s incident velocities.

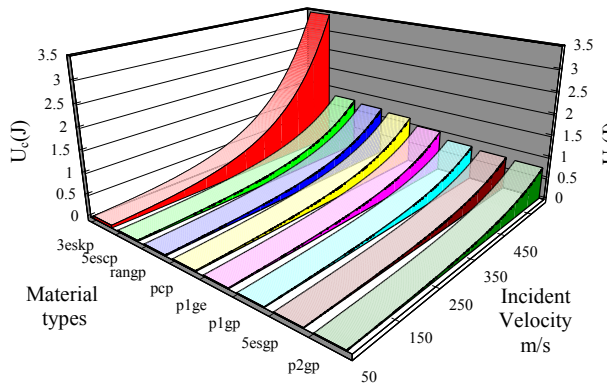

Figure 5-36 contact energy for materials used for plate with 4mm thickness for different incident velocities.

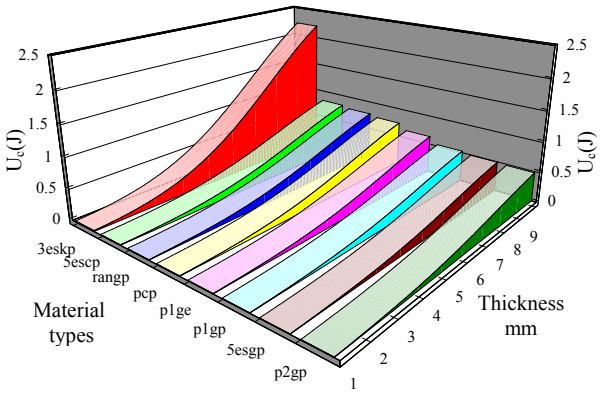

Figure 5-37 contact energy for materials used for plate for different thickness with 250m/s incident velocities.

The contact energy and contact force are in the order for the E-Glass and Carbon Composites while the Kevlar composite has higher values for contact energy and force. The contact force and energy increased with increasing incident velocity because of increasing momentum. And increased with increasing thickness of the composite plate due to the increase of the stiffness.

The remaining absorbing energies were solved together because those energies give the final results for the impact. For example the number of layered delaminated which is entering on the delamination energy should be investigated. Other type of absorbing energies is the penetration for large deformation energy, which must be solved with the delamination energy to calculate the delamination area and penetration radius. And previous type must be solved with the friction losses to estimate the final shape after impact and the type of penetration (partial or fully penetration). The results below for the energies are coupled together to give these results.

The delamination energy for the materials used gives the delamination radius as a side result for this analysis. The delamination radius versus local projectile radius is shown in Fig. 5-38 for different projectile cone angle.

It has been shown that the delamination radius is increased with increasing penetration radius and half cone angle of the projectile. As the projectile penetrates the ply, the local penetration radius will be increased and this gives to increasing the large deformation zone and then the delamination radius will be increased. The cone angle of the projectile has an affect on the penetration hole positively and because of that it depends directly on the delamination radius.

The types of absorbing energies for the plate are shown in Fig. 5-39 for material Plain-woven 2.5*2.5 E-Glass reinforced polyester for 4mm thickness. It has been shown that the contact elastic energy is negligibly small compared with the other types of absorbing energies.

The delamination and large deformation energy increased as the impact velocity increased until reaching the fully penetration zone after that the delamination and large deformation energy stay constant for all velocities upper the

velocity for just penetration. This velocity was called the ballistic limit velocity for the plate.

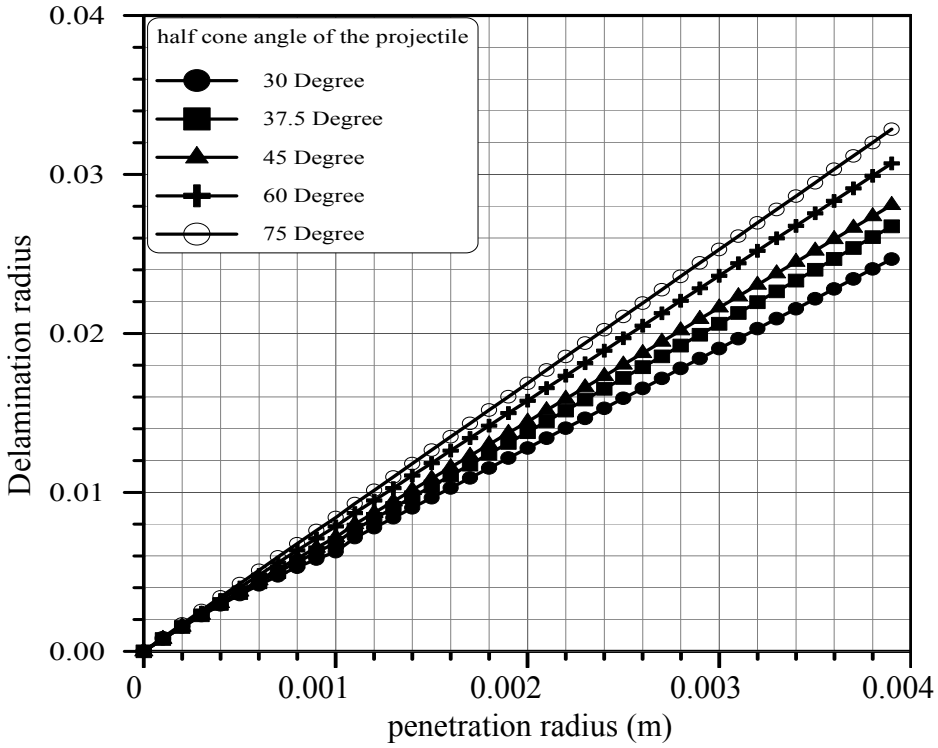

Figure 5-38 Delamination radius versus local projectile radius.

Before the full penetration the velocity increases the penetration depth will be increased causing an increase in the delamination area and large deformation zone, which cause increasing the delamination and large deformation energies. It has been shown that the friction energy continuously increased as the velocity of impact increases, this is because of increase in the momentum of the impact and so the impact force will increases causing an increase in the friction energy.

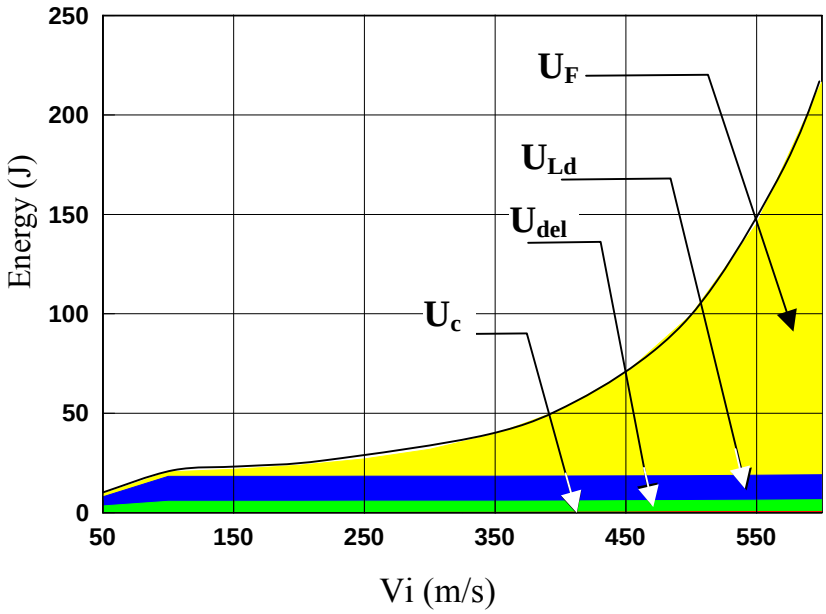

Figure 5-39 The absorbing energies duo to impacting 60^o cone angle 7.5g rigid projectile to a (80*80) mm2 Plain-woven 2.5*2.5 E-Glass reinforced polyester for 4mm thickness

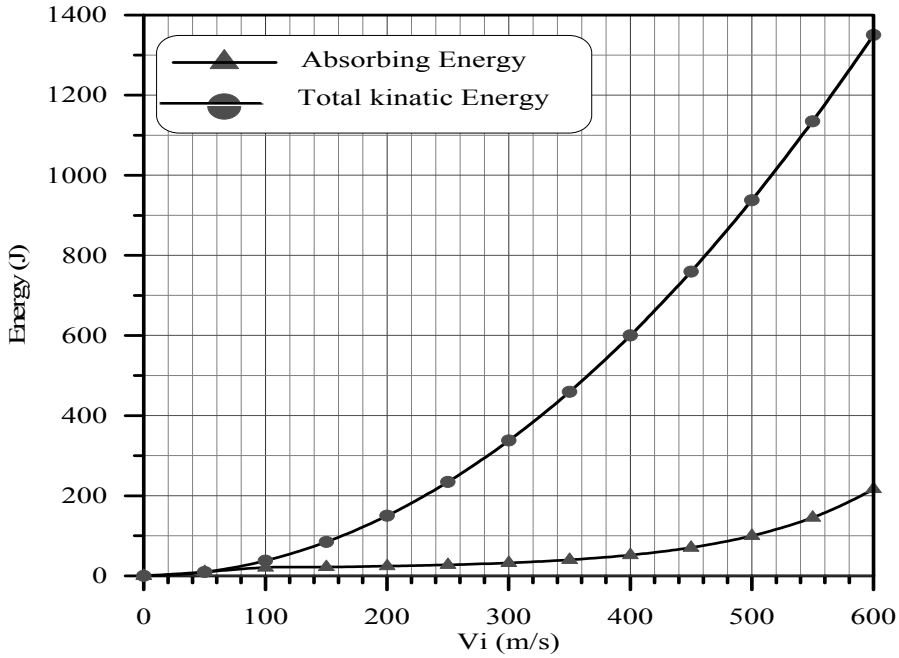

Figure 5-40 The total Kinetic Energy of the projectile and the absorbing energy versus the impact velocity.

The kinetic energy and absorbed energy verses incident velocity for 10 layers (4mm thickness) is shown in Fig. 5-40. It has been shown that the absorbed energy increased as the incident velocity increases in a rate smaller than the rate on

increasing kinetic energy. The kinetic energy was increased with the square power of the incident velocity while the absorbed energy increases as the momentum increases and the friction force increases. It will be noticed that the absorbed energy depends on the incident velocity but to a lesser extent.

5.4 Experimental Results

The impact tests are done for the fabricated specimens will be and discussed in this section. The first parameter studied for these tests is the effect of incident velocity on the resting velocity, penetration time and the absorbing energy. For this reason the 10-layers plain woven E-Glass reinforce polyester composite plate 4mm thickness and 100*100 mm squared. The clamping reduces the dimensions to 80*80mm. The results for these tests are shown in Fig. 5-41. The material used in the tests is the same as that shown in the analytical solution shown in Fig. 5-40. A good agreement was presented for the velocity near the ballistic limits and the experimental amount of the absorbed energy will be greater than that for the analytical solution because excess amount of energy absorbed due to matrix cracks and fragmentation which are not included in the present model. The results of the test shown in Fig. 5-41 shows that the resting velocity increased as the incident velocity increases because the resting energy is not absorbed and increases with the incident velocity. The penetration time measured decreased as the incident velocity increases due to high velocity with constant thickness giving the shortest time. The absorbed energy increases as the incident velocity increases due to increase in the deflection, delamination and fragmentation. These results are similar to the analytical results.

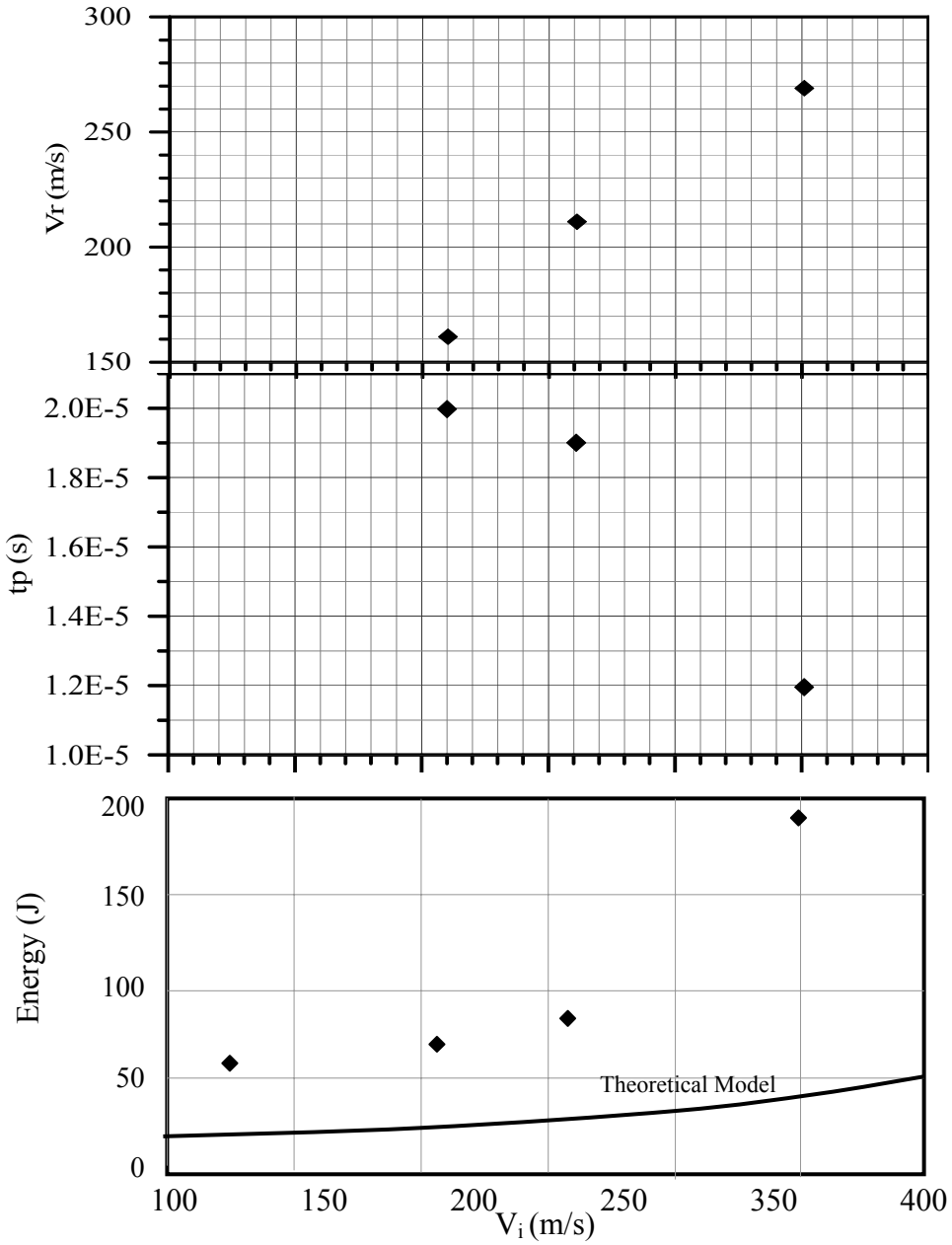

Figure 5-41 The Impact experimental results of the 10-layers p1gp (h=3.9mm), impacted by 60°, 7.5 g steel projectile for various incident velocities.

The projectiles cone angles used in the test was 60, 90, 180°. The effect of these angles on the resting velocity, penetration time and absorbing energy for the 10 layer woven E-Glass fiber reinforced polyester are shown in Fig. 5-42 for Vi~350m/s.

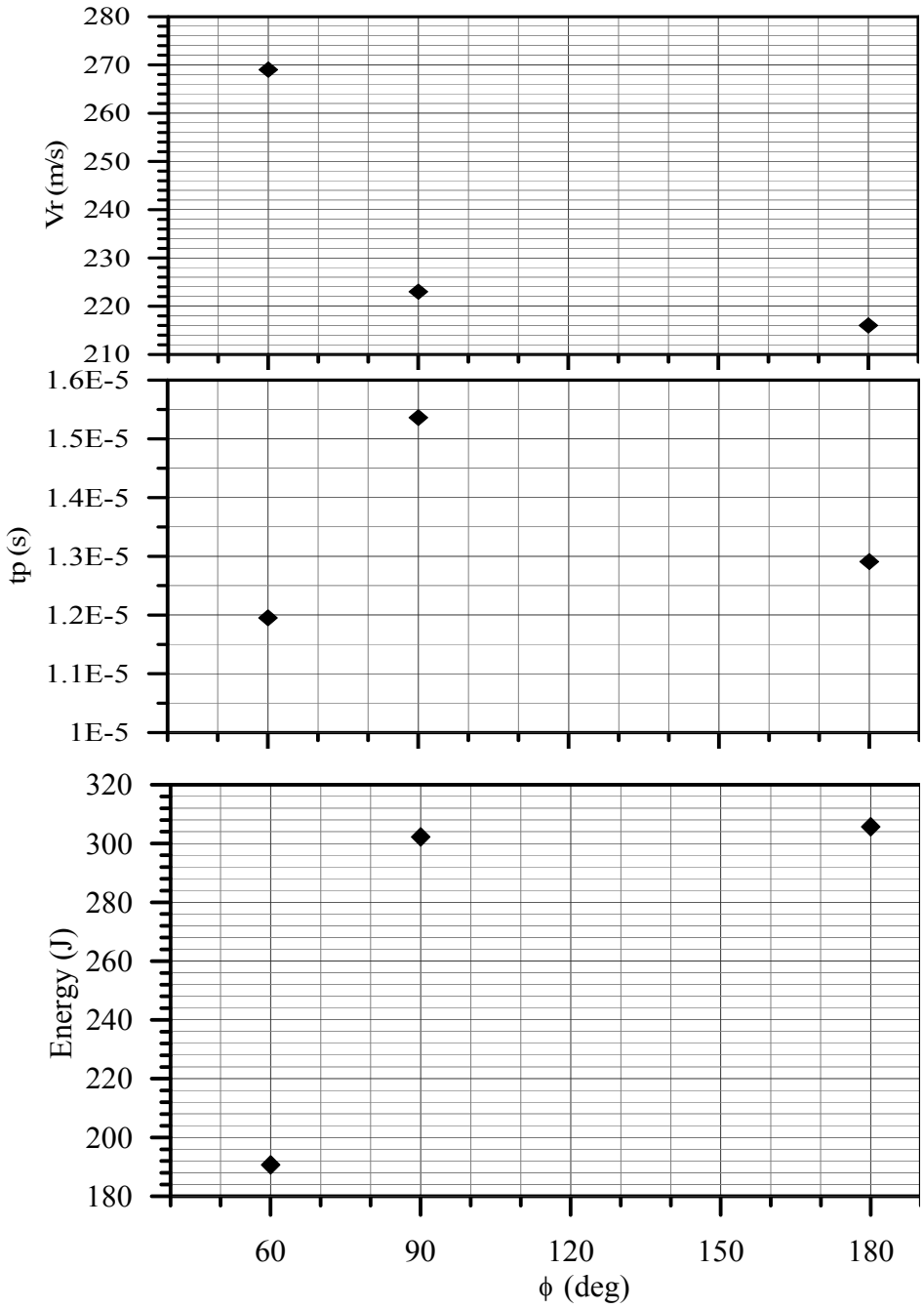

Figure 5-42 The Impact experimental results of the 10-layers p1gp (h=3.9mm), impacted by 7.5 g (Vi~353m/s) steel projectile with various nose angles.

It has been shown that as the cone angle increases the remaining velocity decreases due to increasing the absorbed energy.

The resting velocity, penetration time and absorbing energy are plotted versus the thickness of the fabricated plate in Fig. 5-43. The resting velocity was

decreased as the thickness increases due to increasing the stiffness of the plate then the absorbing energy will be increased. For the same time the penetration time increased with thickness.

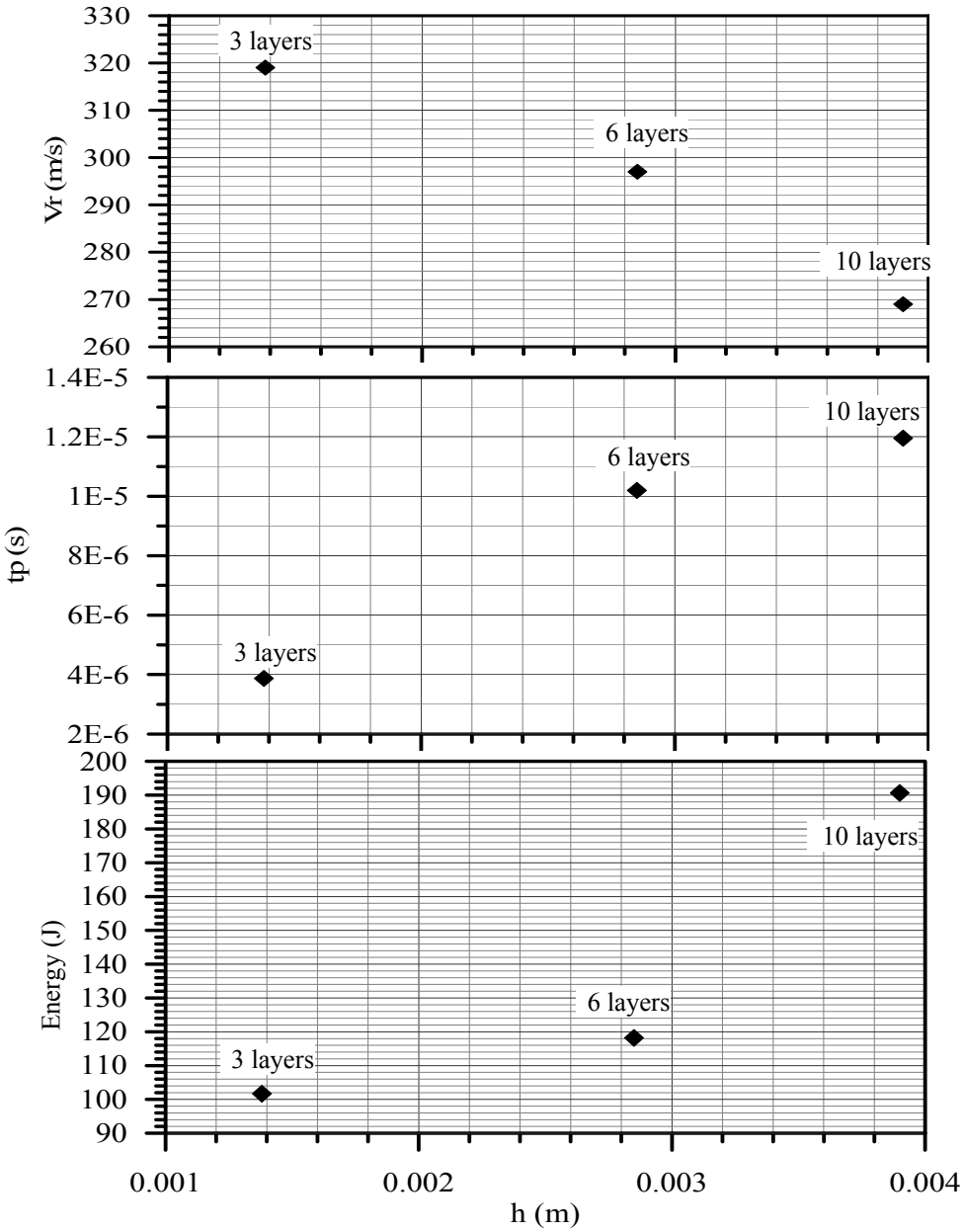

Figure 5-43 The Impact experimental results of p1gp, impacted by 7.5 g (Vi~353m/s) steel projectile with various thickness (No of layers).

Impact tests are carried out for glass-reinforced polyester for different weave styles. The results for these tests are shown in Fig. 5-44. These show that the 5-end satin (5esgp) and small mass per unit area plain weave (p2gp) composites have the largest amount of absorbing energy. This is because the higher number of layers for these weaves give large amount of delamination area and then the delamination energy, in addition to that, the satin weave has higher modulus than the plain weave.

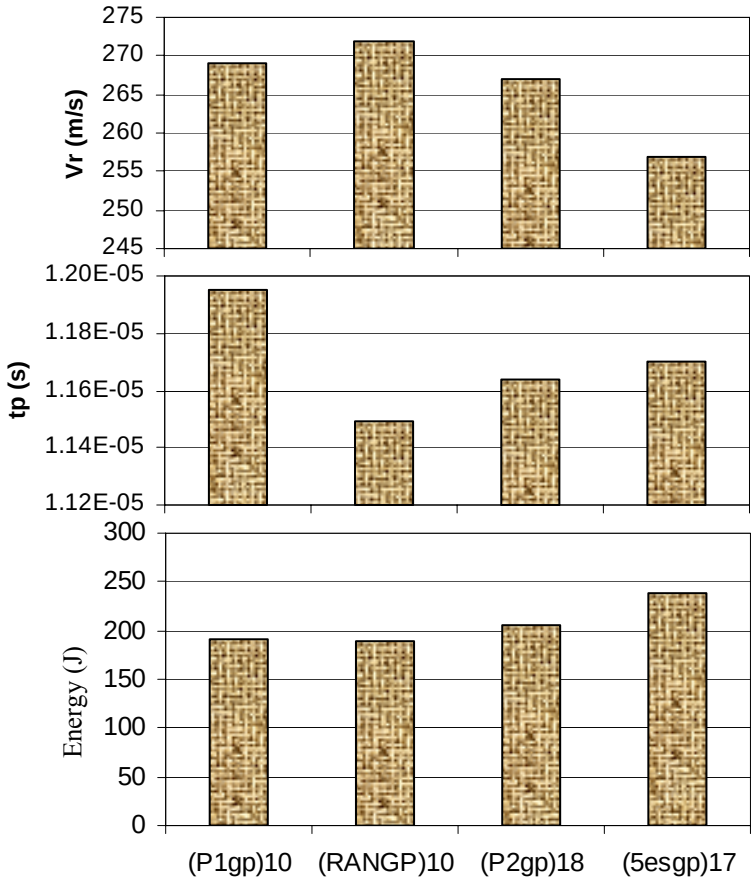

Figure 5-44 The Impact experimental results of the (h~4mm), impacted by 60^{o}, 7.5 g and (Vi~350) projectile for various weave style of glass reinforced polyester.

Although the random fibers composite has a high modulus compared to other glass fiber styles used in this work [Table 5-2)], it has a lower amount of absorbing energy and higher value of resting velocity. This is due to its style behavior of discontinuous fibers and lower amount of delamination area due to lower bonding force between the fibers and the matrix in this type of fiber style. The high mass per unit area plain weave (p1gp) composites has a higher resting velocity and minimum

absorbing energy due to its small amount of delamination layers and the low modulus and the ultimate stress.

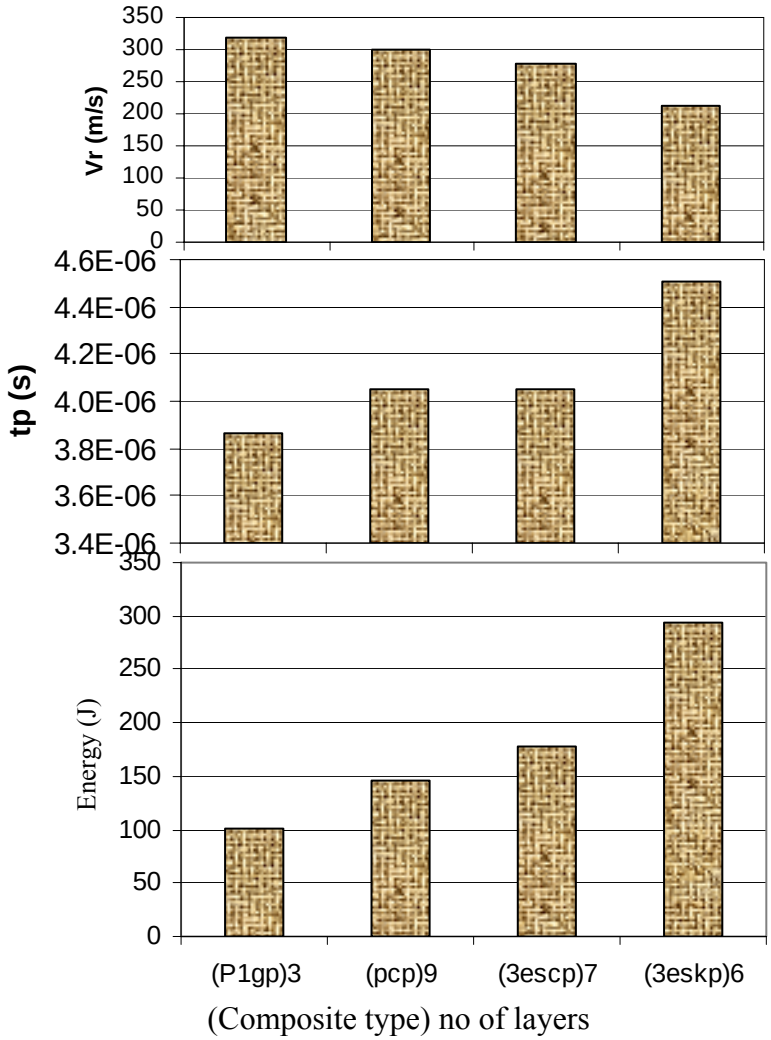

Figure 5-45 The Impact experimental results of the (h~1.4mm), impacted by 60^{o}, 7.5 g and (Vi~350) projectile for various composite materials).

The comparisons of the fiber materials used for the impact are shown in Fig.5-45. It shows that the Kevlar fiber composite has the higher absorbing energy and penetration time and lower resting velocity. The Kevlar composite has the higher modulus and ultimate stresses and because of that it absorbs the higher amount of kinetic energy. The carbon fiber composite has been the second in the absorbing kinetic energy. In fact the resistively of high temperature for the carbon fibers composite give its benefit to use the carbon fiber composite for the

application that need high temperature and impact as in the combustion chamber and the spacecraft nose but with thermal resistive matrix as ceramic. Again the satin weave has the better receptivity to impact and absorbing energy than the plain weave carbon fiber.

The E- glass fiber composite has the lower absorbing energy than the other type of fiber composite material. But because the economic price of the glass fibers and the easy availability of these type of fiber, hoping to improve the impact properties for glass fiber composites, which was investigated by adding layer of strong fiber composite, which is Kevlar fiber composite.

The addition of Kevlar layer in 10 layers plain glass fiber composite was used for different location of the Kevlar fiber, which are front, center and back relative to the impact surface. The resting velocity and approximate penetration time were measured and the absorbing energy was evaluated. These results are plotted against the incident velocity as in Fig. 5-46. It shows that the composite has the higher absorbing energy and penetration time with lower resting velocity when the Kevlar layer was in the rear location. The reason of these results is the deformation shape for the rear of the plate due to impact, which is higher than that for the entrance of the plate impact.

The entrance of the impact projectile to the plate target forms a small hole equal in diameter to that of the projectile. The rear plane of the target has a large deformation and strain energy absorbing the kinetic energy. The location of the stiffened Kevlar layer in the rear of the plate absorbs more kinetic energy because of its high modulus will give it high stiffness.

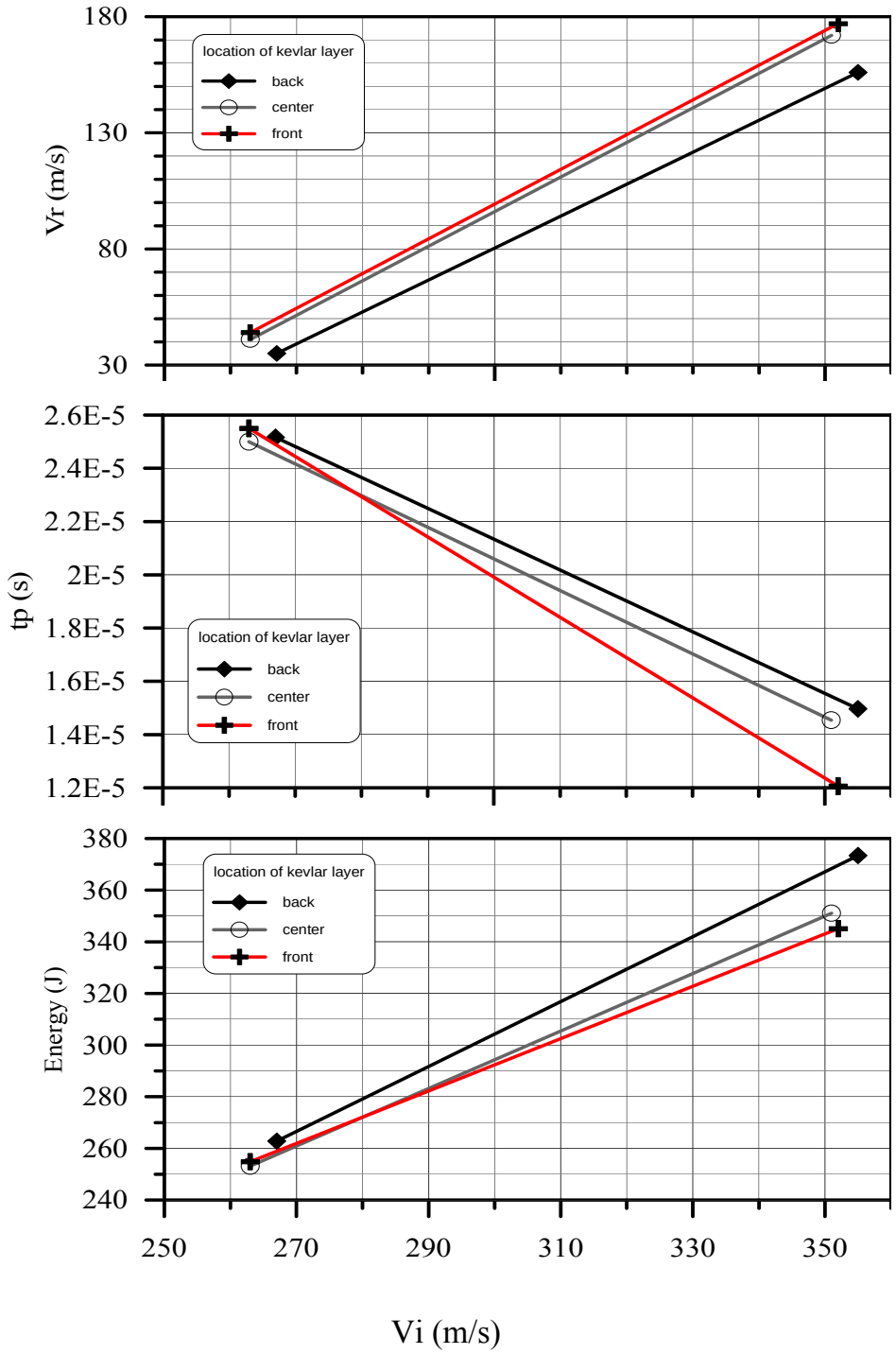

Figure 5-46 The Impact experimental results of verses incident velocity for hybrid composites of 10layers plain E-Glass with different location of Kevlar layer (fiber reinforced polyester composite

The results in Fig. 5-46 shows that as the incident velocity increases the resting velocity and absorbing energy increases and the penetration time decreases.

The rate of absorbing energy for the composite rear Kevlar layer has increased as the incident velocity increased due to increasing the deformation in the backside as the incident velocity increases.

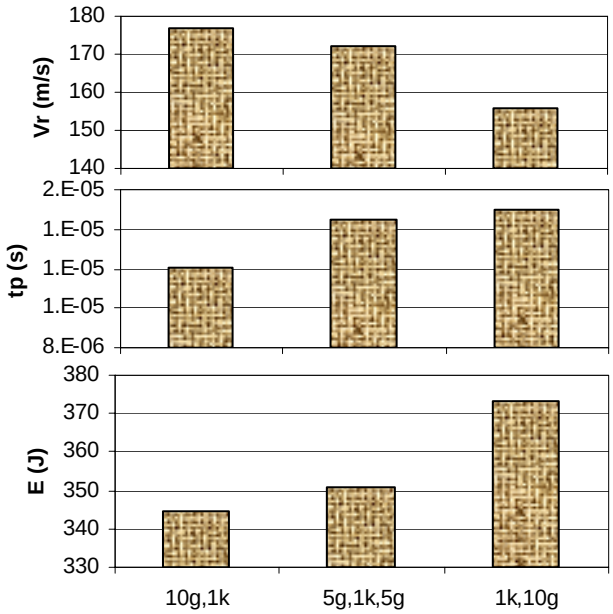

Figure 5-47 The Impact experimental results verses location of Kevlar layer for hybrid composites of 10layers plain E-Glass with different location of Kevlar layer (fiber reinforced polyester composite) for Vi~350m/s.

The comparisons of the Kevlar location for same incident velocity are shown in Fig. 5-47. The higher absorbing energy for the composite with rear Kevlar layer is shown clearly due to the same reasons discussed for Fig. 5-45. Then the best location of the stiffened layer is shown to be in the backside relative to the impact direction.

Chapter Six

Conclusions and Suggestions

6.1 Introduction

In this chapter the conclusions drawn from this work are listed as well as the recommendations for future work.

6.2 Conclusions

The main conclusions of that can be drawn are:

1. From the tests for determining the mechanical properties of woven composite materials, new woven factors were evaluated which were the ratios of mechanical properties for the woven composite to that for equivalent cross play composite. It was found that these factors for carbon fiber composites were higher than that for E-Glass fiber composites and lower than that for Kevlar fiber composites for the same matrix material.

2. The woven factors are higher for fiber-reinforced epoxy than that of the fiber reinforced polyester.

3. The woven factors are increased as the yarn section increased and the end satin increased.

4. The carbon fibers reinforced composites have a higher energy absorbed due to impact than that of the E-Glass reinforced composites and lower than that of the Kevlar reinforced composites theoretically and experimentally.

5. The contact force and energy increases as the thickness of the plate increases, and both the mechanical properties and the incident velocity increase.

6. The wave speed increased as the Young's modulus increases, then the Carbon fibers composites have higher wave speeds than that of E-Glass composites and lower than that of Kevlar composites.

7. The delamination area increases as the cone angle of projectile increases and the radius of projectile increases.

8. In general, as the incident velocity increases the energy absorbed due to impact increases.

9. The contact energy is found to be negligibly small and its effect decreased as the incident velocity increases.

10. The delamination and large deformation energies are found to be increased as the incident velocity increases near the ballistic limit velocity and when the incident velocity increases above these limits the two energies are kept constant.

11. The friction energy has small effect for the velocity range lower the ballistic limits and its effect was increased as the velocity increased above the ballistic limit until it has the main effect for the total absorbing energy.

12. The absorbing energy due to impact is found to be higher for composite materials that have the higher mechanical properties.

13. In hybrid composite materials, the best location for the stiffened layer to absorb the higher energy was the back location relative to the entrance of the impactor.

6.3 Suggestions for Future Works

The treatment of woven composite plate subjected to high velocity impact by a rigid projectile was studied in this work. From this work the following recommendations may be taken into consideration for future work in this field.

1. The woven factor used for this work can be evaluated and studied for dependent sets of woven composite, for this reasons the composite can be fabricated for the weaves roved from same fibers with different satin weaves, mesh size and the future work can be concerned with Leno type of roving, or using the three dimensional weave patterns.

2. The model used in the present work can be developed using the nonlinear relations for material properties specially, for the fiber composites, which have nonlinearities as shown in the present work.

3. The model derived in the present work can be developed by ignoring the energy absorbed due to contact beyond the local indentation because of its small amount. And by adding the matrix cracking and elastic degradation which were noted through the present experiments.

4. The use of different projectile sizes and shapes for the model and the test are useful to optimize and cover all effects of these parameters. Also the development of the model to cover the elastic behavior of the projectile and the effect of density of the projectile.

5. The delamination criterion used is one of the famous criteria used in the impact of models, but because there are many types of delamination criteria and no summing up opinions for one of these criteria, Therefore the tests for these models will be more useful in order to test the criteria and select the best one for every type of impact condition and/ or the composite type.

6. This model can be developed in a way that hybrid composites can be evaluated and optimized for best combination of hybrid arrangements.

7. The models and tests can also be developed for certain conditions such as composites in spacecraft applications due to the ability of impact spacecraft by debris.

8. The impact rig used can be developed to be used for different plate sizes, and the wire screen used for chronograph can be replaced by an easier and more accurate sensor as a laser screen using laser diode and parallel mirrors.

9. Using and testing a ceramic matrix composite is very important because of its ability for using such type of composite in impact applications with high temperature as in a combustion chamber of spacecraft and land base.

REFERENCES

[1] Da-Zhi Jiang ,Wei Shen and Xing-Ye Wang ." ***Simulation of Impact Deformation, Damage and Fracture in Composite Delaminates***". Proceedings of ICCM–11, Gold Coast, Australia, pp 583-592, 14th-18th July (1997).

[2] Reinhart T.J., Dostal C.A., Woods M.S., Frissell H.J., Ronke A.W., Jenkins D.M., O'Keefe K.L., Pilarczyk K.L., Stedfeld R.L. and Mills K.M. ,"***Engineered Materials Handbook. Volume 1, Composites***" ASM International, (1987).

[3] Roger L. Ellis," ***Ballistic Impact Resistance of Graphite Epoxy Composite with Shape Memory Alloy and Extended Chain Polyethylene Spectra Hybrid Components***". M.Sc. Thesis, Virginia University, December (1996).

[4] Sharma S.C., "***Composite Materials***", Narosa Publishing House (2000).

[5] Tsai and Hahn and Delaware, "***Composites Design Encyclopedia***" (1990).

[6] Department of Defense Handbook, "***Composite Materials Handbook. Volume 2. Polymer Matrix Composites Materials Properties***", MIL-HDBK-17-2E, Volume 2 of 5. 17 June (2002).

[7] Department of Defense Handbook, "***Polymer Matrix Composites. Volume 1. Guidelines for Characterization of Structural Materials***" , MIL-HDBK-17-1E, Volume 1of 3. 23 January (1997).

[8] Roy Laible C. "***Ballistic Materials and Penetration Mechanics***", Elsevier Science Publishing Company, (1980).

[9] Fawaz Abbas Taha AL-Najim, ”***An Investigation into the Ballistic Impact Performance Ductile Metallic and Composite Materials Targets***”, PhD. Thesis, University of Technology, June (2000).

[10] Ching H. Yewand Rodney B. Kendrick, ”***Study of Damage in Composite Panels Produced by Hypervelocity Impact***”, Int. J. Impact Engng, Vol.5 PP 729-738, (1987).

[11] Greszczuk L. B.,” ***Response of Isotropic and Composite Materials to Particle Impact***”, Foreign Object Impact Damage to Composite, ASTM STP 568, American Society for Testing and Materials, pp 183-208, (1975).

[12] Jonsan A. Zakus, T. Nicholas, H. F. Swift, L. B. Greszczuk, Curran D.R.,“ ***Impact Dynamics***”, John Wiley and Sons, Inc. (1982).

[13] Enboa Wu and Ching-Shih Yen,” ***The Contact Behavior Between Laminate Composite Plate and Rigid Spheres***” Trans. ASME (Journal of Applied Mechanics), Vol.6, PP 60-67, (1994).

[14] Tan and Sun,” ***Used of Static Indentation Laws in the Impact Analysis of Composite Plates***” , Trans. ASME, Vol.52, pp.6-12, (1985).

[15] Zhidong Guan and Chidar Yang,” ***Low Velocity Impact Damage Process of Composite Laminate***”, Department of Mechanical Engineering, Wichita state University, (2000).

[16] Cairns D.S. and Lagace P.A., “***Thick Composite Plate Subjected to Lateral Loading***”, Journal of Applied Mechanics, Vol.54, pp. 611-616 ,(1987).

[17] Karaogan Levent, ”***Axial Impact of Composite***” PhD. Thesis Stanford University,(1993).

[18] Choi I.H. and Hong C.S.," ***Low Velocity Impact Response of Composite Laminates Considered High Order Shear Deformation and Large Deflection***", Mechanics of composite Materials and Structures, Vol.1, pp.157-170,(1994).

[19] Khalid Abdulaziz Al-Dheylan. , "***A Study of Low Velocity of Whiskers Reinforced Alumina/Silica Carbide Ceramic Composite***" PhD. Thesis, the Pennsylvania State University,(1996).

[20] Kiesling T.C., Chaudhry Z., Paine J.S.N., and Roger C.A., "***Impact Failure Modes of Thin Graphite Epoxy Composites Embedded with Super Elastic Nitnol***" the AIAA/ASME/AHS/ASC 37th SDM Conference, Satlake City, UT, April 15-17,(1996).

[21] Ya-jung Lee and Yan Shyu, "***Low Velocity Impact Failure Analysis of Sandwich Beam***", Proceeding of ICCM-11, Gold Coast , Australia, Vol. II, pp. 495-502,4th-18th July (1997)

[22] William Craft J., Derke Hughes R., and Ajit Kelker D.," ***Low Velocity Impact Damage of Organic Foam Sandwich Composites***", Proceeding of ICCM-11, Gold Coast, Australia, Vol. II, pp. 513-521,4th-18th July (1997).

[23] Markaki A.E. and Clyne T.W.,"***The Effect of Impact Velocity on the Deformation of Layered Metal Foam/ Ceramic Composite***",MIT Verlag (1999).

[24] Markaki A.E and Clyne T.W.," ***Characterization of Impact Response of Metallic Foam/Ceramic Laminates***", Materials Science and Technology, Vol.16 pp. 785-791, (2000).

[25] Majeed Omeer ,"***Numerical Model of Transverse Impact on Composite Coupons***", MENG Thesis Carleton University (Canada),1995.

[26] Wiggenraad J.F.M. and Ubels L.C., "***Impact Damage and Failure Mechanics in Structure Relevant Composite Specimens***", Proceeding of ICCM-11, Gold Coast , Australia, Vol. II, pp. 562-581,4th-18th July (1997).

[27] Florentin Berthet, Pier Devos and Thierry Ansart. ,"***RTM Carbon Composite: Influence of Process Parameters on Compression Strength After Impact***", Proceeding of ICCM-11, Gold Coast , Australia, Vol. II, pp.27-35,4th-18th July (1997).

[28] Kenjiro Komai, Kohji Minoshima and Kazuta Tanaka ,"***Influence of Water Absorption on Delamination Induced by Low Velocity Impact and CAI Strength of FRPS"***. Proceeding of ICCM-11, Gold Coast , Australia, Vol. II, pp. 503-512,4th-18th July (1997).

[29] Parhi P. K., Bhattacharyya S. K. and Sinha P. K., "***Failure Analysis of Multiple Delaminated Composite Plate due tp Bending and Impact***", Bull. Mater/ Sci., Vol. 24, No. 2, pp. 143-149, April (2001).

[30] Apetre N. A., Sankar B. V. and Venkataraman S., "***Indentation of a Sandwich Beam with Functionally Graded Core***", the AIAA/ASME/AHS/ASC 43rd SDM Conference, Denver, Carolado, USA , April 22nd -25th ,(2002).

[31] Chain-Fong Yen and Joe; Patterson," ***Prograsive Failure Analysis of Thin Walled Composite Tubes Under Low Energy Impact***", Material Science Corporation, (1997).

[32] Eduardo Bitencourt and Guillermo J. Creus,” ***Finite Element Analysis of Three-Dimensional Contact and Impact in Large Deformation Problems***”, Computer and Structures, Vol.69, pp. 219-234, (1998).

[33] Moura De M.F.S.F and Goncalves J.P.M., ” ***Modeling the Interaction Between Matrix Cracking and Delamination in Carbon-Epoxy Laminates Under Low Velocity Impact***”, Composites Science and Technology, Vol.64, pp.1021-1027,(2004).

[34] Roger Ellis L.,” ***Ballistic Impact Resistance of Graphite Epoxy Composites With Shape Memory Alloy and Extended Chain Polyethylene Spectra Hybrid Components***” MSc. Thesis, Virginia Polytechnolic Institute and State University,(1996).

[35] Roger Ellis L. and Craig Rogers A.,” ***Ballistic Impact Resistance of Graphite Composites with Superelastic SMA and Spectra Hybrid Components***”, AIAA, pp1-11, (1997).

[36] David Raylance,” ***Influence of Fiber Properties on Ballistic Penetration of Textile Panels***”, Composite Science and Technology, Vol.14, pp.183-190,(1981)

[37] Gupta B. P. and Davids N.,” ***Penetration Experiments with Fiberglass-Reinforced Plastic***”, Experimental Mechanics, pp.445-450, (1966).

[38] Jang B.Z., Chen L.C., Wang C.Z., Lin H.T. and Zee R.H.,” ***Impact Resistance and Energy Absorption Mechanisms in Hybrid composites***”, Composites Science and Technology, Vol.34, pp. 305-335, (1989).

[39] Canwell W.J. and Morton J.,” ***Influence of Varying Projectile Mass on the Impact Response of CFRP***”, Composite Structure, Vol.13, pp.101-114, (1989).

[40] Canwell W.J. and Morton J.," ***Impact Perforation of Carbon Fiber Reinforced Plastic***", Composite Science and Technology, Vol.38, pp.119-141, (1990).

[41] Dutta P.K., Farrell D., Taylor S., Aziz Tadayon and David Hui. ," ***Ballistic Perforation of Graphite/Epoxy Composite***", (Special Report 96-29), US Army Corps of Engineers, December (1996).

[42] Lee B.L., Song J.W. and Ward J.E.," ***Failure of Spectra Polyethylene Fiber-Reinforced Composites under Ballistic Impact Loading***", Journal of Composite Materials, Vol.28, No.3, pp.1202-1226, (1994).

[43] Frank K.Ko, Amotz J.G. and Song W.S.," ***Behavior of Gradient Designed Composite Under Ballistic Impact***", Proceeding of ICCM-11, Gold Coast, Australia, Vol. II, pp.464-473,4th-18th July (1997).

[44] Kasano H. and Abe K.," ***Perforation Characteristics Prediction of Multi-Layered Composite Plates Subjected to High Velocity Impact***" Proceeding of ICCM-11, Gold Coast , Australia, Vol. II, pp.522-531,4th-18th July (1997).

[45] Takahashi K. and Komatsu H.," ***Perforation Characteristics of Fabrics Made of High Strength PE Fibers***" Proceeding of ICCM-11, Gold Coast , Australia, Vol. II, pp.542-551,4th-18th July (1997).

[46] Hosur M.V., Vaidya U.K., Ulven C., Jeelani S.," ***Performance of Stitched/Unstitched Woven Carbon/Epoxy Composite Under High Velocity Impact Loading***", Composite structures, Vol.64, pp.45-466, (2004).

[47] Wisnom M.R. " ***Impact Resistant Carbon Fiber Composite with Tensioned Kevlar Overwind***", M.Sc. Thesis, University of Bristol (2002).

[48] Mark Bower V., " ***Composite Materials***", the University of Alabama in Huntsville, Huntsville, Alabama, copyright 1992-2000.

[49] Hung Cheng Lu. ," ***Ballistic Penetration of GRP Composites: Identification of Failure Mechanics and Modeling***", Ph.D. Purdue University, December, (1998).

[50] Espinosa H.D., Dwivedi S., Lu H.-C.," ***Modeling Impact Delamination of Woven Fiber Reinforced Composites with Contact/Cohesive Laws***", Compt. Methods Appl. Mech, Engrg, Vol.183, pp.250-290, (2000).

[51] Akkerman R., Warnet L.L and van de Ven E.C.," ***Impact Damage in Woven Fabric Reinforced Composite***", Composite Group, Dept. of Mechanical Eng., University of Twente, the Netherlands, (2000).

[52] Nunes L.M., Paciornikand S. and d'Almeida J.R.M.,"***Evaluation of the Damage Area of Glass- Fiber-Reinforced Epoxy-Matrix Composite Materials Submitted to Ballistic Impacts***" Composite Science and Technology, Vol.64, pp. 945-954, (2004).

[53] jenq S.J. and Mo J.J.," ***Ballistic Impact for Two Step Braider Three-Dimensional Textile Composites***", AIAA Journal, Vol.34, No.2, February (1996).

[54] Bazle A. Gama, Md. J. Haque, and John W. Gillespie Jr.," ***Impact, Damage, and Energy Absorption Orthogonal Weave Composite Cell Model***", U.S. Army Research Office, STTR Phase II contract DAAD 19-02-C-0044, (2005).

[55] Alastair Johnson F. and Anthony Pickett K.," ***Impact Tend Crash Modeling of Composite Challenge Structures: a Challenge for Damage Mechanics***", EU project HICA, (2000).

[56] Christof Kindervater M., Alastair Johnson F., Dieter Kohlgrüber, Marius Lützenburger, Nathalie Pentecôte. ," ***Crash and Impact Simulation of Aircraft Structure- Hybrid and FE Base Approaches***", European Congress on Computational Methods in Applied Sciences and Engineering, Barcelona, 11-14 September (2000).

[57] Cheeseman B.A. and Hoppel C.P.R.," ***Simulation the Ballistic Impact of Composite Structural Armor***", Army Research Laboratory, AMSRL-WM-MB ,(2002).

[58] Jensen R.E. ,Madison P.H. and McKnight S.H.," ***Novel Inorganic- Organic Fiber Sizing for Composite Armor Applications***", Army Research Laboratory, Polymers Research Branch, (2002).

[59] Julie Samuels E.," ***Ballistic Resistance of Personal Body Armor***", National Institute of Justice, (2000).

[60] James Shih C., Marc Adams A. and Gene Howald A.," ***Devlopment of a Versatile, Low Cost Cermaic Armor (U)***", TACOM, contract No. DAAE07-99-C-L028, SBIR A98-072., (1992).

[61] Pettit M.J.," ***PSDB Ballistic Body Armour Standard***," Police Scientific Development Branch, Woodcock Hill, Sandridge, St, Albans, Hertfordshire AL4 9HQ, United Kingdom, (1995).

[62] Jason Gomez T., Arun Shukla. ," ***Multiple Impact Penetration of Semi-Infinite Concrete***", International Journal of Impact Engineering, Vo.25, pp.965–979. (2001)

[63] Cynthia Bir A.," ***The Evaluation of Blunt Ballistic Impact of the Thorax***", Ph.D. Thesis, Wayne State University, Detroit, Michigan, (2000).

[64] Rao J.S.," ***Dynamics of Plate***", Narosa Publishing House, 1999.

[65] Bohe Wang," ***The Application of Finite Difference Method and Matlab in Engineering Plates***", M.Sc. thesis, West Virginia University, 1999.

[66] Hussain Ali Al-Qurtany. ," ***Determination of Dynamic Characteristics and Interlaminar Shear Stresses of Composite Laminated Plate under Various Loading***" PhD. Thesis, University of Baghdad, 2004.

[67] Whitny J.M. " ***Shear Deformation in Heterogeneous Anisotropic Plates***" J of Appl. Mech.(37), 1970 pp.1031.

[68] Joseph Earl Thompson, " ***Compaction and Cure of Resin Film Infusion Prepregs***", M.Sc. thesis, the faculty of the Virginia Polytechnic Institute and State University, December 22, (2004)

[69] Hearn E. J.," ***Mechanics of Materials***", volume 2, 2nd edition, Pergamon press, (1985).

[70] Salah M. H ,"***On the Ballistic Impact of Rigid Projectiles on Metallic Target Plates*** ", M.Sc. thesis, University of Technology, (2002).

Appendix A

The Difference Expression of Equation of Motion and Boundary Conditions

The partial differential equation of the equation of motion due to impact, which models the bending of an orthotropic symmetric laminated plates Fig. A-1 with small deflection, is given by equation (3.20)

$$D_{11}\frac{\partial^4 w}{\partial x^4}+2(D_{12}+D_{66})\frac{\partial^4 w}{\partial x^2\partial y^2}+D_{22}\frac{\partial^4 w}{\partial y^4}+\rho h\frac{\partial^2 w}{\partial t^2}=q(x,y,t)$$

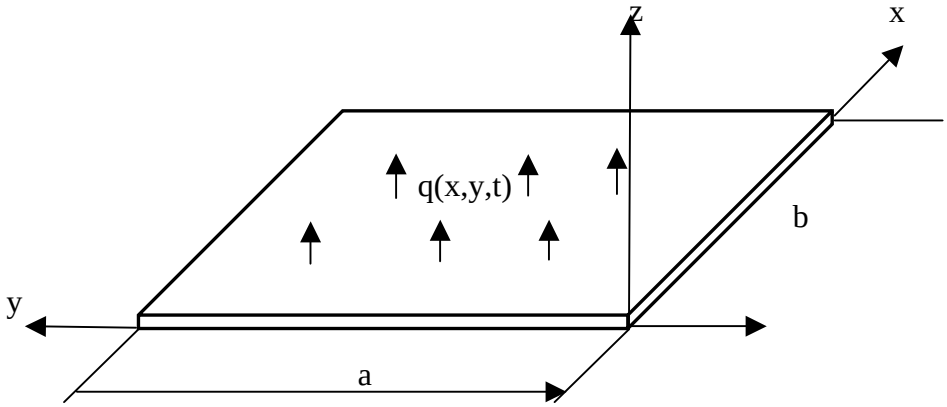

Figure A-1 Rectangular plate subjected to dynamic loading

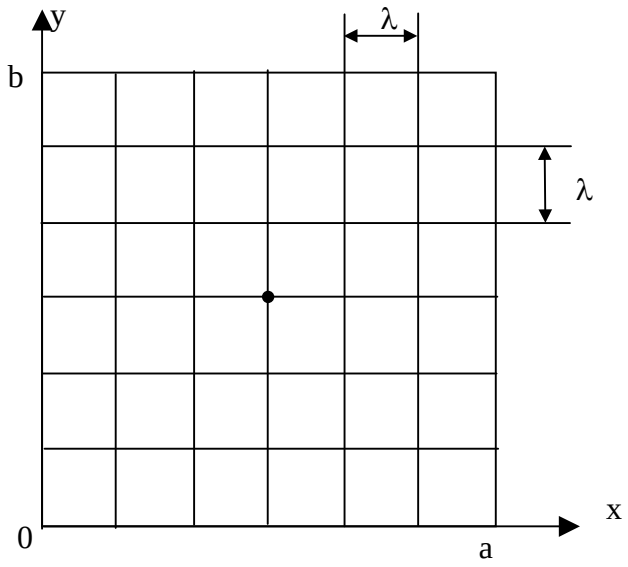

Figure A-2 The shape of the finite difference meshing used for laminate composite plate.

For a node i (Fig. A-2), the pattern of the finite difference coefficients of

$$\left[D_{11}\frac{\partial^4 w}{\partial x^4} + 2(D_{12}+D_{66})\frac{\partial^4 w}{\partial x^2 \partial y^2} + D_{22}\frac{\partial^4 w}{\partial y^4} + \rho h \frac{\partial^2 w}{\partial t^2} \right]_i$$

The acceleration term of in the above, which is, $\rho h \frac{\partial^2 w}{\partial t^2}$ can be simply expressed in the finite difference form as

$$\rho h \left.\frac{\partial^2 w}{\partial t^2}\right|_i \approx \rho h \frac{w_i - 2w_{i,t-1} + w_{i,t-2}}{\Delta t^2} \qquad \ldots(A.1)$$

Where Δt is the time increment which was selected to receive the condition that it is the fraction of the quarter periodic time for the natural frequency of the plate and since the ratio of the length and time increments must satisfy a numerical stability criterion:

$$\frac{\Delta x}{\Delta t} < c_f$$

Where Δx and c_f are the length increment for the plate and the wave speed in the composite respectively, therefore the time increment was limited by

$$\Delta t > \Delta x / \sqrt{E/\rho}$$

Then the total range domain of the applicable time increment Δt is

$$\frac{\pi}{2\omega_n} >> \Delta t > \Delta x / \sqrt{E/\rho}$$

The natural frequency of the clamped laminated plate was derived in the appendix B.

The coefficients A, B, ... in Fig. A-2 are defined in Table A-1. For a node i , saying 7 in Fig. A-3, the finite difference equation applied at it is:

$$(1/\Delta x^4)[F\,D\,B\,D\,E\,C\,A\,C\,E\,D\,B\,D\,F]\{w_1\ w_2\ w_3\ w_4\ w_5\ w_6\ w_7\ w_8\ w_9\ w_{10}\ w_{11}\ w_{12}\ w_{13}\}^T = q_7$$

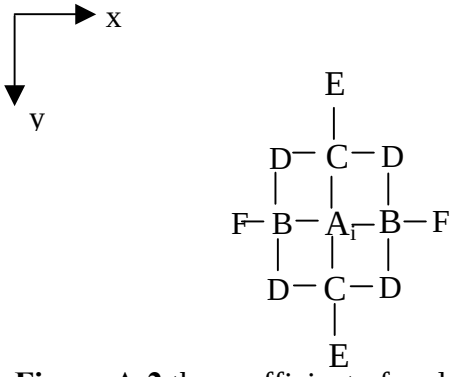

Figure A-2 the coefficient of nodes bounded the interesting node (i)

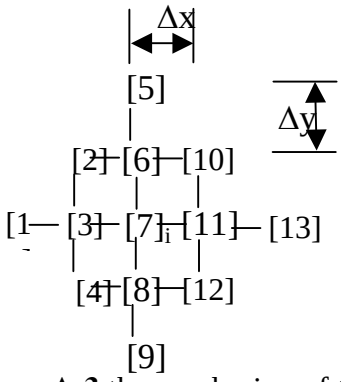

Figure A-3 the numbering of the nodes and increment displacement.

This equation can be applied to an interior node or a node that is on or close to the boundary. When applied to an interior node, the coefficients are shown in Fig. A-2. When applied to a node to be on or close boundary, the coefficients have to be rewritten to satisfy boundary conditions. The boundary conditions Fig. A-4 that we are considering are:

(1). Simply supported

$$for\ x = 0,a \quad w = 0, M_x = -D_{11}\frac{\partial^2 w}{\partial x^2} - D_{12}\frac{\partial^2 w}{\partial y^2} = 0$$

$$for\ y = 0,b \quad w = 0, M_y = -D_{12}\frac{\partial^2 w}{\partial x^2} - D_{22}\frac{\partial^2 w}{\partial y^2} = 0$$

(2). Clamped

$$for\ \ x = 0,a \quad w = 0,\ \frac{\partial w}{\partial x} = 0$$

$$for\ \ y = 0,b \quad w = 0,\ \frac{\partial w}{\partial y} = 0$$

(3). Free

$$for\ \ x = 0,a \quad M_x = 0,\ \frac{\partial M_{xy}}{\partial y} + Q_x = 0$$

$$for\ \ y = 0,b \quad M_y = 0,\ \frac{\partial M_{xy}}{\partial y} + Q_y = 0$$

where,

Mx, My , Mxy : the moment resultant[Fig.A-5].

Qx, Qy: the shear resultant .

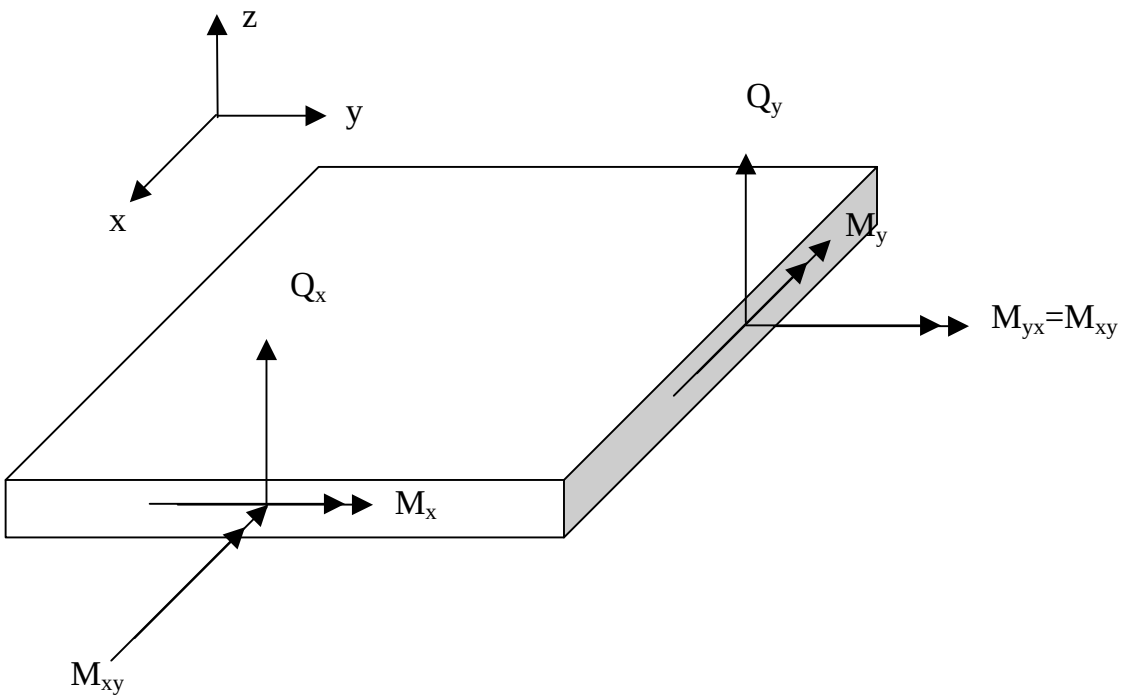

Figure A-5

For the node i in Fig. A.4. (that is 7), we give its difference expressions of *Mx, My, ∂w/∂x, ∂w/∂y, Q_x , Q_y:*

$$M_x\big|_{[7]} = \frac{-1}{\Delta x^2}[\,D_{11} \text{——} - 2(\,D_{11} \begin{matrix} \alpha D_{12} \\ | \\ + \\ | \\ \alpha D_{12} \end{matrix} \text{——} \alpha D_{12}\,)_{[7]} \text{——} D_{11}\,]\{\,w\,\}$$

that is

$$M_x\big|_{[7]} = [\,-1/(\,\Delta x^2\,)][\,D_{11}w_3 + \alpha D_{12}w_6 - 2(\,D_{11} + \alpha D_{12}\,)w_7 + \alpha D_{12}w_8 + D_{11}w_{11}\,]$$

$$\mathrm{M_y}\big|_{[7]} = \frac{-1}{\Delta \mathrm{x}^2}[\mathrm{D_{12}} \text{——} - 2(\mathrm{D_{12}} \begin{matrix} \alpha \mathrm{D_{22}} \\ | \\ + \\ | \\ \alpha \mathrm{D_{22}} \end{matrix} \text{——} \alpha \mathrm{D_{22}})_{[7]} \text{——} \mathrm{D_{12}}]\{\mathrm{w}\}$$

that is

$$M_y\big|_{[7]} = [\,-1/(\,\Delta x^2\,)][\,D_{12}w_3 + \alpha D_{22}w_6 - 2(\,D_{12} + \alpha D_{22}\,)w_7 + \alpha D_{22}w_8 + D_{12}w_{11}\,]$$

$$\frac{\partial w}{\partial x}\bigg|_{[7]} = (\,w_{11} - w_3\,)/(\,2\Delta x\,)$$

$$\frac{\partial w}{\partial x}\bigg|_{[7]} = (\,w_8 - w_6\,)/(\,2\Delta y\,)$$

$$V_x\big|_{[7]} = \frac{-1}{2\Delta x^3}[-D_{11} \text{—} 2(D_{11} + \alpha D_4) \text{—} -2(D_{11} + \alpha D_4) \text{—} D_{11}]\{w\}$$

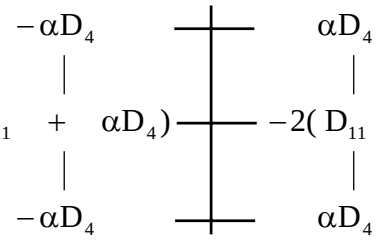

That is

$$V_x\big|_{[7]} = [-1/(2\Delta x^3)][-D_{11}w_1 - \alpha D_4 w_2 + 2(D_{11} - \alpha D_4)w_3 - \alpha D_4 w_4 + \alpha D_4 w_{10} - 2(D_{11} + \alpha D_4)w_{11} + \alpha D_4 w_{12} + D_{11}w_{13}]$$

$$V_y\big|_{[7]} = \frac{-1}{2\Delta x^2 \Delta y}[$$

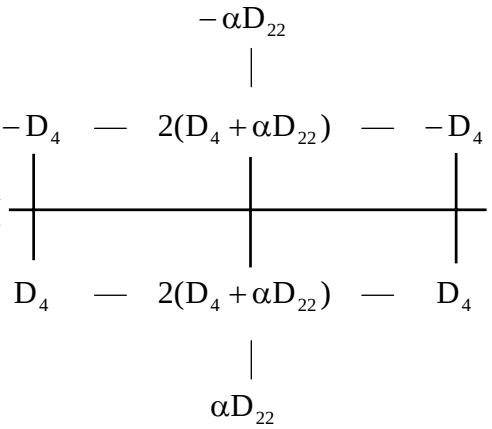

$$]\{w\}$$

That is

$$V_y\big|_{[7]} = -1/2\Delta x^2 \Delta y[-D_4 w_2 + D_4 w_4 + \alpha D_{22} w_5 + 2(D_{11} + \alpha D_4)w_6 - 2(D_{11} + \alpha D_4)w_8 + \alpha D_{22} w_6 - D_4 w_{10} + D_4 w_{12}] = 0$$

Where

$$V_x = \frac{\partial M_{xy}}{\partial y} + Q_x$$

$$V_y = \frac{\partial M_{xy}}{\partial x} + Q_y$$

$$D_4 = D_{12} + 4D_{66}$$

To form the patterns of the finite difference coefficient of orthotropic symmetric laminated plates, we add the fictitious nodes and then apply the finite difference forms of the boundary conditions to eliminate the deflection of fictitious nodes. Finally, the patterns of the finite difference coefficients of orthotropic symmetric laminated plates can be derived and shown in Figure (A.6). Here, simply, we only derive the pattern 3 of Figure (A.6). To show the procedure.

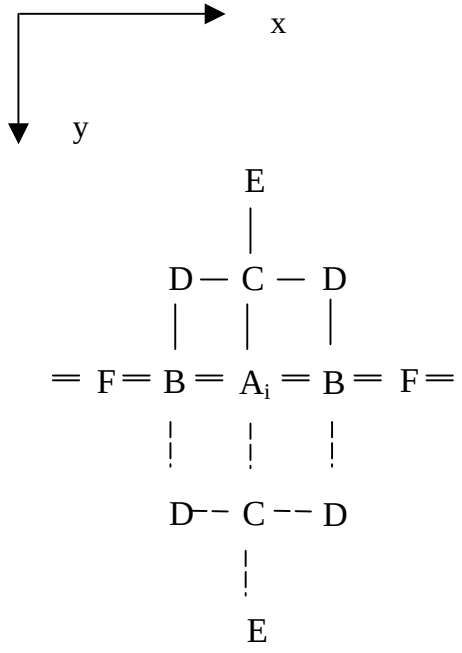

Figure A-6

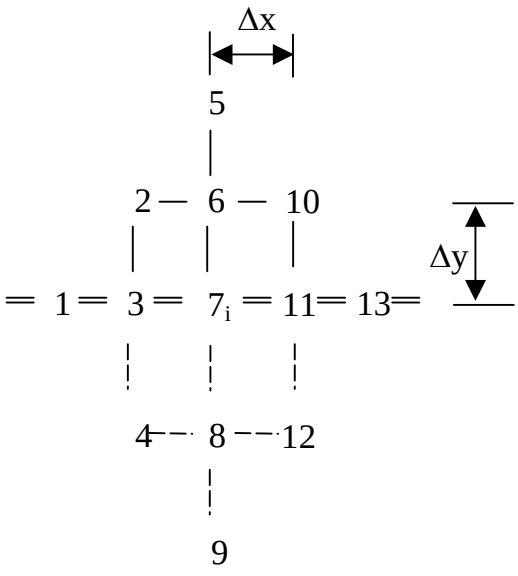

Figure A-7

For the node i (Fig. A-7), at the free edge, adding the fictitious nodes 4, 8, 9, 12, we apply the equation:

$$[F \quad D \quad B \quad D \quad E \quad C \quad A \quad C \quad E \quad D \quad B \quad D \quad F]\begin{Bmatrix} w_1 \\ w_2 \\ w_3 \\ w_4 \\ w_5 \\ w_6 \\ w_7 \\ w_8 \\ w_9 \\ w_{10} \\ w_{11} \\ w_{12} \\ w_{13} \end{Bmatrix} = q_7 \Delta x^4$$

That is

$$Fw_1 + Dw_2 + Bw_3 + Dw_4 + Ew_5 + Cw_6 + Aw_7 + Cw_8 + Ew_9 + Dw_{10} + Bw_{11} + Dw_{12} + Fw_{12} = q_7 \Delta x^4$$

Using boundary conditions, we have:

$$M_y\big|_{[3]} = 0,\ D_{12}w_1 + \alpha D_{22}w_2 - 2(D_{12} + \alpha D_{22})w_3 + \alpha D_{22}w_4 + D_{12}w_7 = 0$$

then

$$\alpha w_4 = -\frac{D_{12}}{D_{22}}w_1 - \alpha w_2 + 2(\frac{D_{12}}{D_{22}} + \alpha)w_3 - \frac{D_{12}}{D_{22}}w_7$$

$$M_y\big|_{[7]} = 0,\ D_{12}w_3 + \alpha D_{22}w_6 - 2(D_{12} + \alpha D_{22})w_7 + \alpha D_{22}w_8 + D_{12}w_{11} = 0$$

Then

$$\alpha w_8 = -\frac{D_{12}}{D_{22}} w_3 - \alpha w_6 + 2(\frac{D_{12}}{D_{22}} + \alpha) w_7 - \frac{D_{12}}{D_{22}} w_{11}$$

$$M_y\Big|_{[11]} = 0,\ D_{12} w_7 + \alpha D_{22} w_{10} - 2(D_{12} + \alpha D_{22}) w_{11} + \alpha D_{22} w_{12} + D_{12} w_{13} = 0$$

Then

$$\alpha w_{12} = -\frac{D_{12}}{D_{22}} w_7 - \alpha w_{10} + 2(\frac{D_{12}}{D_{22}} + \alpha) w_{11} - \frac{D_{12}}{D_{22}} w_{13}$$

$$V_y\Big|_{[7]} = 0,\ [-1/(2\Delta x^2 \Delta y)][-D_4 w_2 + D_4 w_4 - \alpha D_{22} w_5$$
$$+ 2(D_4 + \alpha D_{22}) w_6 - 2(D_4 + \alpha D_{22}) w_8 + \alpha D_{22} w_9 + D_4 w_{10} + D_4 w_{12}] = 0$$

Then

$$\alpha^2 D_{22} w_9 = \alpha D_4 w_2 - \alpha D_4 w_4 + \alpha^2 D_{22} w_5 - 2\alpha(D_4 + \alpha D_{22}) w_6$$
$$+ 2\alpha(D_4 + \alpha D_{22}) w_8 + \alpha D_{22} w_{10} - \alpha D_4 w_{12}$$

Then, we try to eliminate w_4 , w_8, w_{12} :

$$\alpha\, D_{12}\, w_4 = \frac{D_{12}^2}{D_{22}} w_1 - \alpha\, D_{12}\, w_2 + 2(\frac{D_{12}^2}{D_{22}} + \alpha\, D_{12}\,) w_3 - \frac{D_{12}^2}{D_{22}} w_7$$

$$(-2\alpha D_{12} - 2\alpha^2 D_{22}) w_8 = -2(D_{12} - \alpha D_{22}) \alpha\, w_8$$
$$= 2D_{12}(D_{12} / D_{22} + \alpha) w_3 + 2\alpha(D_{12} + \alpha D_{22}) w_6$$
$$- 4(D_{12} + \alpha D_{22})(D_{12} / D_{22} + \alpha) w_7$$
$$+ 2D_{12}(D_{12} / D_{22} + \alpha) w_{11}$$

$$\alpha\, D_{12}\, w_{12} = \frac{D_{12}^2}{D_{22}} w_7 - \alpha\, D_{12}\, w_{10} + 2(\frac{D_{12}^2}{D_{22}} + \alpha\, D_{12}\,) w_{11} - \frac{D_{12}^2}{D_{22}} w_{13}$$

The coefficient of w_1 is

$$F - D_{12}^2 / D_{22} = D_{11} - D_{12}^2 / D_{22} = 2T$$

The coefficient of w_2 is

$$3\alpha D_3 + 2\alpha D_{66} - \alpha D_{12} = \alpha (3D_3 + D_3 - D_{12} - D_{12}) = 2\alpha (2D_3 - D_{12}) = 2H$$

The coefficient of w_3 is

$$\begin{aligned} B + 2(D_{12})^2 / D_{22} + \alpha D_{12} + 2(D_{12})^2 / D_{22} + \alpha D_{12} & \\ = -4D_{11} - 4\alpha D_3 + 4D_{12}^2 / D_{22} + 4\alpha D_{12} & \\ = -4\alpha D_3 + 4\alpha D_{12} - 4D_{11} + 4D_{12}^2 / D_{22} & \\ = 2[-2\alpha (D_3 - D_{12}) - 2(D_{11} - D_{12})^2 / D_{22}] = 2k & \end{aligned}$$

The coefficient of w_5 is $2E$

The coefficient of w_6 is

$$\begin{aligned} C - 2\alpha D_4 - 2\alpha_2 D_{22} + 2\alpha (D_{12} + \alpha D_{22}) = C - 2\alpha D_4 + 2\alpha D_{12} & \\ = -4\alpha D_3 - 4\alpha^2 D_{22} - 2\alpha D_3 - 4\alpha D_{66} + 2\alpha D_{12} & \\ = -4\alpha^2 D_{22} - 6\alpha D_3 - 2\alpha (D_3 - D_{12}) + 2\alpha D_{12} & \\ = -4\alpha^2 D_{22} - 8\alpha D_3 + 4\alpha D_{12} & \\ = 2[-2\alpha (\alpha D_{22} + 2D_3 - D_{12})] = 2O & \end{aligned}$$

The coefficient of w_7 is

$$
\begin{aligned}
&A - D_{12}^{\,2} / D_{22} - 4(D_{12} + \alpha D_{22})(D_{12} / D_{22} + \alpha) - D_{12}^{\,2} / D_{22} \\
&\quad = A - 2D_{12}^{\,2} / D_{22} - 4D_{12}^{\,2} / D_{22} - 4\alpha D_{12} - 4\alpha D_{12} - 4\alpha^2 D_{22} \\
&\quad = A - 6D_{12}^{\,2} / D_{22} - 8\alpha D_{12} - 4\alpha^2 D_{22} \\
&\quad = 6D_{11} + 8\alpha D_3 + 6\alpha^2 D_{22} - 6D_{12}^{\,2} / D_{22} - 8\alpha D_{12} - 4\alpha^2 D_{22} \\
&\quad = 8\alpha(D_3 - D_{12}) + 6(D_{11} - D_{12})^2 / D_{22} + 2\alpha^2 D_2 = 2\psi
\end{aligned}
$$

The coefficient of w_{10} is

$$3\alpha D_3 + 2\alpha D_{66} - \alpha D_{12} = 2H$$

The coefficient of w_{11} is

$$B + 2(D_{12}^{\,2} / D_{22} + \alpha D_{12} + 2(D_{12}^{\,2} / D_{22} + \alpha D_{12}) = 2k$$

The coefficient of w_{13} is

$$F - D_{12}^{\,2} / D_{22} = 2T$$

So the equation applied the node 7 is

$$[\ T\ \ H\ \ k\ \ E\ \ O\ \ \psi\ \ H\ \ k\ \ T\ ]\begin{Bmatrix} w_1 \\ w_2 \\ w_3 \\ w_5 \\ w_6 \\ w_7 \\ w_{10} \\ w_{11} \\ w_{13} \end{Bmatrix} = (q_7/2)\Delta x^4$$

Similarly, we can derive the patterns of the finite difference coefficient of orthotropic symmetric laminated plates with the boundary conditions of simply supported, clamped, free and their combinations (Table A-1 shows the definitions and Fig. A-8 shows the 25 available cases).

Table A-1 Definitions

$A = 6D_{11} + 8\alpha D_3 + 6\alpha^2 D_{22}$

$B = -4(D_{11} + \alpha D_3)$

$C = -4\alpha(D_3 + \alpha D_{22})$

$D = 2\alpha D_3$

$E = \alpha 2D_{22}$

$F = D_{11}$

$G = 5D_{11} + 8\alpha D_3 + 6\alpha^2 D_{22}$

$H = \alpha (2D_3 - D_{12})$

$I = -2(D_{11} + 2\alpha D_3 - \alpha D_{12})$

$J = D_{11} + 4\alpha (D_3 - D_{12}) + 3\alpha^2 (D_{22} - D_{12}^2 / D_{11})$

$K = -2\alpha [D_3 - D_{12} + \alpha (D_{22} - D_{12}^2 / D_{11})]$

$L = \alpha^2 (D_{22} - D_{12}^2 / D_{11})/2$

$M = 5D_{11} + 8\alpha D_3 + 5\alpha^2 D_{22}$

$O = -2\alpha (\alpha D_{22} + 2D_3 - D_{12})$

$P = D_{11} + 4\alpha (D_3 – D_{12}) + 5\alpha^2 (D_{22} – D_{12}^2 / D_{11})/2$

$Q = –2\alpha [D_3 – D_{12} + \alpha (D_{22} – D_{12}^2 / D_{11})/2]$

$R = (D_{11} – D_{12}^2 / D_{22})/2 + 2\alpha (D_3 – D_{12}) + \alpha^2 (D_{22} – D_{12}^2 / D_{11})/2$

$S = – 2(D_3 – \alpha D_{12})– (D_{11} – D_{12}^2 / D_{22})$

$T = (D11 – D_{12}^2 / D_{22})/2$

$U= 2\alpha (D_3 – D_{12})$

$g = 6D_{11} + 8\alpha D_3 + 5\alpha^2 D_{22}$

$k = –2\alpha (D_3 – D_{12}) –2(D_{11} – D_{12}^2 / D_{22})$

$p = 4\alpha (D_3 – D_{12}) + 5(D_{11} – D_{12}^2 / D_{22})/2 + \alpha^2 D_{22}$

$\psi = 4\alpha (D_3 – D_{12}) + 3(D_{11} – D_{12}^2 / D_{22}) + \alpha^{\Pi 2} D_{22}$

$\gamma = 7D_{11} + 8\alpha D_3 + 5\alpha^2 D_{22}$

$\delta = D_{11} + 4\alpha (D_3 – D_{12}) + (7D_{22} – 5D_{12}^2 / D_{11})/2$

$\theta = 4\alpha (D_3 – D_{12}) + (7D_{11} – 5D_{12}^2 / D_{22})/2 + \alpha^2 D_{22}$

$\varphi = 6D_{11} + 8\alpha D_3 + 7\alpha^2 D_{22}$

$\beta = 7D_{11} + 8\alpha D_3 + 6\alpha^2 D_{22}$

:| . . . Simply supported boundary

Clamped boundary

i load point

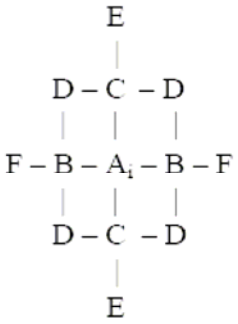

(1)

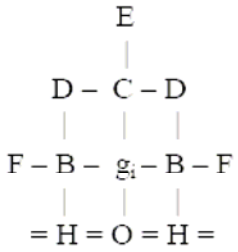

(2)

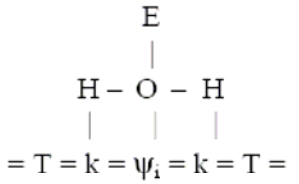

(3)

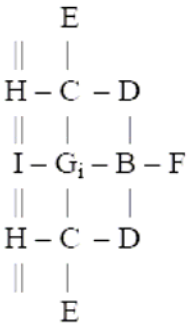

(4)

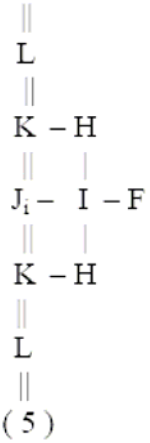

(5)

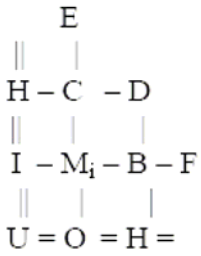

(6)

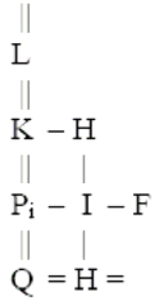

(7)

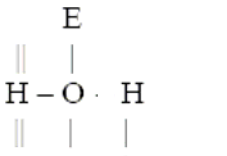

(8)

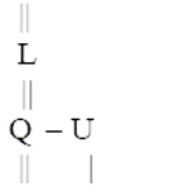

(9)

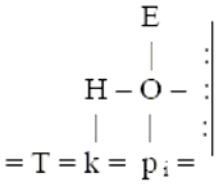

(10)

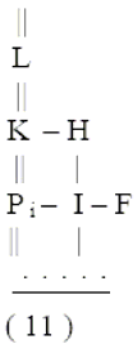

(11)

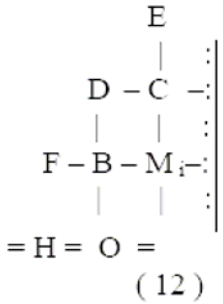

(12)

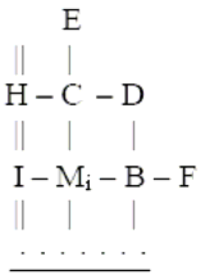

(13)

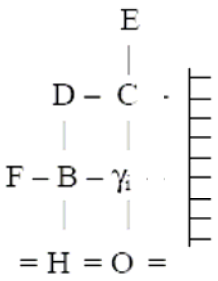

(14)

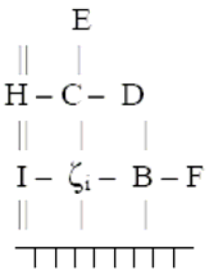

(15)

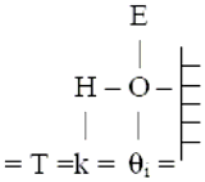

(16)

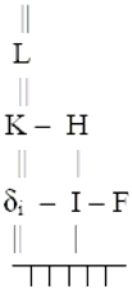

(17)

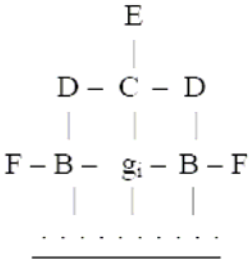

(18)

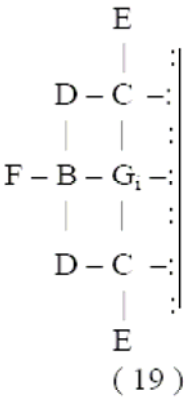

(19)

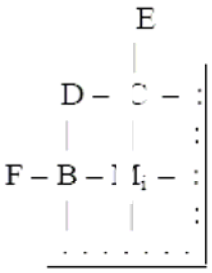

(20)

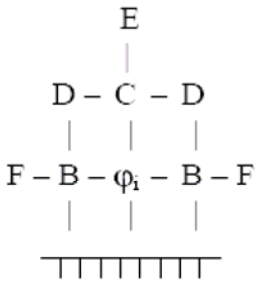

(21)

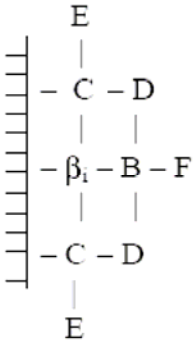

(22)

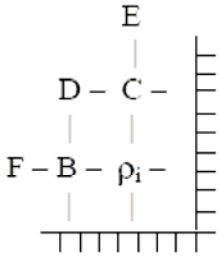

(23)

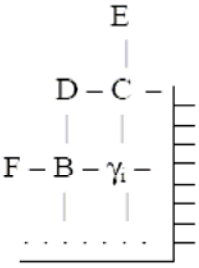

(24)

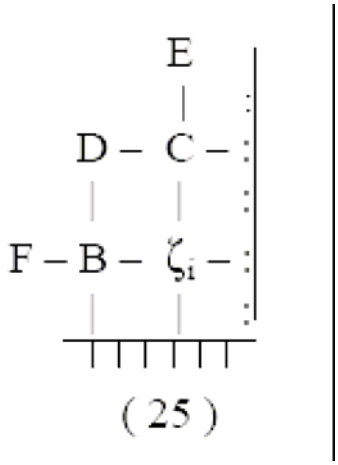

Figure A-8

Employing Fig. A-8 to solve practice problem of orthotropic symmetric laminated plates. Various boundary conditions can be applied to the problem. The edges can be simply supported, clamped, or free.

Appendix B

The derivation of Natural frequency of rectangular CCCC Plate

This derivation modified the Natural frequency derived in {"Dynamics of Plates" by J.S. Rao [62]}.

Clamped Plates

For this case, it not possible to get an exact solution as in the SSSS or SCSC plates, the approximate solution method was used to solve this problem. Let us consider Ritz method for this purpose. The strain energy of the plate is given by

$$U = \frac{1}{2}\iint_A \left[D_{11}\left(\frac{\partial^2 w}{\partial x^2}\right)^2 + 2D_{12}\frac{\partial^2 w}{\partial x^2}\frac{\partial^2 w}{\partial y^2} + D_{22}\left(\frac{\partial^2 w}{\partial y^2}\right)^2 + 4D_{66}\left(\frac{\partial^2 w}{\partial x \partial y}\right)^2 \right] dxdy \quad \ldots(B.1)$$

The work done by a uniformly distributed external force q is

$$W = -V = \iint_A qw dxdy \quad \ldots(B.2)$$

Let the coordinate system be located at the left hand top corner with the x-axis laying on the top edge of width a and the y-axis laying on the left side edge of width b. The boundary conditions for the clamped plate are: -

$$w = \frac{\partial w}{\partial x} = 0 \quad for \quad x = 0, a$$
$$w = \frac{\partial w}{\partial y} = 0 \quad for \quad y = 0, b \quad \ldots(B.3)$$

Let us assume the following series solution for w

$$w(x,y)=\sum_{i=1}^{\infty}\sum_{j=1}^{\infty}a_{ij}\,f_i(x)g_i(y) \qquad \ldots(B.4)$$

Where f and g satisfy the boundary conditions on the edges x constant and y constant respectively. The Lagrangian of the plate is given by

$$L=\frac{1}{2}\iint_A\left[D_{11}\left(\frac{\partial^2 w}{\partial x^2}\right)^2+2D_{12}\frac{\partial^2 w}{\partial x^2}\frac{\partial^2 w}{\partial y^2}+D_{22}\left(\frac{\partial^2 w}{\partial y^2}\right)^2+4D_{66}\left(\frac{\partial^2 w}{\partial x\partial y}\right)^2\right]dxdy \qquad \ldots(B.5)$$
$$-\iint_A qw\,dxdy$$

Submitting (B.3) in the above equation, we get (B.6)

$$L=\frac{1}{2}\iint_A\left[\begin{array}{l}D_{11}\left(\sum_{i=1}^{\infty}\sum_{j=1}^{\infty}a_{ij}\frac{\partial^2 f_i}{\partial x^2}g_i\right)^2\\+2D_{12}\left(\sum_{i=1}^{\infty}\sum_{j=1}^{\infty}a_{ij}\frac{\partial^2 f_i}{\partial x^2}g_i\right)\left(\sum_{i=1}^{\infty}\sum_{j=1}^{\infty}a_{ij}f_i\frac{\partial^2 g_i}{\partial y^2}\right)\\+D_{22}\left(\sum_{i=1}^{\infty}\sum_{j=1}^{\infty}a_{ij}f_i\frac{\partial^2 g_i}{\partial y^2}\right)^2\\+4D_{66}\left(\sum_{i=1}^{\infty}\sum_{j=1}^{\infty}a_{ij}\frac{\partial f_i}{\partial x}\frac{\partial g_i}{\partial y}\right)^2\end{array}\right]dxdy$$
$$-\iint_A q\left(\sum_{i=1}^{\infty}\sum_{j=1}^{\infty}a_{ij}f_i g_i\right)dxdy \qquad \ldots(B.6)$$

For Ritz approximation with m number of terms in f and n terms in g, we have

$$\frac{\partial L}{\partial a_{ij}}=0 \quad for\ i=1,2,...m \ \ and \ \ j=1,2,...n \qquad \ldots(B.7)$$

$$\sum_{k=1}^{\infty}\sum_{e=1}^{\infty}\left[\begin{array}{l} D_{11}\int_0^a \frac{\partial^2 f_k}{\partial x^2}\frac{\partial^2 f_i}{\partial x^2}dx\int_0^b g_e g_j dy \\ + D_{12}\int_0^a \frac{\partial^2 f_k}{\partial x^2} f_i dx\int_0^b g_e \frac{\partial^2 g_j}{\partial y^2}dy \\ + D_{12}\int_0^a \frac{\partial^2 f_i}{\partial x^2} f_k dx\int_0^b g_j \frac{\partial^2 g_e}{\partial y^2}dy \\ + D_{22}\int_0^a f_k f_i dx\int_0^b \frac{\partial^2 g_e}{\partial y^2}\frac{\partial^2 g_j}{\partial y^2}dy \\ + 4D_{66}\int_0^a \frac{\partial f_k}{\partial x}\frac{\partial f_i}{\partial x}dx\int_0^b \frac{\partial g_e}{\partial y}\frac{\partial g_j}{\partial y}dy \end{array}\right] a_{ke} \qquad \text{… (B.8)}$$

$$= q\int_0^a f_i dx\int_0^b g_j dy \quad i = 1,2,...m \quad j = 1,2,...n$$

For a one-term approximation, the assumed solution satisfies the boundary conditions can be taken as:

$$f_1(x) = (x^2 - ax)^2$$
$$g_1(y) = (y^2 - by)^2 \qquad \text{…(B.9)}$$

Equation (B.8) then becomes

$$\begin{aligned} & a_{11}D_{11}\int_0^a \left(12x^2 + 2a^2 - 12ax\right)^2 dx\int_0^b \left(y^2 - by\right)^4 dy \\ & + 2a_{11}D_{12}\int_0^a \left(12x^2 + 2a^2 - 12ax\right)\left(x^2 - ax\right)^2 dx \\ & \times \int_0^b \left(12y^2 + 2b^2 - 12by\right)\left(y^2 - by\right)^2 dy \\ & + a_{11}D_{22}\int_0^a \left(x^2 - ax\right)^4 dx\int_0^b \left(12y^2 + 2b^2 - 12by\right)^2 dy \\ & + 4D_{66}\int_0^a \left(4x^3 + 2a^2x - 6ax^2\right)^2 dx\int_0^b \left(4y^3 + 2b^2y - 6by^2\right)^2 dy \\ & = q\int_0^a \left(x^2 - ax\right)^2 dx\int_0^b \left(y^2 - by\right)^2 dy \end{aligned} \qquad \text{…(B.10)}$$

Upon evaluation of the integrals the above equation and rearranging, yield

$$a_{11} = \frac{\frac{49}{8}q}{7D_{11}b^4 + 4(D_{12} + 2D_{66})a^2b^2 + 7D_{22}a^4} \quad \ldots(B.11)$$

Therefore, the diffraction w is given by

$$w = \frac{\frac{49}{8}q\left(x^2 - ax\right)^2\left(y^2 - by\right)^2}{7D_{11}b^4 + 4(D_{12} + 2D_{66})a^2b^2 + 7D_{22}a^4} \quad \ldots(B.12)$$

The maximum deflection occurs at the center of the plate x=a/2 and y=b/2,

$$w = \frac{\frac{49}{8}qa^4b^4}{2048\left[7D_{11}b^4 + 4(D_{12} + 2D_{66})a^2b^2 + 7D_{22}a^4\right]} \quad \ldots(B.13)$$

Natural Frequency

Since the all edges are clamped, then the solution was assumed to be

$$\begin{aligned} fi(x) = &(\cos r_i a - \cosh r_i a)(\cos r_i x - \cosh r_i x) \\ &+ (\sin r_i a + \sinh r_i a)(\sin r_i x + \sinh r_i x) \end{aligned} \quad \ldots(B.14)$$

$$\begin{aligned} gi(y) = &(\cos r_i a - \cosh r_i a)(\cos r_i y - \cosh r_i y) \\ &+ (\sin r_i a + \sinh r_i a)(\sin r_i y + \sinh r_i y) \end{aligned} \quad \ldots(B.15)$$

The first five roots of $r_i a$ and $r_i b$ are given by

$$\begin{aligned} r_1 a &= r_1 a = 4.73 \\ r_2 a &= r_2 a = 7.853 \\ r_3 a &= r_3 a = 10.996 \\ r_4 a &= r_4 a = 14.137 \\ r_5 a &= r_5 a = 17.279 \end{aligned} \quad \ldots(B.16)$$

For free vibration, the solution is now assumed

$$w = \sum_{i=1}^{m}\sum_{j=1}^{n} A_{ij}\ f_i(x)\, g_j(y) \sin \omega t \qquad \ldots(B.17)$$

substitute equation (B.16) in the above equation (B.17) and minimize the resulting Lagrangian with respect to A_{ij}, yields

$$\sum_{k=1}^{m}\sum_{e=1}^{n}\left[\begin{array}{l} D_{11}\int_0^a \frac{\partial^2 f_k}{\partial x^2}\frac{\partial^2 f_i}{\partial x^2}dx\int_0^b g_e g_j dy \\ + D_{12}\int_0^a \frac{\partial^2 f_k}{\partial x^2}\, f_i dx\int_0^b g_e \frac{\partial^2 g_j}{\partial y^2}dy \\ + D_{12}\int_0^a \frac{\partial^2 f_i}{\partial x^2}\, f_k dx\int_0^b g_j \frac{\partial^2 g_e}{\partial y^2}dy \\ + D_{22}\int_0^a f_k\, f_i dx\int_0^b \frac{\partial^2 g_e}{\partial y^2}\frac{\partial^2 g_j}{\partial y^2}dy \\ + 4D_{66}\int_0^a \frac{\partial f_k}{\partial x}\frac{\partial f_i}{\partial x}dx\int_0^b \frac{\partial g_e}{\partial y}\frac{\partial g_j}{\partial y}dy \end{array}\right] A_{ke}$$

$$= \sum_{k=1}^{m}\sum_{e=1}^{\infty n}\left[\rho h\omega^2 \int_0^a f_i\, f_k dx\int_0^b g_e g_j dy\right] A_{ke} \quad i = 1,2,\ldots m \quad j = 1,2,\ldots n \qquad \ldots(B.18)$$

Hearmon restricted to the first approximation for each natural frequencies and simplified the above to

$$D_{11}\frac{a_1^4}{a} + 2(D_{12} + 2D_{66})\frac{a_2}{a^2 b^2} + D_{22}\frac{a_3^4}{b^4} = \rho h\omega^2 \qquad \ldots(B.19)$$

Where (a) values are obtained from the integrals in equation (B.18)

$$a_1 = 4.73$$
$$a_3 = 4.73$$
$$a_2 = 151.3 \quad for \;\; m = 1, n = 1$$

$$a_1 = 4.73$$
$$a_3 = \left(n + \frac{1}{2} \right) \pi$$
$$a_2 = 12.3 a_3 (a_3 - 2) \quad for \;\; m = 1, \; n = 2,3,4...$$

$$a_1 = \left(m + \frac{1}{2} \right) \pi$$
$$a_3 = 4.73$$
$$a_2 = 12.3 a_1 (a_1 - 2) \quad for \;\; m = 2,3,4,... \; n = 1$$

$$a_1 = \left(m + \frac{1}{2} \right) \pi \qquad \text{…(B.20)}$$
$$a_3 = \left(n + \frac{1}{2} \right) \pi$$
$$a_2 = a_1 (a_1 - 2) a_3 (a_3 - 2) \quad for \;\; m = 2,3,4,... \; n = 2,3,4,...$$

The first mode natural frequency for a square plate can be obtained from the above as

$$\rho h a^4 \omega_{11}^2 = 500.475 D_{11} + 2 \times 151.3 (D_{12} + 2 D_{66}) + 500.547 D_{22} \qquad \text{…(B.21)}$$

i.e.,

$$\omega_{11} = \sqrt[2]{\frac{\left(500.475 D_{11} + 2 \times 151.3 (D_{12} + 2 D_{66}) + 500.547 D_{22} \right)}{\rho h a^4}} \qquad \text{…(B.22)}$$

For an isotropic plate , $D_{11}= D_{22} = D_{12} +2D_{66}$, the above equation further reduced to

$$\frac{\rho h a^4}{D}\omega_{11}^2 = 1303.694$$

i.e.,

$$\omega_{11}^2 = 36.1\sqrt[2]{\frac{D}{\rho h a^4}} \qquad \ldots(B.23)$$

Appendix C

89C51 controller Program for Velocity Measurement Device

Assembly Program used for programming 89C51 controller for application for projectile velocity measuring system

```
org    ooooh
jmp    start
org    oaobh
gmp  In
org    oo4oh
Start:
mov   sp,# 50 h
mov    30 h, # 0
mov    31 h, # 0
mov    32 h, # 0
mov    33 h, # 0
mov    34 h, # 0
mov    35 h ,# 0
mov    ro, # 0
mov    r1, # 0
mov    r2, # 0
mov    r3, # 0
mov    tmod, # 01
mov    ie, # 82 h
st: jb   p1.1, st
t10: jnb  p1.1, t10
setb tro
mov    ro, # 01
```

```
t11: jb p1.1, t11
clr       tro
mov    30 h, t10
mov    31 h, tho
mov    t10, # 0
mov     tho, # 0
setb    tro
mov    ro, # 02
t2:jb    p1.2, t2
clr       tro
mov     32 h, t10
mov     33 h, t ho
mov    t10, # 0
mov    tho, # 0
steb    tro
mov    ro, # 3
t3: jb   p1.3, t3
clr      tro
mov    34 h, t10
mov    35 h, tho
mov    t mod, # 20 h
mov    t con, # 0 d2h
mov    s con, # 52 h
mov    th1, # 0 fdh
setb   scon.6
mov   a, 30 h
set 11: jnb    ti, set11
clr     ti
mov    sbuf, a
mov   a, 31 h
```

```
set 1h: jnb  ti, set 1h
clr     ti
mov   sbuf, a
mov    a, r1
set 1c: jnb  ti, set 1c
clr    ti
mov   sbuf, a
mov   a, 32 h
set 21: jnb  ti, set21
clr    ti
mov    sbuf, a
mov    a, 33 h
set 2h: jnb    ti, set 2h
clr    ti
mov   sbuf, a
mov   a, r2
set 2c: jnb    ti, set 2c
clr   ti
mov  sbuf, a
mov    a, 34 h
set 31: jnb  ti, set 31
clr      ti
mov     sbuf, a
mov    a, 35 h
set 3h; jnb   ti, set 3h
clr    ti
mov    sbuf, a
mov    a, r3
set  3c: jnb    ti, set  3c
clr   ti
```

```
mov   sbuf, a
here: jmp    here
In: ejne    ro, # 1, I2
Inc        r1
Jmp       rtn
I2: ejne   ro, # 2, I3
I3: ejne    ro, # 3, rtn
Inc   r3
Rtn:   reti
end
```

الزجاج و البلاط السيراميكي و رقائق التصوير الطبي باشعة اكس. تم قياس الخواص الميكانيكية المطلوبة من خلال تجارب قياسية. من خلال هذه التجارب تم حساب معامل جديد سمي بمعامل النسج و الذي يمثل نسبة الخواص الميكانيكية للمواد المركبة المصنعة من النسيج الى مثيلاتها للمواد المركبة المصنعة من الالياف الطولية المتعامدة. وجد ان هذا المعامل يكون اعلى للمواد المركبة بالكفلر عنه في باقي الالياف و لنفس مادة الربط. كذلك وجد ان معامل النسج للمواد المركبة بالابوكسي هو اعلى لمثيلاتها المستخدمة للبولستر كمادة ربط. ان معامل النسج يزداد مع زيادة مساحة الحزمة المستخدمة في النسج و كذلك مع زيادة المسافة بين الحنيات خلال النسج.

الجزء الثاني هو تصنيع واختبار صفائح مركبة في الاصطدام البالستي ولهذا الغرض تم تصميم وبناء منظومة تصادم باستخدام بندقية صنعت لهذا الغرض ولعينات مربعة ذات تثبيت مقيد. تم تصميم وبناء عداد حاسوبي زمني لقياس سرعة الدخول والخروج للاطلاقة ولتقييم الزمن التقريبي للاختراق. استخدمت هذه المنظومة لمقارنة النتائج النظرية مع الاختبارات العملية وايضا لدراسة تاثير ترتيب الطبقات في الصفائح الهجينة على التصادم.

اظهرت النتائج ان طاقة التلامس لها اقل القيم نسبة للطاقات الممتصة، وان طاقات التفصخ والتشويه الكبير قد ازدادت مع زيادت سرعة التصادم لحين الوصول الى الحدود البالستية وبعدها تبقى ثابتة. ان الطاقة الممتصة بالاحتكاك ازدادت مع سرعة التصادم بغض النظر عن الحدود البالستية. ان الطاقة الممتصة قد ازدادت بزيادة سمك الصفيحة. ان مقاومة اهداف الكاربون المركبة للتصادم كانت اقل من مقاومة اهداف الكفلر المركبة واعلى من اهداف الزجاج المركب.

لتحسين خواص التصادم لمواد الزجاج المركبة تم اضافة طبقة كفلر الى الصفيحة الطباقية وفي ثلاثة مواقع هي امام، خلف وفي مركز الصفيحة. اثبتت النتائج ان اضافة طبقة الكفلر قد ادت الى زيادت الطاقة الممتصة للتصادم وان هذه الطاقة تكون اعلى ما يمكن عندما تكون طبقة الكفلر خلف الهدف نسبة الى اتجاه دخول الاطلاقة

الخلاصـــة

ازداد استخدام المواد المركبة المكونة من الالياف المقواة في العديد من التطبيقات المدنية والعسكرية نتيجة امتلاكها خواص ميكانيكية ممتازة كالمقاومة النوعية و الجساءة النوعيةومقاومة التاكل وامتلاكها عمر كلل اكبر من المواد الاخرى. رغم ذلك, فان احد اهم الماخذ على المواد المركبةهي خواصها التداخلية,والتي تكون ذات فعالية في احمال التصادم.ان بعض الاجزاء المكونة للمركبات الفضائية والطائرات وقواعد الاطلاق قد تتعرض الى تصادم بسرع عالية كاجزاء المحرك المكسورة, وريش التوربينات او الشضايا المتطايرة الى المضخات والقذائف والمدافع ...الخ.

في هذا العمل, تم دراسة الطاقة الممتصة نتيجة تصادم اطلاقة جاسئة صغيرةعلى اهداف لمواد مركبةدراسة نظرية وعملية.نظرذيا تم دراسة تصادم اطلاقات مخروطية المقدمة علىمواد مركبة متعددة الطبقات. تم التعامل مع اربعة انواع من الطاقات الممتصة والتي هي طاقة الانفعال نتيجة تشويه الصفيحة (طاقة التماس), طاقة التشويه الكبير قرب منطقة التصادم, طاقة التفصخ للطبقات و الطاقة المفقودة في الاحتكاك.

تم تطويروحل معادلة الحركة للصفائح متعددة الطبقات لظروفها الحدية. تم اشتقاق معادلة الطاقة لمنطقة التشويه العالي المعرضة للتفصخ تحت فرضية شكل التشويه لحساب عمق الاختراق وقطر دائرة منطقة التفصخ. تم حساب طاقة التفصخ من خلال حل معادلتي نظرية فشل التفصخ مع معادلة الحركة. طاقة الاحتكاك حلت بفرضية ثبات معامل الاحتكاك.

قسم العمل النظري الى محورين رئيسين. اولا, تم صناعة واختبار خواص المواد المركبة النسيجية المستخدمة في البحث. استخدمت ثلاثة انواع من الالياف هي الالياف الزجاجية والياف الكاربون والياف الكفلر ولمختلف اشكال النسج وسمك حزم الالياف. استخدم نوعين من مواد الربط هي البولستر والابوكسي. تم صناعة عينات مواد الربط والمواد المركبة يدويا باستخدام مواد بديلة متوفرة وبنجاح كقوالب للعينات كمعجون لصق

شكر وتقدير

الحمد لله على ما انعم وله الشكر على ما الهم و الثناء على ما اقدم ...

أود ان اعبر عن امتناني وشكري وتقديري لكل من المشرفين, **الاستاذ الدكتور هشام توفيق** و **الدكتور كاظم حمزة غليم** و المغفور له **الدكتور طلال يوسف النائب** لما بـذلوه من جـهد وارشادات وتوجيهات طيلة مدة البحث.

اود ايضا ان اشكر جميع اساتذتي الذين لم يبخـلوا علي بالنصح و الارشـاد كلمـا دعتني الحاجة الى الاستاناس بارائهم. شكرا جزيلا لكل زمـلائي واصـدقائي في القسـم وخـارجـه علي المساندة والمساعدة.

ويعجز القلم عن التعبير عن حبي وتقديري لابي وامي واخوتي واخواتي لمساندتهم وحثهم لي,وجزيل شكري وحبي لزوجتي العزيزة وابنتي التي ولدت خلال فترة انهائي لهذا العمل .

ادعو من الله ان يحفظ الجميع ويسدد على طريق الصلاح خطاهم.

علي حسـين محمد الحلي

دراسة تحليلية وعملية للتصادم بسرع عالية على صفائح مركبة

أطروحة
مقدمة الى كلية الهندسة في جامعة النهرين
وهي جزء من متطلبات نيل درجة دكتوراه فلسفة
في الهندسة الميكانيكية

من قبل

علي حســين محمد الحلي

بكلوريوس علوم في الهندسة الميكانيكية/1996
ماجستير علوم في الهندسة الميكانيكية/1999

وذلك في

محرم **1427 هـ**
ايلــول **2006 م**